ORNL-TM-2307

OAK RIDGE NATIONAL LABORATORY LIBRARIES

3 4456 0539391 8

OAK RIDGE NATIONAL LABORATORY

operated by

UNION CARBIDE CORPORATION

NUCLEAR DIVISION

for the

U.S. ATOMIC ENERGY COMMISSION

ORNL-TM-2307

77

ID LIBRARY APR 24 '69

DESORPTION OF CARBON MONOXIDE FROM TUNGSTEN BY BOMBARDMENT WITH ELECTRONS

(Thesis)

Robert Eugene Clausing

Submitted as a thesis to the Faculty of the School of Engineering and Applied Science of the University of Virginia in partial fulfillment of the requirements for the degree of Doctor of Science.

LEGAL NOTICE

This report was prepared as an account of Government sponsored work. Neither the United States, nor the Commission, nor any person acting on behalf of the Commission:

A. Makes any warranty or representation, expressed or implied, with respect to the accuracy, completeness, or usefulness of the information contained in this report, or that the use of any information, apparatus, method, or process disclosed in this report may not infringe privately owned rights; or

B. Assumes any liabilities with respect to the use of, or for damages resulting from the use of any information, apparatus, method, or process disclosed in this report.

As used in the above, "person acting on behalf of the Commission" includes any employee or contractor of the Commission, or employee of such contractor, to the extent that such employee or contractor of the Commission, or employee of such contractor prepares, disseminates, or provides access to, any information pursuant to his employment or contract with the Commission, or his employment with such contractor.

ORNL-TM-2307

Contract No. W-7405-eng-26

METALS AND CERAMICS DIVISION

DESORPTION OF CARBON MONOXIDE FROM TUNGSTEN BY BOMBARDMENT WITH ELECTRONS

Robert Eugene Clausing

Submitted as a thesis to the Faculty of the School of Engineering and Applied Science of the University of Virginia in partial fulfillment of the requirements for the degree of Doctor of Science

APRIL 1969

OAK RIDGE NATIONAL LABORATORY
Oak Ridge, Tennessee
operated by
UNION CARBIDE CORPORATION
for the
U.S. ATOMIC ENERGY COMMISSION

ACKNOWLEDGMENT

The author wishes to express his sincere appreciation to Professors Avery Catlin and Kenneth R. Lawless of the Materials Science Department of the University of Virginia and to Drs. J. S. Faulkner and C. J. McHargue of the Oak Ridge National Laboratory for their many helpful suggestions during the course of this investigation and the preparation of the dissertation. Thanks are due also to Dr. R. A. Strehlow for several stimulating discussions and to P. Patriarca for his constant encouragement.

The author has been privileged to conduct the experimental work both in the Materials Science Department of the University of Virginia and in the Metals and Ceramics Division of the Oak Ridge National Laboratory and wishes to thank the many members of the staffs of both the University and the Laboratory who have helped in the research. Special thanks are due to the members of the Metals and Ceramics Division Reports Office, who under the direction of Meredith R. Hill, helped to prepare this document under a very tight time schedule. The specific assistance of Jeanette Jenkins, who did such a fine job in typing the rough draft and most of the final copy, is greatly appreciated. Harry Livesey deserves special mention for the graphic arts work in most of the original drawings.

The author is grateful to the Oak Ridge National Laboratory for the privilege of participating in its educational assistance program. The research was supported by the United States Atomic Energy Commission under contract with the Union Carbide Corporation.

ABSTRACT

A mass spectrometric technique has been developed to measure the quantity of neutral molecules released by electron impact from metallic surfaces covered with adsorbed gases and was used to investigate the electron bombardment induced desorption of carbon monoxide from tungsten. The method is sensitive enough to detect the desorption of about 10^9 molecules during an eight-second bombardment pulse. This sensitivity permits frequent sampling of a surface without significantly perturbing the gas-metal surface; therefore, reactions can be followed as they occur. This technique for studying gas-metal interactions is compatible with other methods including low-energy electron diffraction, flash filament measurements, and the desorption of ions and secondary electrons due to electron bombardment.

It was possible to separate the effects of thermal desorption due to the very small amount of target heating that accompanied the electron bombardment from the effects of electron impact *per se*. The thermal effects were shown to be negligible for the conditions of this study. They were also shown to be pressure dependent so that they would make an important contribution for the desorption of carbon monoxide from the tungsten target at 300°K for 500 electron volt electrons at ambient carbon monoxide pressures greater than 10^{-8} torr.

The desorption of neutral carbon monoxide molecules from a tungsten ribbon with predominantly [100] poles normal to the surface was measured for electron energies in the range from 30 to 8,000 electron volts. Between 3×10^{-6} and 6×10^{-5} molecules were desorbed per incident electron, depending upon the electron energy. The desorption appears to be from the alpha form of chemisorbed carbon monoxide, whose measured population was about 10^{13} molecules per square centimeter. The desorption cross section for neutral carbon monoxide from this alpha state is then calculated to be about 4×10^{-18} square centimeters for electrons having energies of 100 electron volts. The threshold of electron energy necessary to cause desorption is approximately 20 electron volts.

The relationship of the desorption cross section to the electron energy is discussed, and a tentative explanation involving several processes is offered.

CONTENTS

CHAPTER		PAGE
I.	INTRODUCTION	1
	Definition of the Study	1
	Purpose, Need, and Scope of the Study	2
	Purpose	2
	Need	3
	Scope	5
	Organization of the Dissertation	5
II.	REVIEW OF THE LITERATURE	6
	Electron Bombardment Induced Desorption	6
	Experimental results	6
	Theoretical treatments of EBID	27
	Adsorption of Carbon Monoxide on Tungsten	38
III.	EXPERIMENTAL METHOD, APPARATUS, AND TECHNIQUES	42
	Method	42
	Apparatus	43
	Pressure measurement	43
	Vacuum system	45
	Tungsten specimens	58
	Bombardment cell and mode of operation	59
	Target temperature measurement and control	65

CHAPTER PAGE

Technique 68

Measurement of neutral gas produced by EBID 68

Measurement of ions produced by EBID 72

IV. EXPERIMENTAL RESULTS 74

The EBID of Carbon Monoxide as a Function of Electron Energy 74

Thermal and Pressure Effects on the Desorption Signal . . 77

Mass Spectrometer Sensitivity 80

Measurement of the Amount of Carbon Monoxide Adsorbed on the Target 80

V. DISCUSSION OF THE RESULTS 89

The Effect of Electron Energy on the Desorption Cross Section 89

Electron Bombardment Induced Desorption as a Function of Pressure 97

Thermal Desorption as a Function of Pressure 97

Quantity of Gas Adsorbed on the Target at 300° K 99

Measurement Errors 103

VI. CONCLUSIONS AND RECOMMENDATIONS 106

Conclusions 106

Recommendations 108

BIBLIOGRAPHY 113

CHAPTER PAGE

APPENDIX A. EBID of Hydrogen from Tungsten at 300° K 123

APPENDIX B. Thermal Desorption 128

APPENDIX C. Temperature Distribution in the Target During EBID and Ohmic Heating 134

LIST OF TABLES

TABLE		PAGE
I	Summary of Electron Bombardment Induced Desorption Data . . .	25
II	Summary of the Adsorption States for Carbon Monoxide on Tungsten	40
III	Typical Analysis of Gases	55
IV	Full Coverage Values for Carbon Monoxide on Tungsten at 300°K	83
V	Full Coverage Values for Nitrogen and Hydrogen on Tungsten at 300°K	84

LIST OF FIGURES

FIGURE PAGE

1. Experimental Arrangement Used by Moore to Study the Interaction of Electrons with Adsorbed Gases 9

2. Oxygen Ion Current as a Function of Electron Bombardment Current 10

3. Oxygen Ion Current as a Function of the Energy of the Bombarding Electrons 11

4. Schematic Diagram of the Retarding Field Apparatus Used by Redhead to Study the EBID of Ions from Oxygen Chemisorbed on Molybdenum 13

5. Normalized Ionization Probability as a Function of Electron Energy for Oxygen Adsorbed on Molybdenum at 300° K (Solid Curve) and Atomic Oxygen in the Gas Phase (Dashed Curve) 15

6. Ion Energy Distributions for Carbon Monoxide on Tungsten at 300° K and Above. The ion energy distribution for adsorbed oxygen at 300° K is also shown for comparison . . . 16

7. Normalized Ion Current as a Function of Electron Energy, V_e (Electron Volts), for Carbon Monoxide Adsorbed on Tungsten at 300° K 18

FIGURE PAGE

8. Correlation of EBID of Ions from Carbon Monoxide and Hydrogen Adsorbed on Molybdenum with the Thermal Desorption of Hydrogen and Carbon Monoxide as the Temperature of the Molybdenum Target Was Increased 19

9. Hydrogen Ion Signal Due to EBID from Hydrogen Adsorbed on Molybdenum as a Function of Time During a Thermal Excursion to 1000°C in an Ultrahigh Vacuum System at 5×10^{-9} Torr Residual Gas Pressure 20

10. Hydrogen Ion Current from Type 303 Stainless Steel as a Function of Electron Energy Near the Threshold Energy . . . 22

11. Hydrogen Ion Current as a Function of Electron Energy from 400 to 6,000 Electron Volts 23

12. Schematic Representation of the Potential Energy for Several States of an Adsorbed Molecule or Atom 30

13. Schematic Representation of the Possible Consequences of Excitation to the Ionized State 34

14. Schematic Representation of the Possible Consequences of Excitation to the Antibonding State 36

15. Schematic Diagram of the Electrical Systems Associated with the Mass Spectrometer 46

16. Mass Spectrum of the Residual Gases in the Experimental Chamber of the EBID Apparatus 49

17. Schematic Diagram of the Experimental Chamber Showing the Gas Handling for the EBID System 50

FIGURE PAGE

18. Block Diagram of the Complete Vacuum System 52

19. Photograph of the EBID Apparatus 53

20. Photograph of the Vacuum System 54

21. Photomicrograph of the Surface of the Tungsten Target 60

22. Schematic Drawing of the Bombardment Cell 61

23. Photograph of the Bombardment Cell 62

24. Photograph of the Tungsten Target in Its Shielded Mounting . . 63

25. Schematic Diagram of the Electrical Apparatus Associated with Target Heating and the Bombardment Cell 64

26. Electron Bombardment Induced Desorption of Carbon Monoxide from Tungsten as a Function of Electron Energy 75

27. Electron Bombardment Induced Desorption and Thermal Desorption of Carbon Monoxide from Tungsten at 300° K as a Function of the Partial Pressure of Carbon Monoxide in the Experimental Chamber 78

28. Electron Bombardment Induced Desorption Data for Desorption of Carbon Monoxide from Tungsten Taken Using the 0.0025-Centimeter-Thick Target and a Carbon Monoxide Pressure of 5×10^{-8} Torr 79

29. A Typical Calibration Curve for the Mass Spectrometer Output Signal as a Function of the Pressure Indicated on the Chamber Ion Gauge 81

30. Thermal Desorption Spectra 86

FIGURE PAGE

31. Carbon Monoxide Pressure as a Function of Time During (a) Adsorption of the Gas Onto a Clean Tungsten Target and (b) Thermal Desorption of the Gas from the Target . . . 88

32. An Analysis of the EBID Data of Figure 26 92

33. Electron Bombardment Induced Desorption of Hydrogen from Tungsten at 300° K as a Function of Electron Energy 123

34. Electron Bombardment Induced Desorption and Thermal Desorption of Hydrogen from Tungsten at 300° K as a Function of the Partial Pressure of Hydrogen in the Experimental Chamber 125

35. Typical Thermal Desorption Data for Carbon Monoxide from Tungsten. (a) Using Ehrlich's technique. (b) Using Redhead's technique 129

36. Thermal Desorption of Carbon Monoxide from Tungsten Using the Technique of Bell and Gomer. (a) Alpha (and beta) step-desorption spectrum, obtained by heating a full 20° K layer to 600° K for 60 seconds, and then redosing with an excess of carbon monoxide. (b) Step-desorption spectra of full and partial 20° K layers 131

FIGURE PAGE

37. Temperature Distributions in a One-Dimensional Model of the Tungsten Target (I), Ohmic Heating (II), Electron Bombardment Only at the Midpoint of the Target (III), Electron Bombardment of the Center Half of the Target (IV), Electron Bombardment of the Center Third of the Target (V), and Ohmic Heating with 150 Per Cent of the Power Input of Curves I, II, III, and IV 137

LIST OF SYMBOLS

The following symbols will have the indicated meanings unless otherwise specified:

A	Amperes.
AC	Alternating current.
°C	Degrees centigrade.
DC	Direct current.
E	Activation energy for a process (electron volts).
E_0	Energy of the incident electron in an elastic collision (electron volts).
E_a	Heat of adsorption (electron volts).
E_b	Potential energy of an adsorbate ion at infinite separation from the metal surface (electron volts).
E_{th}	Threshold energy for EBID of an ion with no extra kinetic energy (electron volts).
E_T	Maximum energy transferred to a free molecule by an elastic momentum transfer process.
e	Electron in Figure 5 (taken from the literature), otherwise it denotes the charge associated with one electron.
EBID	Electron bombardment induced desorption.
ev	Electron volt.
FEM	Field emission microscope.
−HV	Negative high voltage.

LIST OF SYMBOLS (continued)

+HV	Positive high voltage.
I^+	Current of positive ions.
i^+	Positive ion current (amperes).
i—	Bombarding electron current (amperes).
IG	Ion gauge.
IGC	Experimental chamber ion gauge.
IGM	Gas manifold ion gauge.
IGTSP	Ion gauge which indicates the pressure in the titanium sublimation pump.
°K	Degrees Kelvin.
K	The rate of reaction.
L/S	Liters per second.
l/s	Liters per second.
M	Molecular weight of a molecule.
Ma	Milliampere.
Meg	1,000,000 ohms.
M/e	$\frac{\text{Molecular weight}}{\text{Electronic charge}}$
N	Number of gas molecules striking one square centimeter per second.
NA	Not available.
n	The surface concentration (molecules per square centimeter).
P	Pressure (torr).

LIST OF SYMBOLS (continued)

ΔP	A small change in P.
Q	Influx of gas into the vacuum system (torr liters per second).
ΔQ	A small change in Q (usually the rate of gas desorption due to electron bombardment or thermally pulsing the target) (torr liters per second).
Q_0	Influx of gas from outgassing of the vacuum components (torr liters per second).
Q_s	Rate of reversible adsorption on the vacuum system walls (torr liters per second).
Q_L	Influx of gas from a controlled supply (torr liters per second).
q	The heat flux in arbitrary units.
R	The gas constant $\approx 8.7 \times 10^{-5}$ electron volt per atom °K.
S	Volumetric rate of gas removal (liters per second).
T	Temperature (°K).
ΔT	Small change in T.
T_{av}	Average temperature.
$(\Delta T)_{av}$	Average change in temperature.
T_0	Temperature of the heat sink.
$(\Delta T)_{max}$	Maximum temperature change.
t	Time.
t_c	Adsorption time accumulated.

LIST OF SYMBOLS (continued)

V	Volts.
$\frac{\Delta V}{V_0}$	Ratio of the amount of gas desorbed on a given step in Figure 36(a) to the total desorbable gas.
V_e	Electron accelerating voltage (volts).
V_R	Retarding voltage for ions (volts).
W	Watt.
X	Distance.
Z	Atomic number.
α, α', β_1, β_2, β_3	Designations for different adsorbed states of carbon monoxide on tungsten.
μa	Microampere.
ν_x	Frequency factor usually approximated as 10^{13} per second.
T_s	The cross section for the elastic collision of an electron with an atom (square centimeters).
χ	Separation distance.
χ_0	Equilibrium separation distance of an adsorbate from the metal surface.
Ω	Ohm.
$<$	Less than.

LIST OF SYMBOLS (continued)

$>$	More than.
$\sim$	Approximately.
$\approx$	Approximately equal.

CHAPTER I

INTRODUCTION

Definition of the Study

The desorption of ions and gases from metal surfaces by bombardment with electrons per se has been observed in many circumstances.[1-10*] The quantities of desorbed gases and ions are sometimes very large. Such desorbed gases and ions shorten the life of high-power electron tubes and can be an important factor in the operation of vacuum systems and the use of ion gauges. Though these and other technically important processes are being explored empirically, a better understanding of the processes contributing to the phenomenon would expedite the solution to problems caused by unwanted desorptions and help optimize the desirable applications. As more is learned about electron bombardment induced desorption (EBID), it is becoming an important tool for studying gas-metal surface interactions.

The motivation for this study initially came from a desire to understand EBID and exploit it for vacuum system processing and as a tool for studying the gas-metal surface interactions that are so important to vacuum technology. Because of the complex nature of both the EBID process and the gas-metal interactions, it is desirable during the

---

*Denotes references. See pages 113 through 120.

development of apparatus and techniques to use simple gas-metal combinations that are convenient to manipulate experimentally. Tungsten was chosen because it can be cleaned of surface contaminants, except carbon, by heating in a vacuum to 2200 to 2400°K, and even the carbon may be removed by heating in oxygen at 10^{-6} torr. Initially, both carbon monoxide and hydrogen were investigated because they are common gases in ultrahigh vacuum systems; however, there is much more information in the literature on the carbon monoxide-tungsten system, and the adsorbed hydrogen is more difficult to maintain free of contamination than is the carbon monoxide. Therefore, the study was concentrated on carbon monoxide.

The experimental equipment developed for this study has been designed to study the EBID of neutral gas during electron bombardment; the desorption of ions may also be measured; however, since others were studying the desorption of ions, it was decided to concentrate on neutral particle measurements.

Purpose, Need, and Scope of the Study

Purpose. The two main goals of this study were (1) to develop sensitive techniques for studying the desorption of gases from metallic surfaces by electron bombardment, and (2) to provide information that will be useful in practical applications of EBID and in understanding of the desorption processes.

Need. The three main justifications for studying the desorption of gases by electron bombardment are (1) its potential value as a tool for investigating gas-metal interactions, (2) its immediate value to modern technology, and (3) a scientific interest in the desorption mechanisms.

It should not be necessary to show the great importance of the interactions of solid surfaces with gaseous environments. One need only to be reminded that corrosion and catalysis are surface phenomena. Though knowledge of gas-metal reactions is increasing rapidly, we still lack much of the basic information needed for understanding the processes we use so widely.

In 1964, L. H. Germer said:[11]

> One should reflect upon the enormous importance of catalytic processes, and upon the absence of basic understanding of these processes. It seems to me that getting to understand catalysis will have a greater impact upon the world than will all the solid state devices that can ever be developed.[11]

Surface phenomena are, of course, the heart of the matter.

The surfaces of solids are difficult to study experimentally and are poorly understood because of the number and variety of phenomena involved and the difficulty of measuring and controlling them. No one technique is best for studying surface phenomena; rather, each technique provides a certain kind of information, and it is the combination of a variety of techniques that gives the most complete understanding of surface phenomena. The EBID of gases and ions may be used with thermal desorption methods and mass spectrometry to provide a very useful

combination. Thermal desorption measures activation energies for desorption, the abundance of the adsorbed species, and helps identify phases; mass spectrometry identifies the kind and amount of the desorbing species; and EBID provides both a sensitive measure of the abundance of certain adsorbed species and information about the bonding to the surface. Since electron bombardment can be accomplished with low-intensity, narrow electron beams, it can be used as a probe to follow surface changes as they occur without interfering significantly with the phenomena as would be necessary with the thermal desorption technique.

The second justification for studying EBID is the importance of this phenomenon to modern technology. Perhaps the most obvious application is "cleaning up" vacuum systems. The use of EBID with thermal desorption has been reported to lower the base pressure of vacuum systems by as much as a factor of 100 (references 12 and 13). The EBID can also be used to monitor the "cleanup" of gases by thermal or other techniques or to monitor the contamination of vacuum with hydrocarbons. It may also be useful in inducing chemical changes and in certain cases for producing clean surfaces without heat or radiation damage.

The third justification is scientific curiosity. None of the published explanations for EBID fit all of the observations. It seems likely that several mechanisms are important and that some or all of them are directly related to the nature of the bond between the substrate and the adsorbate. If this is so, it should be possible to get new information about bonding from EBID data.

Scope. This work was limited to developing a technique for studying EBID of gases and ions from metal surfaces and a study of the desorption of carbon monoxide from tungsten for the reasons mentioned earlier. However, Appendix A, page 123, contains some data for the EBID of hydrogen from tungsten. A few ion measurements were made in this study and were in good qualitative agreement with published data. They are not reported here, however, since the experimental effort concentrated on obtaining neutral particle data.

Organization of the Dissertation

The following chapters (1) develop the historical and theoretical background for the study of EBID to provide a basis for the discussion of the experimental results; (2) summarize the state-of-the-art knowledge about the adsorption of carbon monoxide on tungsten; (3) describe the experimental method, apparatus, and techniques used in this study; (4) present the experimental data; and (5) discuss the experimental results in relation to the information in the literature and the relevant desorption mechanisms.

CHAPTER II

REVIEW OF THE LITERATURE

This chapter provides an historical introduction to EBID, summarizes subsequent developments up to the present, and reviews the desorption and adsorption mechanisms described in the literature. The literature review is not intended to be complete but rather to recount some of the most important developments and provide background for the present study.

Electron Bombardment Induced Desorption

Experimental results. The first account of desorption from surfaces due to electron bombardment is apparently reported by A. J. Dempster[14] in 1918. He was searching for sources of "positive rays" to be used with his "New Method of Positive Ray Analysis," which was an early version of the magnetic mass spectrometer.

> It was thought that the bombardment of salts by electrons might break up the chemical compounds and give rise to many positive ions. . . . Although the aluminum phosphate was chemically pure, the rays obtained under the bombardment of 128 volt electrons were very complex; the following ions were observed besides a couple of unresolved groups: H_1, H_2, Li (weak), O_1 (strong), Na (strong), O_3 (?) (weak), M = 62 (weak, possibly Na_2O), M = 67 (strong, possibly H_3PO_2 = 66), M = 76 (strong), M = 86 (weak, possibly Rb = 85.5), M = 112 (strong, possibly P_2O_3 = 110). . . . From the bombardment of aluminum phosphate to which a little lithium chloride and sodium chloride had been added strong bundles of

> hydrogen atoms and hydrogen molecules were obtained. . . . The experiments indicated the convenience of the method of obtaining positive rays and opened up an interesting field for investigation.[14]

In spite of this promising start and the subsequent rapid development of the mass spectrometer there is nothing more in the open literature until about 1950 regarding the use of electron bombardment of surfaces to produce ions or neutral particles.

In the period 1950 to 1959 several investigators examined the use of electron bombardment to decompose compounds and to sputter oxides and metals (Dart,[15] Plumlee and Smith,[16] Moore and Hughes,[17] Moore,[18] and Wargo and Shepard[19]). These investigations established that (1) electron bombardment could decompose compounds, but that the threshold energy for decomposition is not directly related to the heat of formation of the compound and that the decompositions are not all proportional to the electron current; (2) electron bombardment was not effective in causing sputtering of oxides or metals; (3) electron bombardment removed adsorbed gases as both ions and molecules; and (4) electron bombardment produced some O^+ ions with kinetic energies of several electron volts.

In 1960 Young[20] reported desorption efficiences of about 10^{-5} O^+ ions per incident 90 electron volt electron from oxidized metal surfaces; Todd, Lineweaver, and Kerr[3] reported efficiences of up to 7×10^{-2} oxygen molecules per electron from glass, and Moore[1] reported the results from the first experiment specifically designed to study EBID of gases from a well-characterized metal surface. He used a molybdenum ribbon target mounted in front of a mass spectrometer ion source so

that desorbed ions could be measured directly by the mass spectrometer. In 1961 Moore gave a comprehensive report of his findings on the interaction of electrons having energies up to 325 electron volts with carbon monoxide adsorbed on polycrystalline molybdenum and tungsten.[21] Figure 1 shows schematically his experimental arrangement. Figure 2 shows that the desorption efficiency for O^+ ions does not change even though the bombarding current was varied five orders of magnitude. This is good evidence that the desorption process is a first order process, that is, it requires only one electron. No C^+ or CO^+ ions were detected. The yield of O^+ ions per electron is plotted as a function of electron energy in Figure 3. Curves A and D are supposedly for only carbon monoxide on the target, and the maxima are 2 and 6×10^{-6} ions per electron when corrected for the probability that a liberated ion will pass through the spectrometer. Moore used oxygen in his system, so his target may have been contaminated with oxygen thus giving O^+ desorptions higher than for a pure carbon monoxide adsorption. He attributed the observed desorption to the beta state of carbon monoxide since his measurements were at 950°K or higher. The threshold electron energy was between 17.0 and 18.3 electron volts which is 6 volts lower than the energy required to produce O^+ from carbon monoxide in the gas phase.

In 1962 Degras, Pétermann, and Schram[22] gave the first of a series of papers built around the measurement of EBID of neutral gas molecules from nickel surfaces using an omegatron mass spectrometer. This paper proposed using EBID with 10 to 150 electron volt electrons

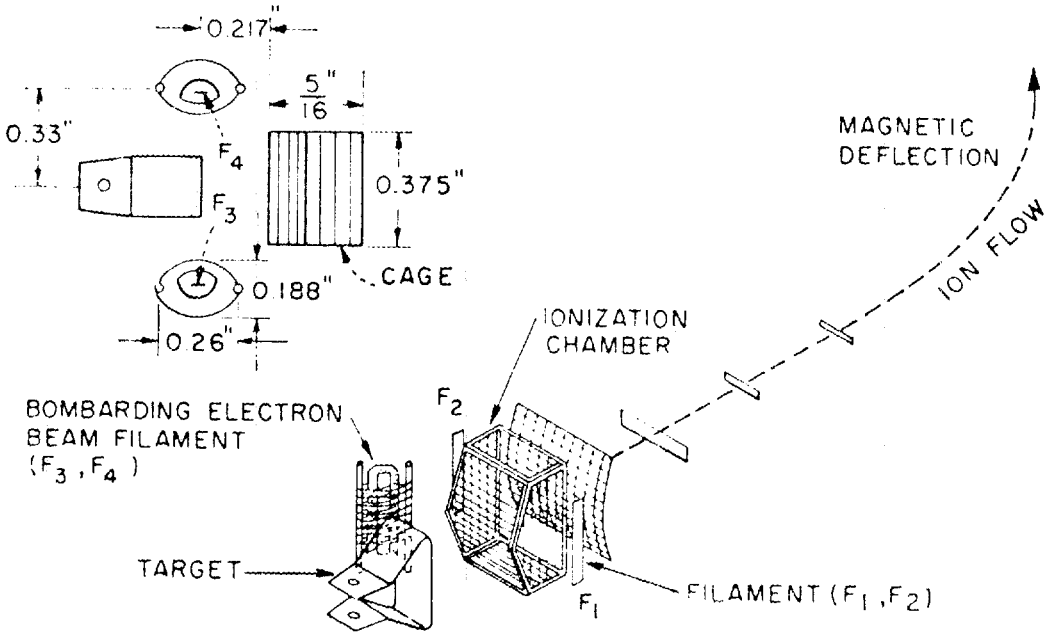

Figure 1. Experimental arrangement used by Moore to study the interaction of electrons with adsorbed gases. (Reprinted from G. E. Moore, "Dissociation of Adsorbed CO by Slow Electrons," Journal of Applied Physics, 32:1241, 1961.)

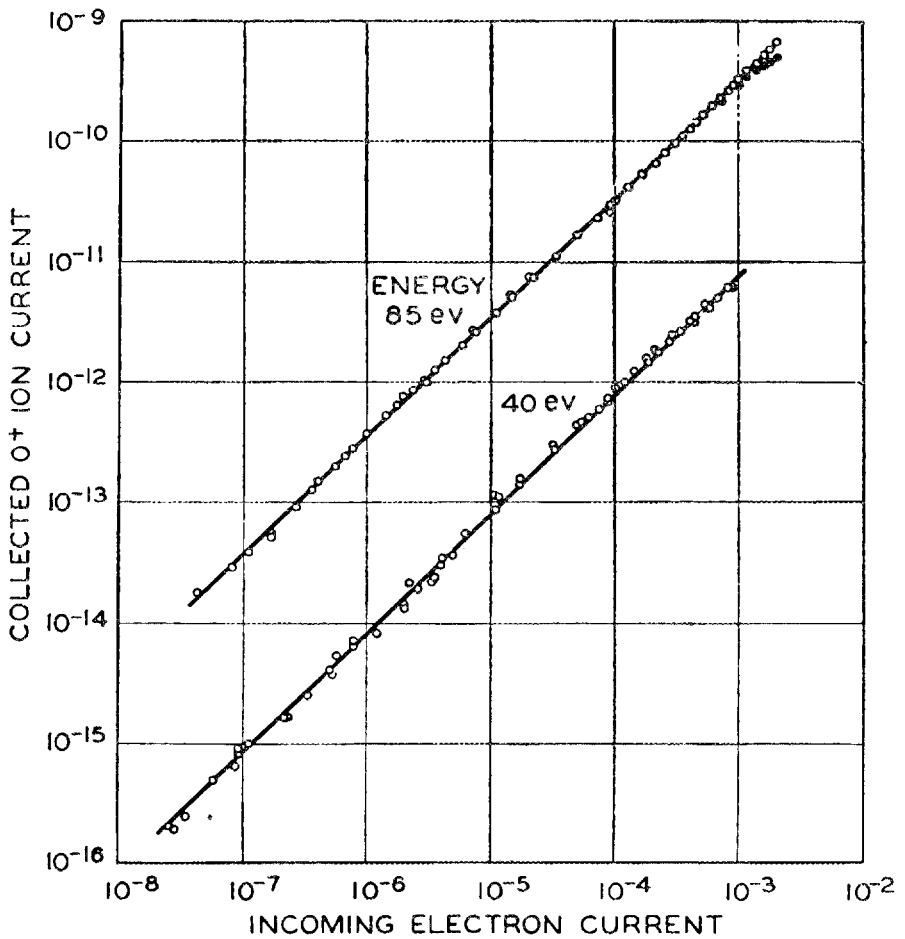

Figure 2. Oxygen ion current as a function of electron bombardment current. (Reprinted from G. E. Moore, "Dissociation of Adsorbed CO by Slow Electrons," Journal of Applied Physics, 32:1245, 1961).

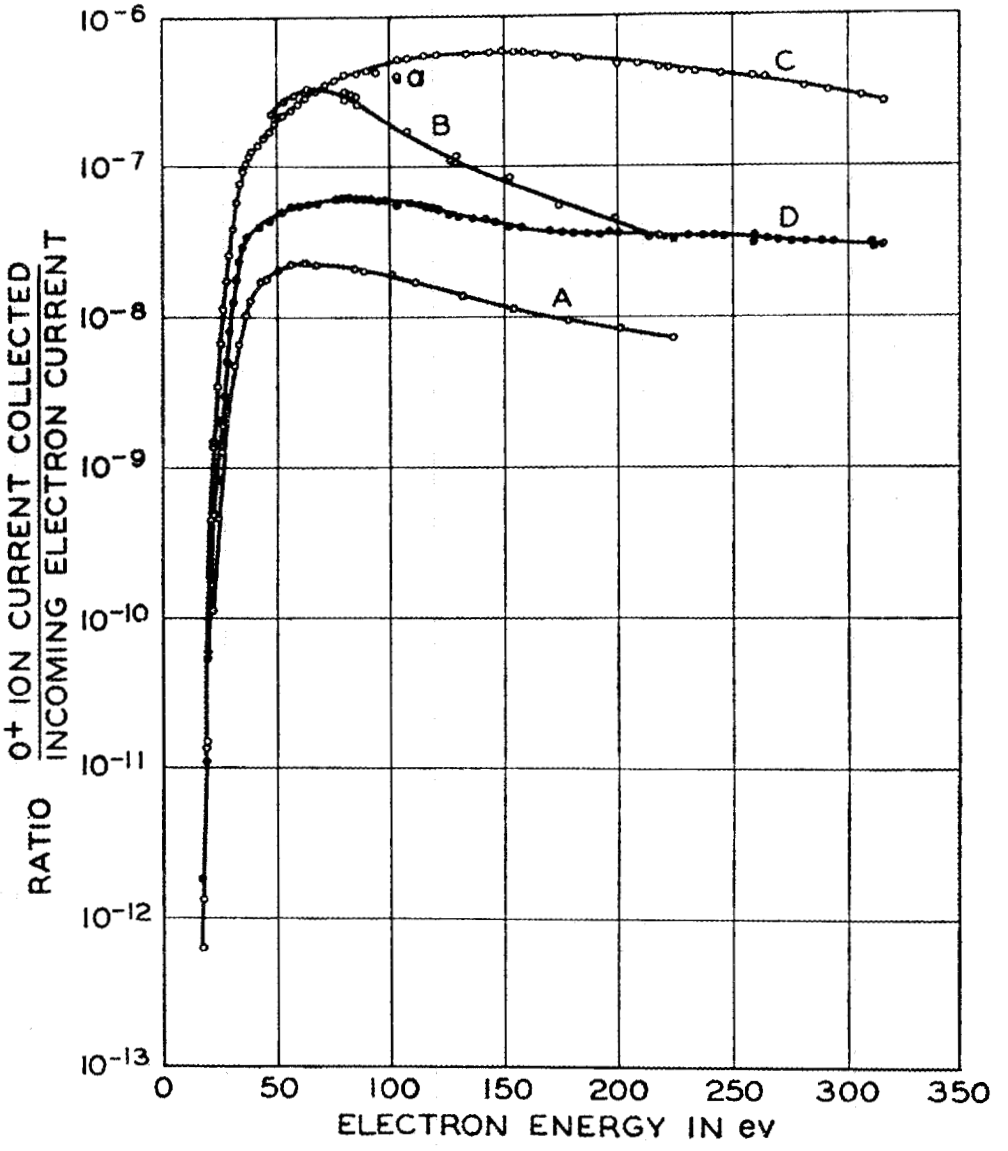

Figure 3. Oxygen ion current as a function of the energy of the bombarding electrons. (Curve A: oxygen was less than 10^{-3} as abundant as carbon monoxide. Curve B: oxygen was 0.14 as abundant as carbon monoxide. Curve C: oxygen was about 0.90 as abundant as carbon monoxide. Curve D: oxygen valve closed. Oxygen was 1.6×10^{-3} as abundant as carbon monoxide in ambient.) (Reprinted from G. E. Moore, "Dissociation of Adsorbed CO by Slow Electrons," Journal of Applied Physics, 32:1246, 1961.)

to remove gas strictly from surfaces, thus making possible a differentiation between surface and bulk gas sources. They also proposed to determine sticking probabilities but gave no results on either proposal. Later papers[8,23] report a yield of 1.9×10^{-2} gas molecules per incident electron from a nickel surface that was covered with carbon monoxide. This yield was independent of current (2–20 microamperes per square centimeter) and electron energy (100–300 electron volts). The yield of carbon monoxide from a nickel oxide surface was 8×10^{-8} molecules per electron and was proportional to the beam power. Another paper gives some data that indicates that on an unbaked nickel specimen the surface is covered with carbon monoxide and hydrogen quite rapidly by diffusion from the bulk, and that bulk diffusion is still an important contributor to the adsorbed surface gases after the sample has been baked at 400°C for 35 hours.[24]

In 1962 and 1963 a large number of papers appeared that recognized that both ion gauges and mass spectrometers may produce large spurious signals due to the EBID of ions and/or nuetral molecules from grids or other surfaces.[4,25-31] In an effort to understand the relatively large effect of adsorbed oxygen on measurements with ion gauges, Redhead studied the EBID of ions from oxygen absorbed on a polycrystalline molybdenum ribbon.[4,32] He used the retarding field arrangement shown schematically in Figure 4. The tungsten filament is the source of electrons, and the anode is the electron target. This arrangement and a later improvement, that uses a hemispherical geometry for the grids and collector,[33] permits accurate

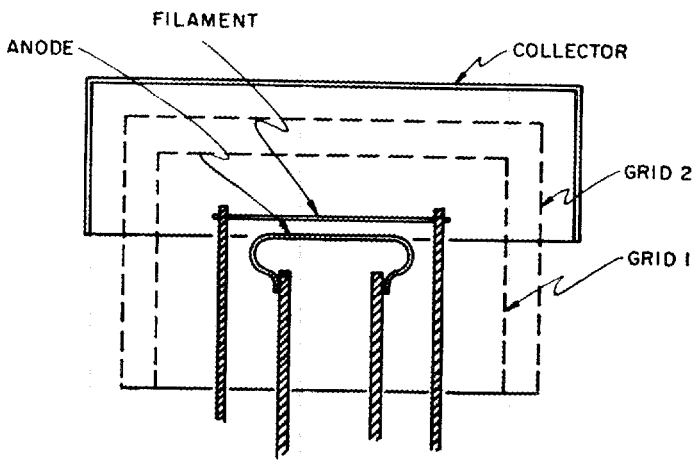

Figure 4. Schematic diagram of the retarding field apparatus used by Redhead to study the EBID of ions from oxygen chemisorbed on molybdenum. (Reprinted from P. A. Redhead, "Interaction of Slow Electrons with Chemisorbed Oxygen," Canadian Journal of Physics, 42:887, 1964.)

measurements of the total ion production due to EBID. By using suitable electrical potentials on the various elements of the apparatus an energy analysis of the ions also may be obtained. This method does not, however, identify the ion species. The anode can be heated so that thermal cleaning and thermal desorption measurements are practical. A series of experiments has been reported by Redhead in which he used this technique to determine the threshold energy for desorption, the ion energy distributions, and the EBID yields of ions (and indirectly neutral molecules) from both molybdenum and tungsten polycrystalline targets covered with adsorbed oxygen or carbon monoxide. The threshold for desorption of oxygen from molybdenum was reported to be 17.6 ± 0.2 electron volts;[4,32] the threshold for desorption of ions from carbon monoxide on molybdenum was found to be 15.5 electron volts.[5] Using this value, he estimated the heat of desorption of carbon from tungsten to be 9 electron volts. The threshold for ion desorption from carbon monoxide on tungsten was found to have two branches with values of 15.1 electron volts and 18.7 electron volts which he associated with two adsorbed states of carbon monoxide on tungsten.[33] Figure 5 shows the yield of ions from oxygen adsorbed on molybdenum as a function of electron energy and compares this result with the ionization probability for atomic oxygen. Redhead uses this obvious similarity as support for his model of the desorption process, which is discussed in the next section. Figure 6 shows the energy distribution of the ions produced from carbon monoxide and oxygen adsorbed on tungsten. It is suggested that the peak that occurs at a retarding voltage, V_R, ≈ 1.5 volts is

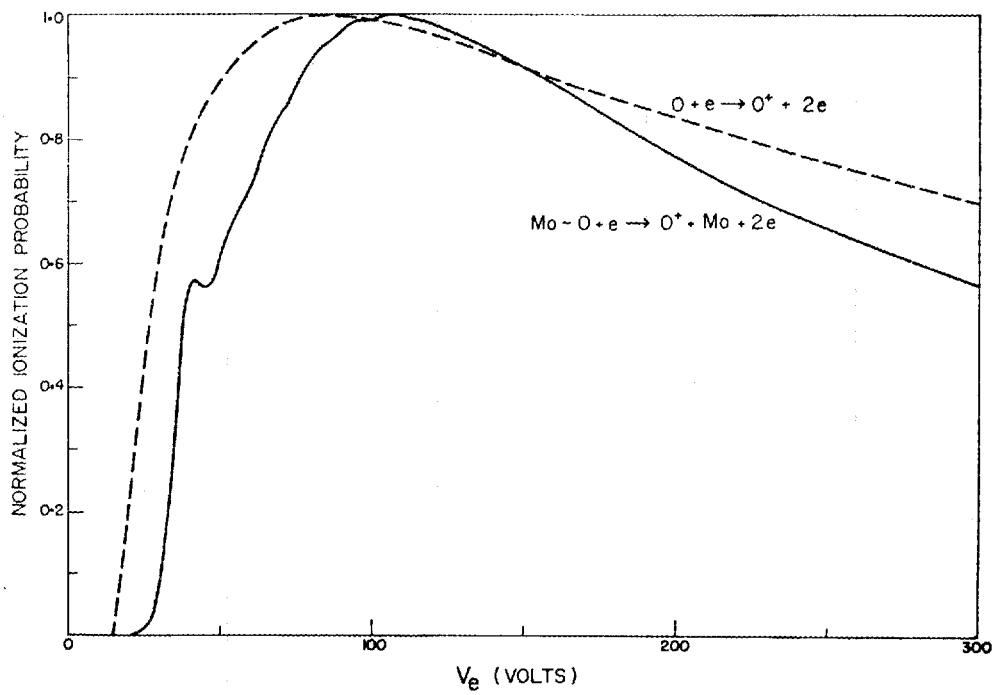

Figure 5. Normalized ionization probability as a function of electron energy for oxygen adsorbed on molybdenum at 300° K (solid curve) and atomic oxygen in the gas phase (dashed curve). (Reprinted from P. A. Redhead, "Interaction of Slow Electrons with Chemisorbed Oxygen," Canadian Journal of Physics, 42:891, 1964.)

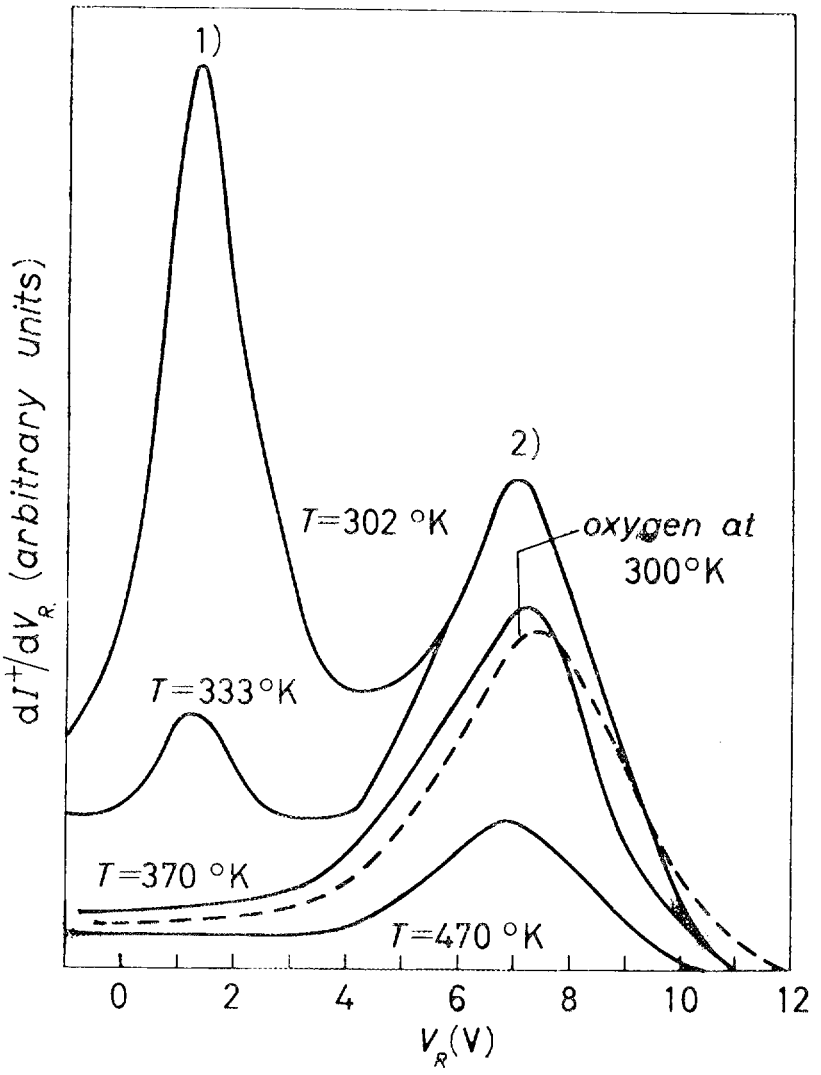

Figure 6. Ion energy distributions for carbon monoxide on tungsten at 300° K and above. The ion energy distribution for adsorbed oxygen at 300° K is also shown for comparison. [Electron energy equals 100 volts, pressure equals 8×10^{-8} torr. Reprinted from P. A. Redhead, "Electron-Impact Desorption of Carbon Monoxide from Tungsten," Supplemento al Nuovo Cimento, 5(2):589, 1967.]

due to desorption of CO^+ from the "virgin" state of carbon monoxide on tungsten and that the peak at $V_R = 7$ volts is due to O^+ ions from the alpha state of carbon monoxide on tungsten. Figure 7 shows the variation of ion current with energy for the two states of carbon monoxide on tungsten. Note that the ion current does not fall at higher energies in contrast to the behavior of the curve for oxygen on molybdenum shown in Figure 5, page 15. This represents a departure from the behavior predicted by both his desorption mechanism and the one proposed by Menzel and Gomer.[34]

In 1963 Lichtman[6,35] began a series of experiments using equipment basically similar to that of Moore except that he used an electron beam to bombard the target surface instead of an unfocused electron emitter and an electron multiplier to increase the sensitivity of his mass spectrometer. (The increased sensitivity permits the use of very small electron currents and therefore negligible perturbation of the surface by the electron bombardment.) Figure 8 shows the correlation of EBID of ions from carbon monoxide and hydrogen adsorbed on molybdenum with the thermal desorption of hydrogen and carbon monoxide as the temperature of the target was increased. Note that he is able to relate the decrease in the H^+ signal to the desorption of hydrogen at about 800°C and that the decrease in the O^+ signal occurs at about the same temperature as the carbon monoxide desorption at 1150°C. The desorption temperatures for both hydrogen and carbon monoxide are higher than those usually observed, but this may be due to measuring the temperature in the center of the target where it was hottest. Figures 8 and 9 illustrate

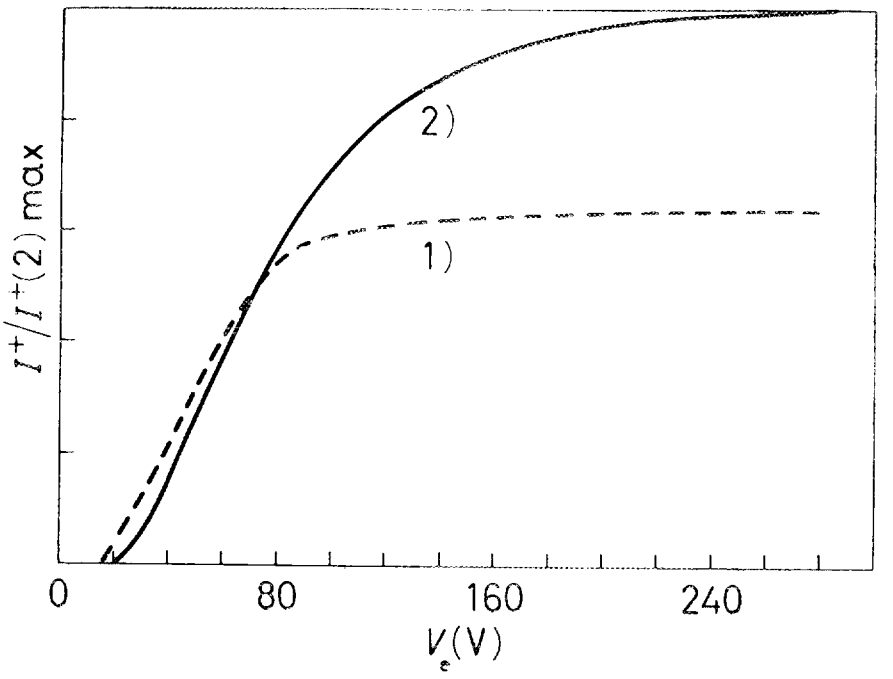

Figure 7. Normalized ion current as a function of electron energy, V_e (electron volts), for carbon monoxide adsorbed on tungsten at 300° K. [The solid curve is for state (1) and the dashed curve is for state (2) tentatively identified as virgin and alpha states, respectively, by Redhead.] [Reprinted from P. A. Redhead, "Electron-Impact Desorption of Carbon Monoxide from Tungsten," Supplemento al Nuovo Cimento, 5(2): 592, 1967.]

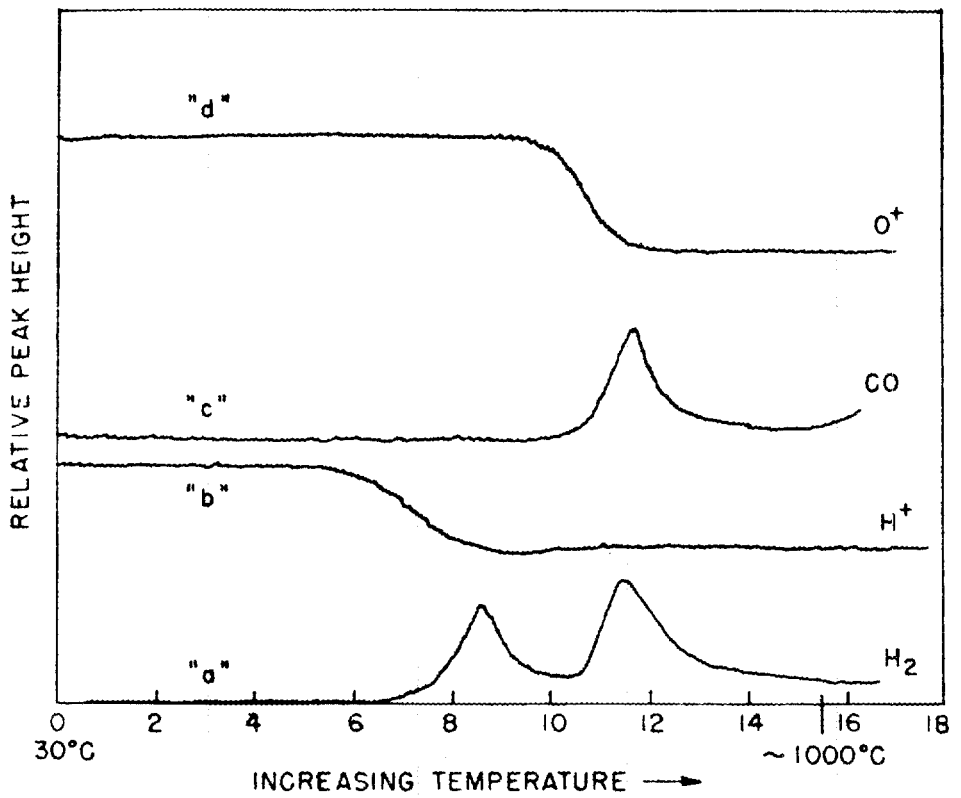

Figure 8. Correlation of EBID of ions from carbon monoxide and hydrogen adsorbed on molybdenum with the thermal desorption of hydrogen and carbon monoxide as the temperature of the molybdenum target was increased. (Reprinted from David Lichtman, "Adsorption-Desorption of Residual Gases in High Vacuum," The Journal of Vacuum Science and Technology, 2:73, 1965.)

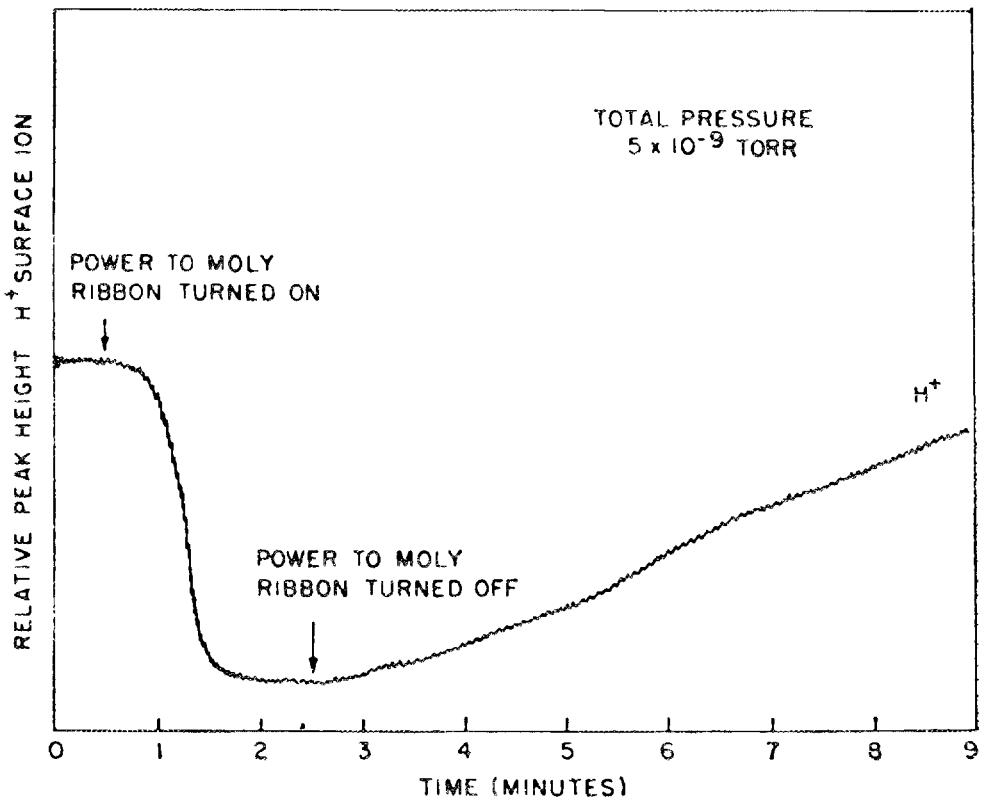

Figure 9. Hydrogen ion signal due to EBID from hydrogen adsorbed on molybdenum as a function of time during a thermal excursion to 1000°C in an ultrahigh vacuum system at 5×10^{-9} torr residual gas pressure. (Reprinted from David Lichtman, "Adsorption-Desorption of Residual Gases in High Vacuum," The Journal of Vacuum Science and Technology, 2:73, 1965.)

the very useful ability of EBID techniques to follow without affecting adsorption-desorption reactions as they occur. Figure 9 shows the desorption and readsorption of hydrogen on a molybdenum target in an ultrahigh vacuum system. Figure 10 shows the energy dependence of the H^+ desorption from type 303 stainless steel near the threshold energy. The shape of this curve is like that predicted by the theory to be discussed in the next section; however, Figure 11 shows data obtained at higher electron energies, which does not behave as the basic theory would predict. Data for EBID of Na^+ and Cl^+ do exhibit behavior that is consistent with the theory in that they have well-defined thresholds in the 10 to 20 electron-volt range, and the ion current rises steeply to a maximum and then decreases as the ion energy increases.[36] Lichtman has used his apparatus to explore a variety of problem areas and has shown the technique to be very useful.[6,36-41] His results for the EBID of O^+ from carbon monoxide on molybdenum[41] differ substantially from those of Redhead. His threshold values are 20 electron volts for both the alpha and beta phases of carbon monoxide, and his ion yields are approximately 30 times those of Redhead. It is not evident why a discrepancy of this magnitude in the results should exist. It would seem to be outside the range of experimental error.

In 1964 Menzel and Gomer published the results of a study of EBID using the field emission microscope (FEM).[9,34,42] They obtained results for hydrogen, oxygen, carbon monoxide, and barium on a tungsten emitter tip. The results for carbon monoxide are in fair quantitative

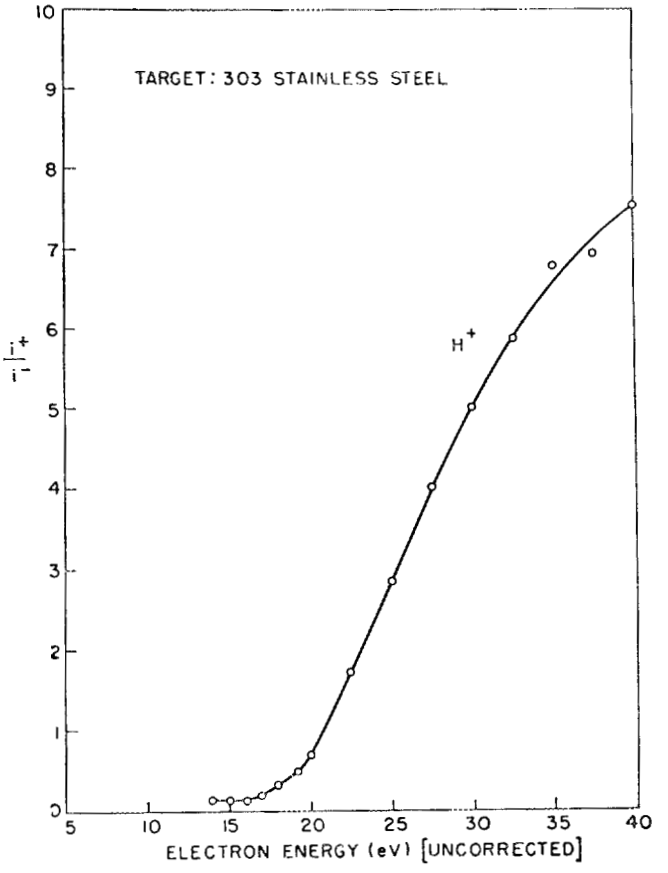

Figure 10. Hydrogen ion current from type 303 stainless steel as a function of electron energy near the threshold energy. [The ratios on the ordinate are relative, not absolute. Reprinted from David Lichtman and R. B. McQuistan, "Slow Electron Interaction with Adsorbed Gases," Progress in Nuclear Energy Series IX. Analytical Chemistry (Vol. 4, New York: Pergamon, 1965), p. 117.]

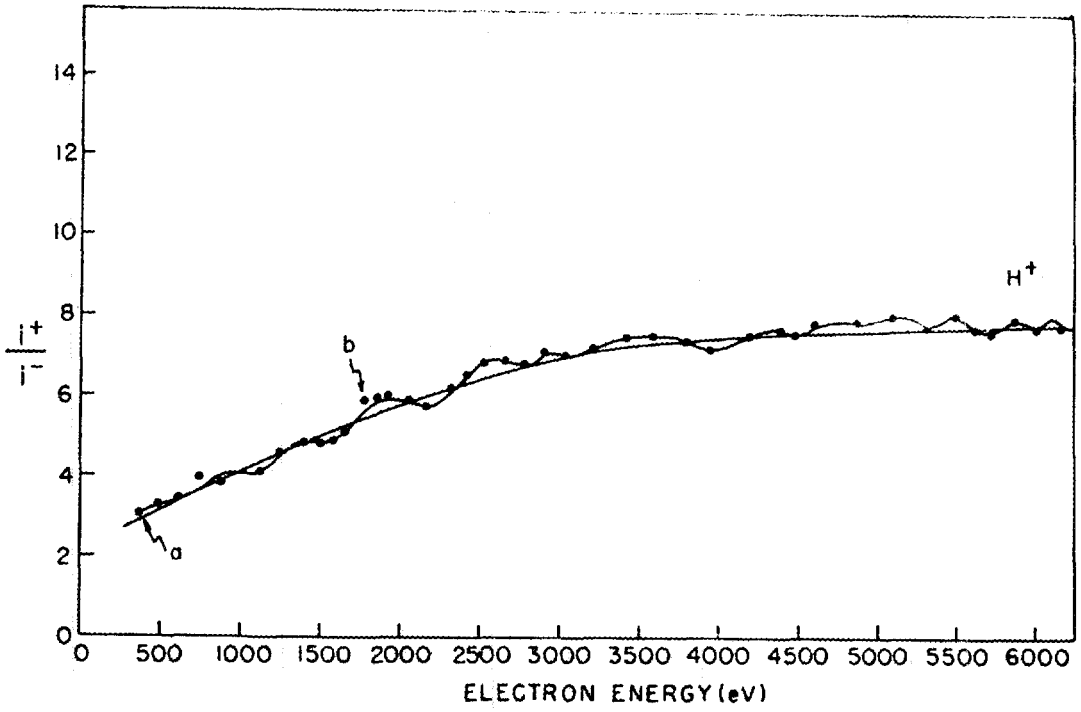

Figure 11. Hydrogen ion current as a function of electron energy from 400 to 6,000 electron volts. [The ratios on the ordinate are relative, not absolute. Reprinted from David Lichtman and R. B. McQuistan, "Slow Electron Interaction with Adsorbed Gases," Progress in Nuclear Energy Series IX. Analytical Chemistry (Vol. 4, New York: Pergamon, 1965), p. 113.]

agreement with those of Redhead. They independently developed a theory of EBID that is almost the same as that proposed by Redhead; both are discussed in the next section.

Recently other investigators have adopted and modified the techniques of Redhead, Lichtman, Gomer, and Menzel. Table I is a compilation of the results of some of these studies.

Yates, Madey, and Payn[43] have equipment very similar to Redhead's and report results for the EBID of ions from carbon monoxide, nitric oxide, and oxygen on polycrystalline tungsten that are consistent with Redhead's results. Sandstrom, Leck, and Donaldson[47] have an apparatus which is similar to Redhead's except that a quadrapole mass analyzer is used in place of the collector. They have reported only qualitative results which seem to be in reasonable agreement with Redhead's results. Coburn[44] has reported data from a similar modification of Redhead's technique except that he uses an electron beam to bombard the target so that his technique also has a resemblance to Lichtman's. Coburn's results are qualitatively similar to Redhead's but differ appreciably in absolute values.

Several other methods of obtaining EBID data have been used,[2,48-51] and this study and the qualitative results are reported in Table I.

A number of EBID investigations have been of an applied or engineering nature.[7,10,13,15,52-59] These studies utilize a wide variety of techniques on a variety of materials, but in general they share the following features:

TABLE I

SUMMARY OF ELECTRON BOMBARDMENT INDUCED DESORPTION DATA

Yield of Neutrals Per Electron[a]	Yield of Ions Per Electron	Technique	Author	Reference	Date
		CO on Tungsten			
β 10^{-5}		b	Menzel and Gomer	34	1964
α 3×10^{-4}		b	Menzel and Gomer	34	1964
α 10^{-4}	2×10^{-7}	c	Yates *et al.*	43	1967
α 3×10^{-4}	1.5×10^{-6}	c	Redhead	33	1967
β $\sim 3 \times 10^{-3}$	2×10^{-7}	d	Coburn	44	1968
α 3×10^{-5}		e	Clausing	This Study	1968
		CO on Molybdenum			
	4×10^{-6}	d	Moore	21	1961
2×10^{-3}	3×10^{-7}	c	Redhead	5	1964
1.6×10^{-3}	6×10^{-6}	c	Degras and Lecante	45 46	1965 1966
	1.2×10^{-4}	d	Lichtman *et al.*	41	1966
9×10^{-6}		b	Singata *et al.*	51	1966
2×10^{-5}	1×10^{-5}	f	Singleton	48	1967
5×10^{-3}	3.2×10^{-6}	c	Degras and Lecante	49	1967
		Oxygen on Molybdenum			
	7×10^{-5}	d	Moore	21	1961
7×10^{-4}	1.3×10^{-5}	c	Redhead	32 4	1963 1964
	4×10^{-4}	d	Lichtman and Kirst	39	1966
		Oxygen on Tungsten			
3×10^{-4}		b	Menzel and Gomer	34	1964
3×10^{-4}		c	Yates *et al.*	43	1967
		Hydrogen on Tungsten			
10^{-5}		b	Menzel and Gomer	34	1964
1.3×10^{-5}		d	Clausing	This Study	1968

TABLE I (Continued)

Yield of Neutrals Per Electron[a]	Yield of Ions Per Electron	Technique	Author	Reference	Date
		CO on Nickel			
2×10^{-2}		e	Petermann	8	1963
2×10^{-2}		g	Theodorou and Love	50	1967
		H_2O on Nickel			
3×10^{-3}		e	Klopfer	52	1967

[a]Calculated from data in the listed reference.

[b]Field emmission microscope.

[c]Measurement of ion current from the surface.

[d]Mass spectrometer measurements of surface ions.

[e]Mass spectrometer measurements of neutral molecules.

[f]Current from ion gauge grid.

[g]Chemical reaction of released CO with an alkali metal covered photo cathode.

1. The partial or total system pressures were used to measure the effects of EBID.
2. The yields are usually higher than those of Table I. They typically range from 10 or more neutral gas molecules released per incident electron down to 10^{-4} molecules per electron, but some results after extensive bombardment were as low as a few times 10^{-6} molecules per electron.
3. The yields decreased as bombardment time accumulated.
4. The results do not fit neatly into the theory discussed in the next section because large yields are found at high energies and thresholds are as low as a few electron volts. The desorbed gases were usually hydrogen and carbon monoxide with hydrocarbon fragments in some systems.

Theoretical treatments of EBID. Although there are several possible mechanisms for electrons to interact with adsorbed gases, only two mechanisms have been discussed in any detail. These mechanisms provide qualitative explanations for most of the experimental data from simple systems although neither can make quantitative predictions of gas release rates.

In 1964 both P. A. Redhead[32] and Menzel and Gomer[9,34] offered theoretical treatments of their data on the desorption of gases from molybdenum and tungsten surfaces. The treatments are very similar; Menzel and Gomer consider a slightly broader range of interactions. Both theories are based on the assumption that the desorption is the

result of an electronic excitation of the adbond* by the incoming electron and that this primary excitation is similar to the electronic excitation of atoms or molecules in the gas phase. Both theories assume that the cross sections for the excitation of the adbond are approximately the same as for gas phase phenomena. The experimental desorption cross sections are much smaller than the primary excitation cross sections. This, they hypothesize, is because of the high probability of a transition back to the ground state through an interaction with electrons from the metal. Thus, the essential features of this mechanism are: (1) an electronic excitation of the adbond and (2) either the desorption of the adsorbate or, more likely, the de-excitation and recapture of the adsorbate by electron tunneling into the broken bond. The recapture process is in most cases quite efficient so that typically only 1 in 10^4 excited adsorbate atoms or molecules escapes. The escape probability varies widely, however, from nearly unity to less than 10^{-6} depending upon the particular gas-metal combination and the particular surface state of the adsorbate. According to Menzel and Gomer,[34] if bonding occurs via "nonlocalized electrons," for example as in metallic bonding, it is almost impossible for electronic excitation processes to cause desorption, because electrons from the metal reestablish the bonds so rapidly. They predict virtually no desorption for electropositive adsorbates from metals and maximum desorption for electronegative adsorbates from insulators.

---

*The term adbond is used to designate the bond between the adsorbate and the metal.

Figure 12 is a schematic diagram showing the potential energy for the interaction of an adsorbate with a metal surface as a function of the distance between the adsorbate and the surface. The diagram is similar to that for the various states of the hydrogen molecule.[60] The zero of potential energy is arbitrarily chosen to represent the energy when the electrically neutral adsorbate is removed to infinity and is free of any interaction with the surface. The curve for the first ionized state shows a potential energy of E_b for the ion at infinity. Redhead uses an E_b equal to the energy required to produce ionization of the adsorbate if it were in the gas phase. The interaction of the ion with the surface can be considered as the sum of the following forces: (1) the electrical image force, (2) the repulsive force due to the overlap or interpenetration of the electron clouds, (3) the van der Waal's attractive force, and (4) an exchange force like those which make possible covalent bonds. As the ion is positioned closer to the metal surface, the long-range attractive coulomb image forces together with the intermediate range exchange force and the small van der Waal's force form a potential well and the ion can reduce its potential energy by moving closer to the surface until the short-range repulsive force arises. This force increases rapidly as the electron clouds of the adsorbate and metal overlap and electrons are forced into higher energy levels due to the Pauli exclusion principle. A minimum exists therefore in the potential energy curve and determines the equilibrium distance of the ion from the surface. The ionized state shown here is metastable and will decay into the ground state if sufficient time is allowed.

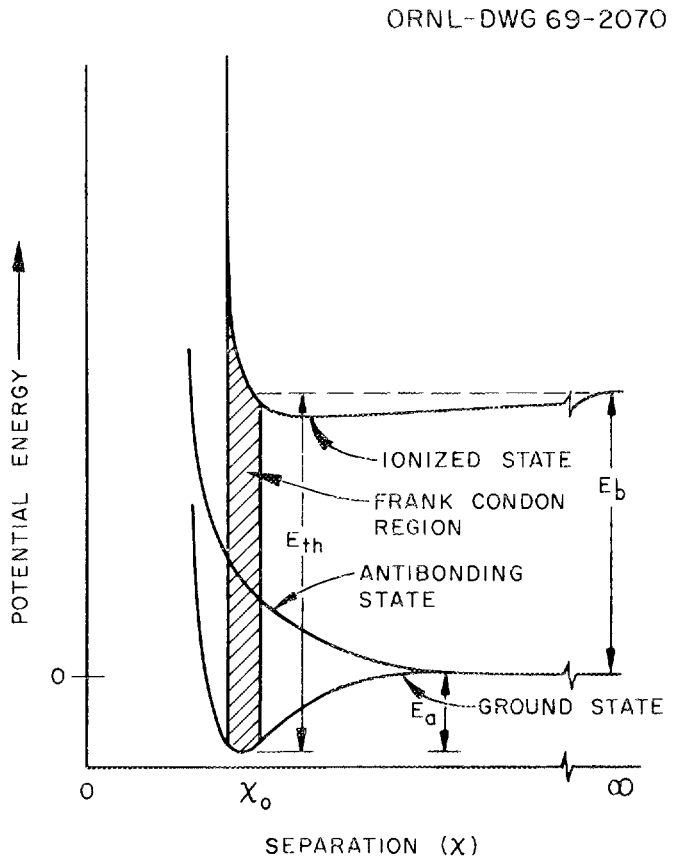

Figure 12. Schematic representation of the potential energy for several states of an adsorbed molecule or atom.

In the case of the ground state curve for the neutral adsorbate the image force does not exist unless the adsorbate is polarized and then only at close separations. The basic attractive forces in the case of chemisorption are due to the tendency for the adsorbate to form an ionic, covalent, or metallic bond at the metal surface. These forces have a much shorter range than the attractive coulomb image force acting on an ion. The repulsive forces are similar to those acting in the case of the ion and again a minimum exists in the potential energy curve which determines the equilibrium separation, χ_o, of the chemisorbed adsorbate and the surface. The depth of the potential well at the lowest energy level is E_a, the heat of adsorption; this is the same as the activation energy for desorption in this case.

The threshold energy E_{th} for the desorption of an ion with no kinetic energy is given by

$$E_{th} = E_a + E_b \ . \tag{1}$$

Thus, if the heat of adsorption and the ionization energy are known, one can calculate what the threshold energy for desorption of an ion with zero kinetic energy should be.

A significant quantitative difference between the treatment of Menzel and Gomer and that of Redhead concerns the fate of the electron released from the adbond by the electron impact. Redhead uses E_b as the normal gas-phase ionization potential which implies that the electron is a free electron. Menzel and Gomer require the electron to be raised only to the Fermi level of the metal; thus, their E_b is given by subtracting the energy required to overcome the work function of the

metal from the gas-phase ionization energy. The result of this difference is that Menzel and Gomer's E_{th} is lower than Redhead's by the energy required to remove an electron from the Fermi level to infinity.

The antibonding state may be considered as a state with an antisymmetrical wave function for the binding electrons or as a state in which the binding electrons have parallel spins. It is any quantum state that creates net repulsive forces between the adsorbate and the substrate. If the adsorbate is placed into this state it will either be repelled from the surface or an eletronic transition will occur which will drop the adsorbate to the ground state.

Because of the Frank-Condon principle, only vertical transitions occur with appreciable probability. Hence, transitions from the lowest vibrational state will occur to excited levels only within the shaded area above the ground state. The electronic states will change, but neither the position nor the kinetic energy of the adsorbate will change during the transition. Only adiabatic transitions from the ionic curve or a repulsive state to the ground state are allowed. A suitable energy level must also exist in the ground state. (Adiabatic here means no interchange of nuclear and electronic energy and no change of total system energy.) The energy given up in a downward transition is electronic in origin and is radiated or given to the electrons in the metal. It is now possible to trace the course of events that may occur when an electron interacts with the adsorbate via an electronic excitation.

If the electron impact causes an upward transition from the ground state to the ionized curve one of several things may occur as shown in Figure 13 by the numbered curves:

1. An immediate transition back to the ground state may occur with the electronic energy being dissipated by interactions with the electrons of the metal or the emission of radiation.
2. The ionized adsorbate may escape as an ion if (a) it has received energy equal to or greater than E_{th} and (b) it is not neutralized as it moves away from the surface by exchanging its potential energy for kinetic energy.
3. A transition back to the ground state may occur after the ion has started to move away from the surface, in which case the ion will have converted some of its potential energy into kinetic energy. This kinetic energy may be enough to allow the adsorbate particle to escape as a neutral particle, shown by Curve 3a in Figure 13, but if it is not the adsorbate will remain bound to the surface and its kinetic energy will merely put it into a higher vibrational state, shown by Curve 3b in Figure 13. The adsorbate will subsequently give up this additional energy by radiation or by interaction with the metal lattice.
4. The ionized adsorbate might undergo an electronic transition to the repulsive state and be desorbed as a neutral particle.

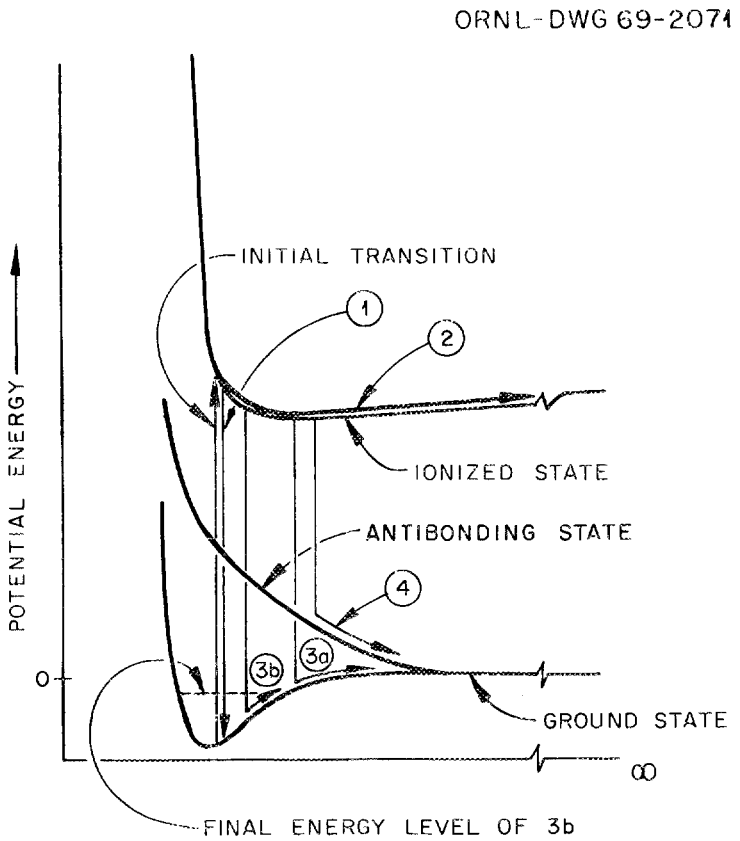

Figure 13. Schematic representation of the possible consequences of excitation to the ionized state.

5. If the ionized adsorbate has received less energy than E_{th} it cannot be desorbed as an ion but may still follow any of the other alternatives, Curve 1, 3a, 3b, or 4.

The numbered curves in Figure 14 show what may happen if the electron impact causes a transition to the antibonding curve:

1. As in the case of ionization, the particle could immediately fall back to the ground state. The electronic energy would be radiated or given to the electrons in the metal.
2. The adsorbate may be desorbed by moving away from the surface along the antibonding curve, exchanging its potential energy for kinetic energy in the process. This process would result in energetic neutral particles being desorbed.
3. The adsorbate could move away from the surface, acquiring kinetic energy as in Curve 2 but fall back to the ground state before being completely desorbed. If the adsorbate has acquired enough kinetic energy while moving away from the surface in the antibonding state the particles will be desorbed as shown by Curve 3a in Figure 14, but if it does not have sufficient kinetic energy to overcome the potential energy requirements to escape from the ground state it will be recaptured into the chemisorbed ground state as in Curve 3b. The particle's increased kinetic energy will put it into a higher vibrational energy level but this will soon decay back to a lower level with the emission of infrared radiation or by interaction with the metal lattice.

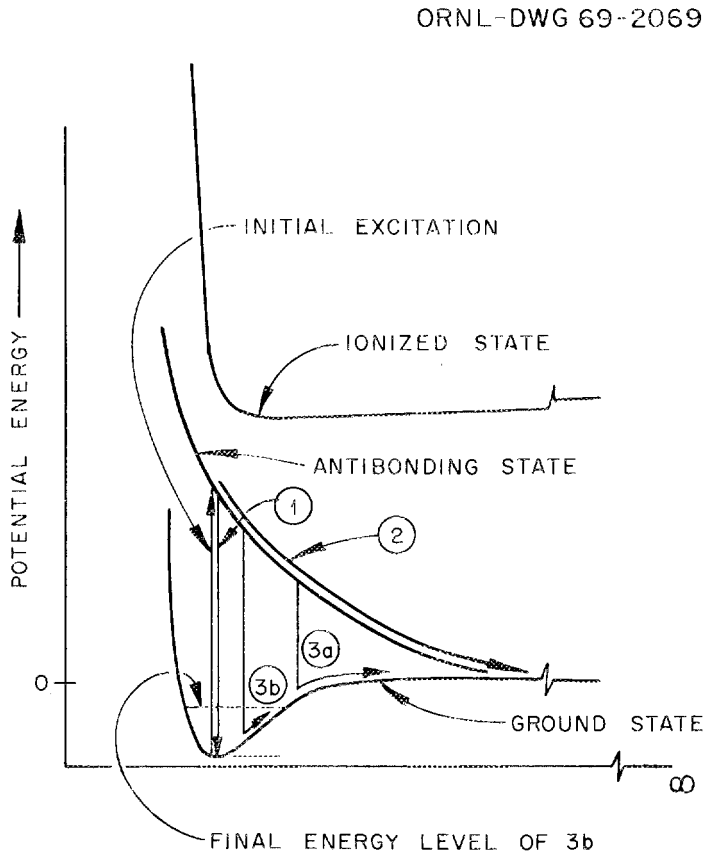

Figure 14. Schematic representation of the possible consequences of excitation to the antibonding state.

Both Menzel and Gomer[9] and Redhead[32] have shown that the predictions of this kind of model fit the results observed in their experiments. In particular, Menzel and Gomer's data show that the probability for EBID is relatively high for carbon monoxide, considerably lower for hydrogen, and completely undetectable for barium adsorbed on tungsten in qualitative agreement with their predictions. They also show in some detail[42] how the desorption probabilities for carbon monoxide vary for various adsorbed states.

Redhead uses the model to explain the desorption of both ions and neutrals from oxygen on tungsten,[32] carbon monoxide on molybdenum,[5] and carbon monoxide on tungsten.[33] He measures the ion desorption and infers neutral desorption rates from this. He interpreted his data in terms of excitation to the ionized state to produce the observed ions and Auger neutralization of the ions to either recapture the adsorbate or produce a neutral with enough kinetic energy to desorb. He is also able, by making some assumptions, to fit his measurements of desorbed ion energies to the model and to estimate bond strengths, neutral particle energies, and even the bonding energy of carbon monoxide, carbon, and oxygen to the substrate.

The electronic excitation mechanism seems to account well for most of the features of the data reported for EBID of CO, NO, and O_2 (references 5, 9, 32, 33, 42, 43) chemisorbed on tungsten and molybdenum. No direct measurement of the total desorption of neutral gas from these systems has been reported although neutral desorption rates may be

obtained indirectly from both Redhead's ion measurements and Menzel and Gomer's field emission studies.

The success of the above model does not imply that other important EBID mechanisms do not exist. In fact, there is considerable data on electron bombardment induced desorption which is not readily explained by the above model.[7,8,10,12,13,22,50,55-59] It is also possible that other mechanisms producing neutral particle desorption are operating on the systems investigated by Redhead and by Menzel and Gomer without being obvious from the data recorded. Menzel and Gomer mention that a momentum transfer mechanism might account for the rapid removal of physisorbed hydrogen implied from the initial data points in one series of experiments.[9] Mechanisms such as momentum transfer might become the dominant mechanism in favorable circumstances.

Adsorption of Carbon Monoxide on Tungsten

From the work of many investigators it seems that there are at least seven identifiable adsorption states* for carbon monoxide on tungsten and perhaps more. In all cases the adsorption is nondissociative, and thermal desorptions take place by first-order reactions. Ehrlich identified four states that form at 300°K (α, β_1 , β_2, β_3) by the thermal desorption technique.[61] Swanson and Gomer[62] used field emission techniques and reported the existence of a virgin state that formed on

---

*The term adsorption state as used in this dissertation means any adsorbed state that is identifiable as distinct from other bound states by any experimental method.

initial adsorption at 20°K and a weak adsorption on top of the saturated virgin layer at 20°K. Pure physisorption was reported by Gomer to occur on surfaces at 4.2°K (reference 63). These states, their heats of adsorption, and proposed geometries are summarized in Table II. The geometries are speculative but have reasonable bases.[42,62,64-67] Some confusion has arisen in the identification of the states since the introduction of EBID studies of ions. Information from the thermal desorption, field emission, and EBID studies is not completely consistent. The EBID techniques indicate that the virgin state formed at 95°K has a small cross section for ion desorption; but as it is warmed up to approximately 200°K, it converts to a new state or states that exhibit larger ion desorption cross sections.[43] No significant thermal desorption is observed at the conversion temperature.[68] The state that formed on heating from 95°K to above 200°K is referred to by Yates, Madey, and Payn[43] as alpha. This state also forms on adsorption onto a clean surface at 300°K (references 33, 43), but Redhead[33] calls this same state the virgin state. This state, which is listed in Table II as α', apparently desorbs thermally between 300 and 370°K. A separate state that desorbs thermally or converts to another state at 500°K (reference 33), 680°K (reference 43), or 750°K (reference 44) and has a large ion desorption yield, is identified as alpha by Redhead,[33] and as β_1 by Yates, Madey, and Payn.[43] Coburn,[44] also using EBID of ions, agrees with Yates <u>et al</u>. and identifies these states as alpha and β_1, respectively, but his thermal desorption spectra show no desorption at 750°K when the ion signal from "β_1" diminishes. His thermal desorption data show "β_1"

TABLE II

SUMMARY OF THE ADSORPTION STATES FOR CARBON MONOXIDE ON TUNGSTEN

State	Temperature of Adsorption (°K)	Heat of Adsorption (ev)	Configuration	Approximate Temperature of Desorption (°K)	Dipole Moment	Reference
Physisorbed	4.2	0.2–0.3		90	Positive	63 62
Second layer over virgin layer	20	0.25–0.5	"resemble α but more weakly bound"	180		62
Virgin	20	0.7 or larger	"probably lying down"	converts to α and β or desorbs 200–400	Negative	62 42 68 33
α′ (virgin?)	200–300	0.7–0.8	?	320 (300–370)	?	33 43 44
α	300	1.26 1.0	O O ‖ ‖‖ C or C ‖ | W W	470 (350–470)	Positive	67 79 42 69 64 65 33
β_1	300	2.5 2.6 2.7	O ‖ C W W Second Valence Bond	1000 (950–1050) (700–1000)	Negative	67 79 33
β_2	300	3.0	C=O W W Lying Down or O ‖ C W W First Valence	1175 (1160–1180)	Negative	67 66 42
β_3	300	3.2 3.3		1260 (1230–1300)	Negative	69 81 33

being desorbed from 800 to 1000°K. The thermal desorption spectra of Bell and Gomer[68] do show a β_1 desorption beginning at about 700°K and extending up to about 1000°K. It is not entirely clear how these three or four states are related at this time.

The thermal desorption spectra of Bell and Gomer are shown in Figure 36 in Appendix B, page 132. An examination of these data, especially Figure 36, indicate that the number of adsorbed states is probably much larger than the eight given in Table II, page 40, and that the adsorption energies, indicated by the desorption temperatures, change with coverage. It is pointed out in Chapter V, page 89, that the atomic structure of the surface, the carbon monoxide pressure, and the temperature during and after adsorption are all very important in determining the population of the various adsorption states. It is also well known[69] that the adsorption energy for a given state usually changes with the population because of interaction with previously adsorbed molecules. One must therefore consider the names listed in Table II as identifying a group of adsorbed states having adsorption energies within a certain range and perhaps having similar adsorption geometries. One must also recognize the differences in the nomenclature used by various authors.

Data on the amount of gas adsorbed according to various authors are given in Chapter IV, page 74. The scatter in this data is also discussed briefly in Chapter V.

CHAPTER III

EXPERIMENTAL METHOD, APPARATUS, AND TECHNIQUES

Method

The method chosen for these experiments is based on measuring the change in pressure in the specimen chamber caused by the release of gas associated with the bombardment of the gas covered surface by electrons of selected energy. The steady-state pressure in a vacuum chamber is determined by the relation

$$Q = PS \ , \tag{2}$$

where

Q = influx of gas into the vacuum (torr liters per second),

P = pressure in the system (torr),

S = volumetric removal rate from the system (liters per second).

Assuming the value of S remains constant, a small change in Q, ΔQ, would produce a small change in P, ΔP, related by

$$\Delta Q = \Delta PS \ . \tag{3}$$

Thus, ΔP can be related to ΔQ if S is known. This type of measurement is the same as that used in thermal desorption (flash filament) experiments for many years, except that in the case of thermal desorption measurements the quantities of gas are usually quite large, 10^{13} to 10^{15} molecules, compared to the amounts to be measured in these experiments (10^{9} to 10^{11} molecules per pulse). There are several

serious problems in measuring these small amounts of gas. Perhaps the most difficult arises as the result of the background signal due to Q, which is frequently large compared with that due to ΔQ.

The background signal due to the residual gases or intentionally added gases in the experimental system was always larger and most of the time was 10 to 100 times larger than the expected signal due to EBID. The source of the background signal (steady-state gas pressure) is usually quite constant, however, and in the worst cases varied only slowly with time. It was possible, therefore, to observe a small perturbation on the large signal by subtracting a large constant signal from the steady background and observing only the difference between the two signals. If the small perturbation is produced by a controlled pulsing of the electron bombardment, a series of corresponding pressure pulses will be observed whose amplitude can be accurately measured in spite of the fact that they represent a very small part of the total signal. From this ΔP one can calculate the ΔQ if S is known and thus determine the rate of release of gas due to the electron bombardment.

Apparatus

Pressure measurement. The pressure measurements can be made with an ionization gauge or a partial pressure analyzer. The UHV-12 ion gauge sold by Varian Associates was used with the Varian 971-0003 gauge control. The ion gauge, of course, records only total pressure and has a minimum detectable pressure of about 2×10^{-11} torr in

normal operation. The partial pressure analyzer used was the 22PC110 model magnetic sector instrument manufactured by General Electric. Either ion energy or magnetic field strength could be varied to select the $\frac{\text{molecular mass}}{\text{electron charge}}$ (M/e) ratio of interest. Although the minimum detectable pressure is well below 10^{-12} torr, measurements of pressures below 10^{-12} torr were not usually made.

The ion gauge outputs were quite stable over long time periods and reacted quickly to small changes in pressure. The output of the mass spectrometer, on the other hand, was very noisy and unstable. The output shifted ±5 per cent or more in a very erratic way and could not be held on a peak reading. This is not inherent in the mass spectrometer but was due to poorly regulated power supplies and an inadequate electrometer for this application. One by one regulated power supplies were substituted for the original supplies and a better electrometer was obtained. It is now possible to reproducibly detect signals of about 10^{-3} times the background. This is accomplished by bucking out (suppressing) the steady background signal and using a more sensitive electrometer scale to read the small variations in the total signal which are the result of an EBID pulse. It is possible, for example, to suppress signals of 10^{-8} ampere and by using the 10^{-10} ampere scale to read reproducibly 10^{-11} ampere signals. Ion gauge signals from the standard supply can be read almost this well if appropriate suppression circuitry is used. However, primary reliance was placed on the mass spectrometer for ΔP measurements since it provided partial pressure readouts and could read smaller pressures than the ion gauges.

The mass spectrometer sensitivity was determined by comparison with the ion gauge over a wide range of pressures of carbon monoxide (from the system base pressure of about 2×10^{-10} to 10^{-7} torr). The smallest reproducible ΔP for carbon monoxide was about 2×10^{-12} torr in normal operation with a carbon monoxide background of about 5×10^{-11} torr.

The original alternating current mass spectrometer filament supply was not used; it was replaced by a well-regulated, constant-current, direct-current supply. An emission current of 1 milliampere was normally used. The thoriated tungsten filament was used, with an ionizing potential of 75 volts. Figure 15 is a schematic diagram of the mass spectrometer electronics which identifies each piece of equipment and its function.

The ion gauges were operated at 4 milliamperes emission. The gauges and mass spectrometer ion source were operated continuously and always allowed to come into equilibrium with the system. They were rarely outgassed because of the long time required to come back into equilibrium with the system at pressures below 1×10^{-9} torr.

Vacuum system. In a study such as this one where it is important to have a good knowledge and control of the amount and kind of gas adsorbed on a metal surface, it is necessary to use ultrahigh vacuum techniques. From the kinetic theory of gases as discussed by Dushman,[70] one can compute that at 10^{-6} torr an initially clean surface is struck by about 10^{15} molecules of gas per square centimeter every 2 seconds.

ORNL-DWG 69-2063

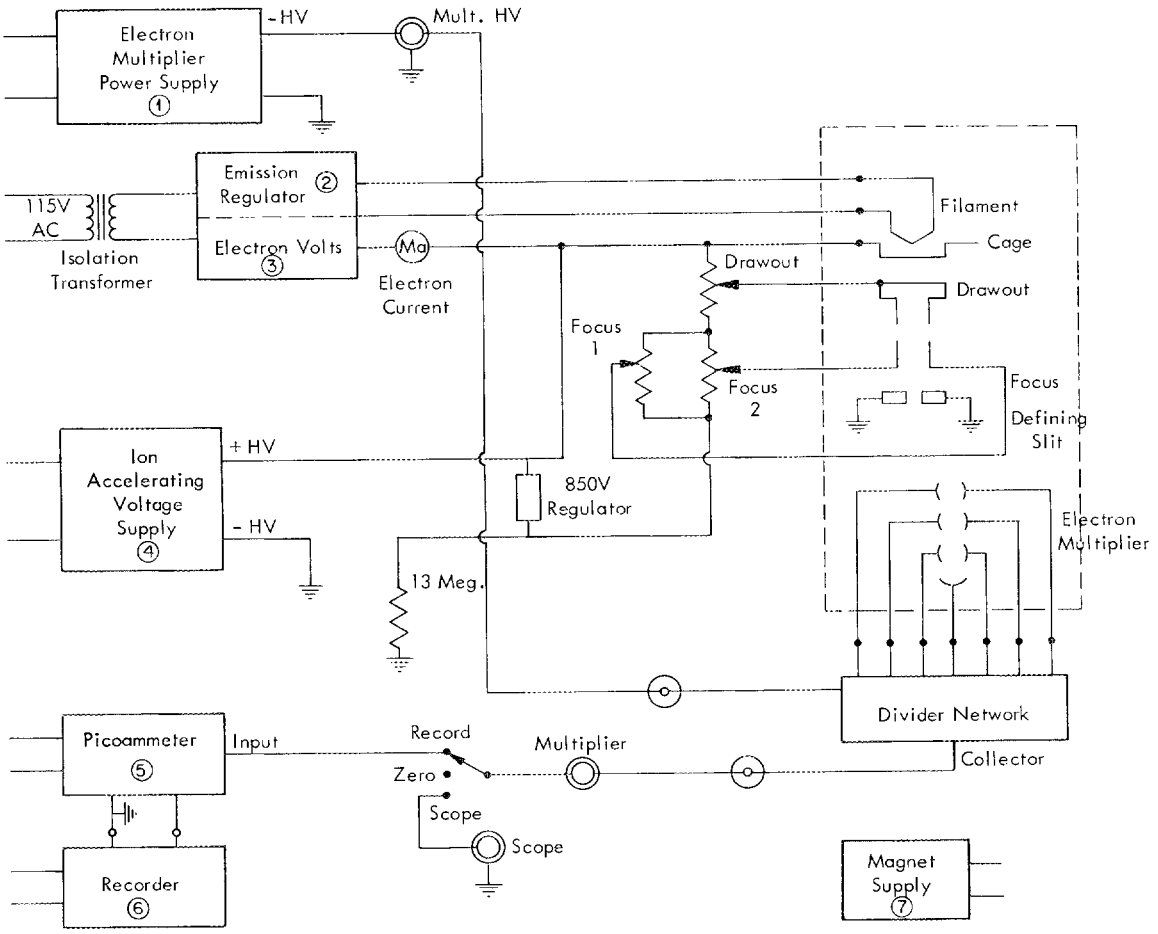

① Power Designs Pacific Model 1569 Regulated 500V-5000V DC

② NJE Model TR 18-3 Regulated 0-3A DC

③ Kepco Model ABC-425M Regulated 0-425V DC

④ Keithly Model 242 Regulated 300V-3500V DC

⑤ Keithly Model 417 Picoammeter with Current Suppression

⑥ Sanborn 150 High Speed Recorder Dual Channel with Model 150-1800 Stabilized DC Preamplifier

⑦ General Electric Electromagnet Control 22 PM 203 Regulated

Figure 15. Schematic diagram of the electrical systems associated with the mass spectrometer.

This is enough gas to form a complete layer 1 molecule deep on a plane surface. At a pressure of 10^{-9} torr, the same coverage would require 40 minutes.*

Thus, to maintain a surface in a known condition for a length of time in which it is reasonable to make a series of measurements, pressures below 1×10^{-9} torr are required.

In order to attain and maintain these pressures routinely it is necessary to keep the influx of gas, Q, as small as possible and to use gas removal rates, S, which are the highest practical but still consistent with the other requirements of the experiment. In this experiment, increasing S decreases both P of Equation (2), page 42, and ΔP of Equation (3), page 42, in the same ratio. As long as the ratio of $\Delta P/P$ controls the minimum detectable EBID, one is well advised to increase S, but when the detection of ΔP is no longer controlled by the ratio of $\Delta P/P$ but rather by the absolute amplitude of ΔP (which occurs for this equipment at about 10^{-12} torr) a further increase in S is undesirable, because it requires a corresponding increase in ΔQ to provide the minimum

---

*This illustration assumes the molecular weight of the gas is 28, the temperature is 300°K, and all of the molecules striking the surface stick to it and are distributed by surface diffusion to form a uniform layer. The number of gas molecules, N, striking a unit area per unit time is given by

$$N = 3.513 \times 10^{22} \frac{P(\text{torr})}{\sqrt{MT}} \text{ cm}^{-2} \times \text{sec}^{-1} ,$$

where

P = pressure in torr,
M = molecular weight of gas,
T = temperature in °K.

usable signal. An increase in ΔQ is undesirable, because this gas is supplied by EBID from the tungsten surface and thus results in changing the surface concentration of gas. Increasing ΔQ also requires an increase in electron current, which means increasing the power dissipated at the target thereby making any thermal desorption effects accompanying the EBID larger. For low electron energies the thermal effects may not be a problem, but space charge effects may limit the current available at the target and thereby limit the ΔQ.

A gas removal rate of 10 liters per second for carbon monoxide was chosen for this experiment. This speed was provided by a commercial titanium sublimation pump equipped with an orifice to provide the selected speed. The pressure attained in the working volume was normally about 4×10^{-10} torr total, or about 5×10^{-11} torr carbon monoxide. The other gases were methane, neon, argon, water vapor, carbon dioxide, and hydrogen as shown by the mass spectrometer trace of Figure 16.

Figure 17 is a flow diagram of the experimental chamber showing the gas handling. Note that Q_L, the gas coming into the system from a controlled leak, and Q_o, the gas coming into the system via outgassing, are steady-state gas sources, while ΔQ, the gas desorbed by electron bombardment, is the only pulsed source; Q_s, which is usually a function of pressure and temperature, is associated with the presence of a "surface phase" of weakly adsorbed gas on the vacuum system walls. This quantity may be positive, negative, or zero depending on whether or not the "surface phase" is in equilibrium with the gas phase. The importance of this gas source or sink is discussed in Chapter V, page 89;

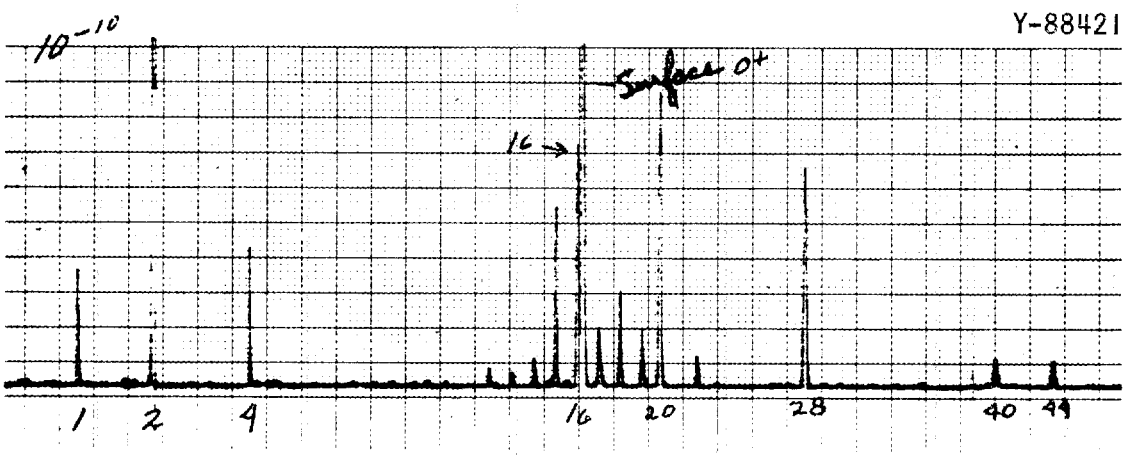

Gases	Approximate Partial Pressure, torr
H_2	8×10^{-10}
He	2×10^{-10}
CH_4	1×10^{-10}
H_2O	4×10^{-11}
Ne	3×10^{-10}
CO	6×10^{-11}
A	1×10^{-11}
CO_2	1×10^{-11}
	Total 1.5×10^{-9}

Figure 16. Mass spectrum of the residual gases in the experimental chamber of the EBID apparatus. (Ion gauge reading 8×10^{-10} torr.)

ORNL-DWG 69-2068

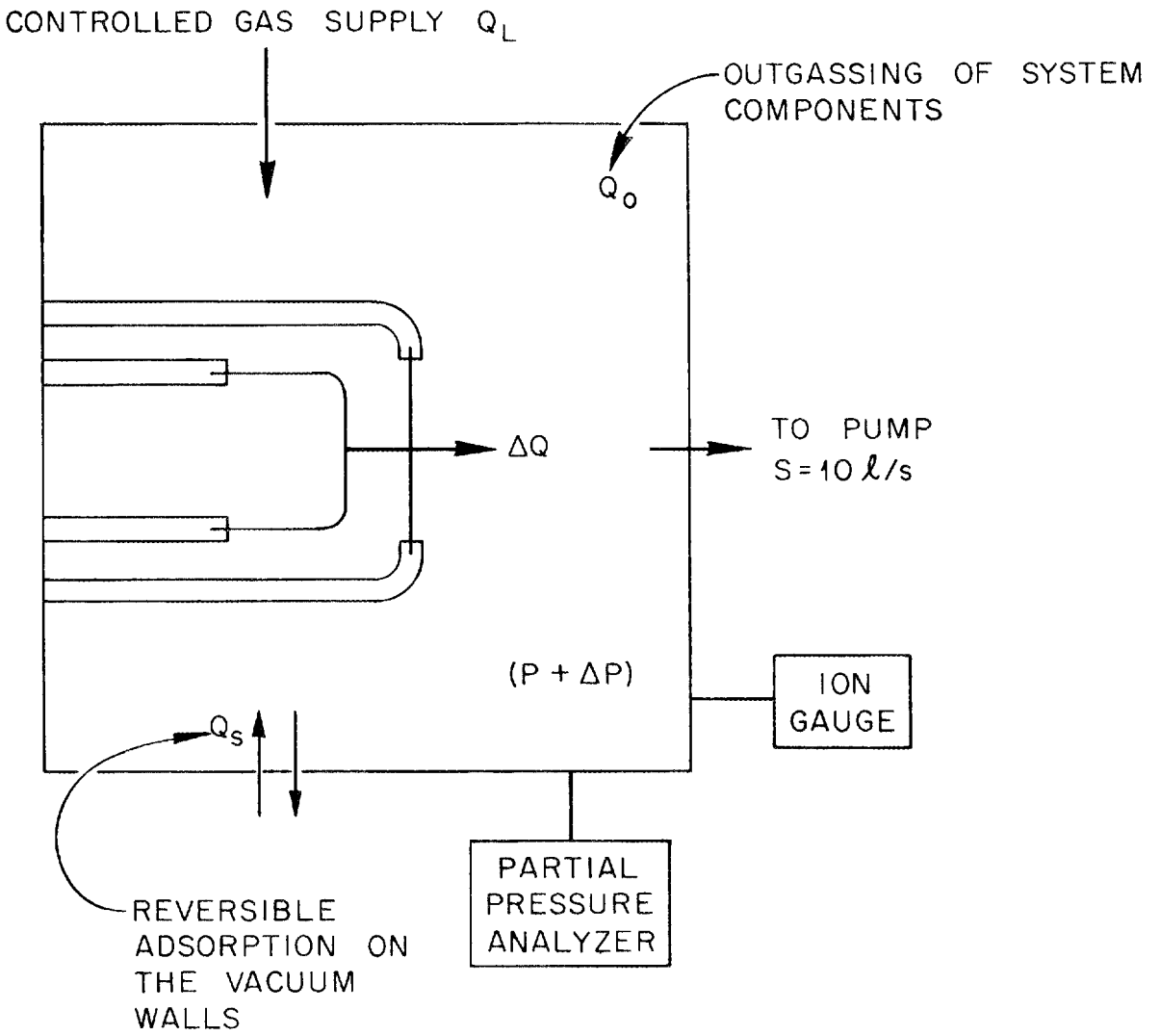

$$P + \Delta P = \frac{Q_L + Q_O + \Delta Q + Q_S(PT)}{S}$$

Figure 17. Schematic diagram of the experimental chamber showing the gas handling for the EBID system.

it may be a very important term or completely negligible depending upon the gas being studied, the materials, the system configuration, and the experimental technique. The relation

$$P + \Delta P = (Q_L + Q_o + \Delta Q + Q_s)/S \qquad (4)$$

that determines the total pressure in the chamber combines Equations (2) and (3), page 42, but has the added term, Q_s, which is difficult to treat and may influence both the steady-state pressure, P, and the pulse pressure, ΔP. The discussion in Chapter V argues that Q_s does not have an important effect on ΔP for the conditions of this experiment.

Figure 18 shows schematically the complete vacuum system, Figure 19 is a photograph of the entire apparatus, and Figure 20 is a close-up view of the vacuum system. Any one of five gases may be admitted to the system from high-pressure sources through individual leak valves. The gases are good grades but not spectroscopic quality. They are supplied in lecture bottles. A typical analysis is given in Table III. The gases are supplied to the leak valve at 100 to 150 pounds per square inch to minimize contamination by the unbaked portions of the gas handling system. Spectroscopic gases could have been used. However, as a practical consideration, one is not usually able to utilize the initial high purity to good advantage because of the background of residual gases in the vacuum system and the interactions of the gas with the vacuum system components, which result in the release of considerable quantities of impurities. It is a rare occasion when the impurities in the vacuum

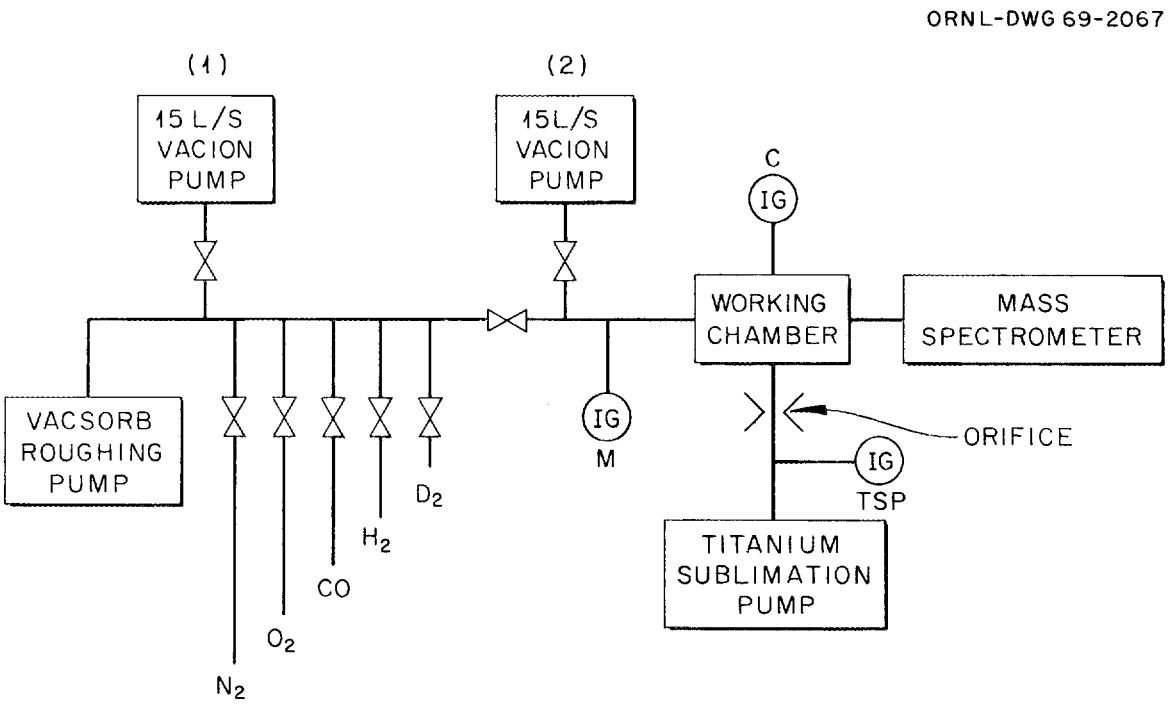

Figure 18. Block diagram of the complete vacuum system.

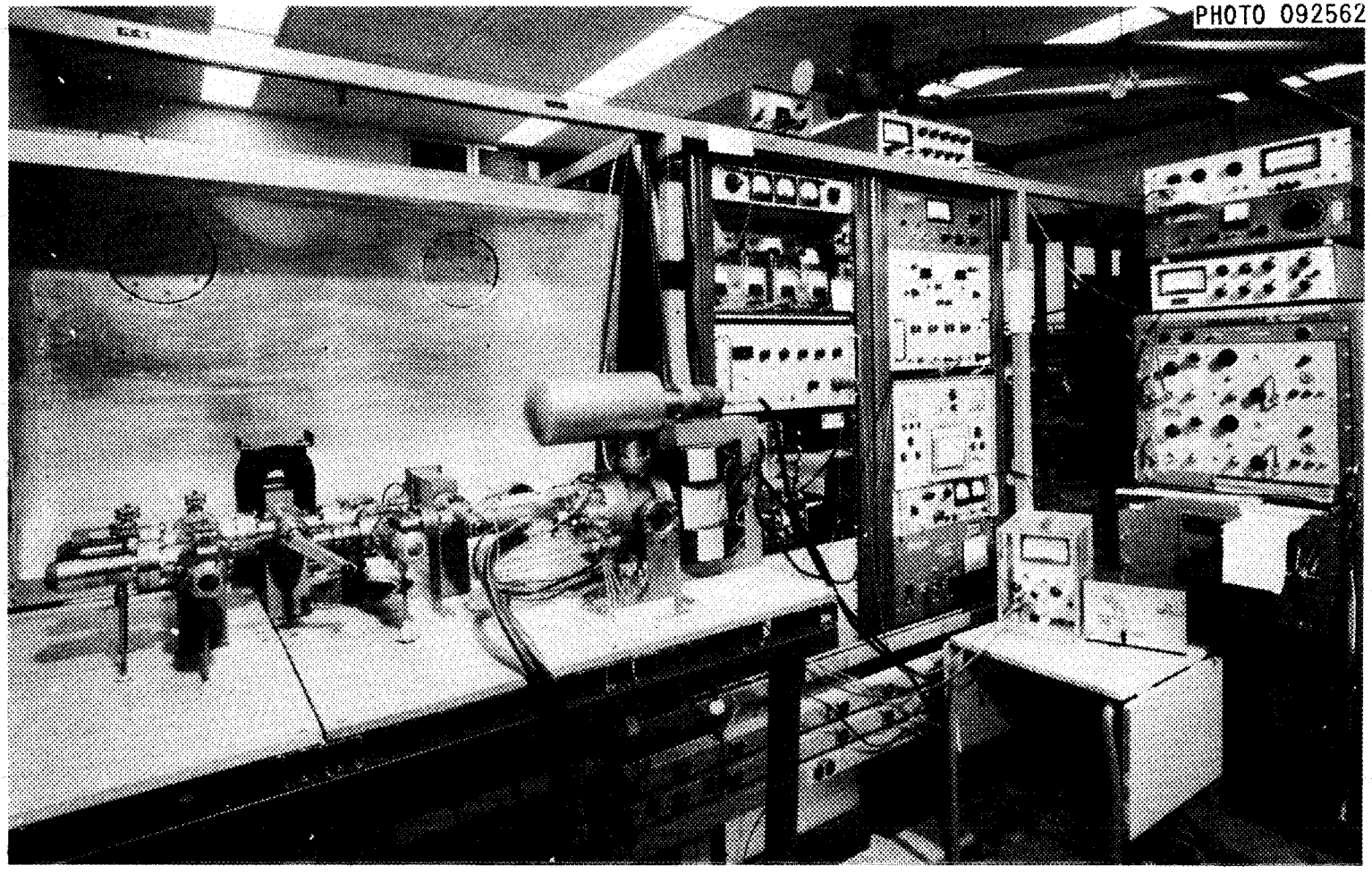

Figure 19. Photograph of the EBID apparatus.

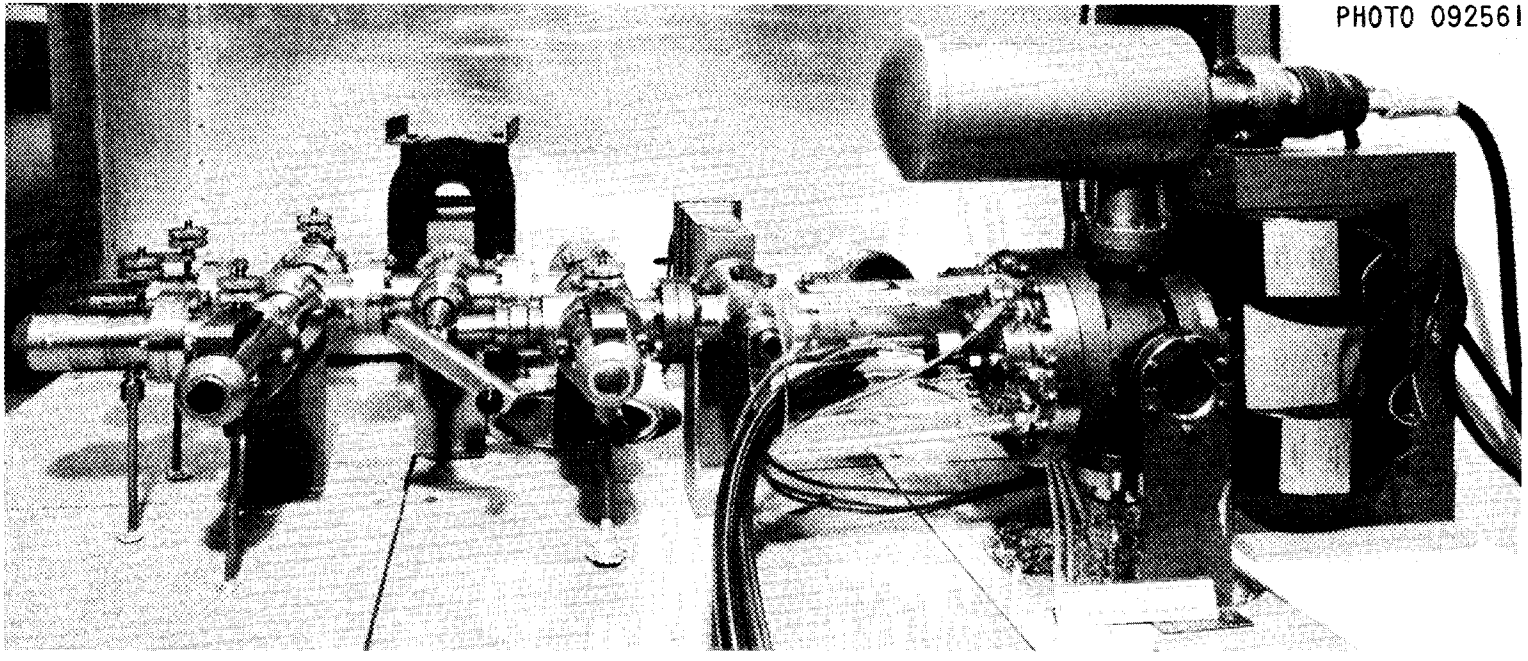

Figure 20. Photograph of the vacuum system. The test chamber is on the lower right side, and the gas leak valves are on the left and left center.

TABLE III

TYPICAL ANALYSIS OF GASES

Gas	Grade	Purity[a] (%)
Oxygen	ED	99.6 Mole
Carbon Monoxide	CP	99.5 Mole
Nitrogen	Prepurified	99.997 Mole
Hydrogen	Prepurified	99.95 Mole
Deuterium		99.5 Atom

[a]According to The Matheson Company, Inc., 932 Paterson Plank Road, East Rutherford, New Jersey 07073.

environment at pressures below 5×10^{-8} torr are measured to be less than 1 per cent of the total even when the ion gauges are off and the sputter ion pumps are valved closed.

The leak valves were Varian Model 951-500. All of the components of the vacuum manifold are built using standard bakable ultrahigh vacuum (UHV) components of the type marketed by Varian and Granville-Philips and are sealed with conflat-style copper gaskets. The vacuum is brought to about 10^{-3} torr with a Vacsorb pump, and then the system is switched to the 15-liters-per-second, water-cooled VacIon pump number one. This pump is used for all vacuum processing of the system but is frequently throttled or valved off during an experiment because of its effect on the impurity content of the gas. VacIon pump number two was intended to be operated only at the end of bakeouts and to provide lower base pressures when the gas inlet manifold could be closed off. In fact, however, it was not used at all during the collection of the data reported in this dissertation, because its use did not appreciably improve the conditions in the working chamber. The presence of the pump magnet also influenced the ion gauge readings on the Ion Gauge M shown in Figure 18, page 52. The pump magnet was removed, but the valve to the pump was left open.

The chamber, which can be seen in Figure 20, page 54, is $3\frac{1}{2}$ inches in inside diameter and 4 inches long. It has four $1\frac{1}{2}$-inch connections around its diameter for connection to the gas manifold, the titanium sublimation pump, a view port, and a tubulated ion gauge. The nude source of the mass spectrometer intrudes about 2 inches into the chamber

from one end, and the tungsten sample and electron bombardment source are mounted on a 6-inch outside-diameter conflat flange, which closes the other end of the chamber. The whole vacuum system rests on a transite table top and can be enclosed by a bakeout oven. The oven can be separated into two sections so that different temperatures may be used to bake the gas handling manifold and the main experimental area. The usual bakeout treatment is about 16 hours at 250°C for the experimental area and 16 hours at 150°C for the gas handling manifold and VacIon pump number one. All filaments, the tungsten target, and the titanium sublimators are outgassed at the end of the bakeout period while the system is at about 100°C. The pressure before cool down is usually in the low 10^{-6} torr range and drops into the low 10^{-9} torr range after several hours at room temperature with all filaments operating and down to mid 10^{-10} range after titanium is evaporated in the sublimation pump. At this time, the VacIon pump number one becomes more of a liability than an asset and is useful only to pump inert gases and methane. When gas is leaked into the system, it is best to close off this pump entirely, because impurities released from the pump under the increased pressure contaminate the gas being introduced. The pressure in the titanium sublimation pump chamber is normally close to 1×10^{-10} torr when the pressure in the working chamber is 10^{-9} or less. This pressure remains 10 to 100 times lower than the pressure in the experimental chamber when any of the gases from the gas manifold are admitted. Only a small error is introduced by neglecting the pressure on the downstream side of the orifice when calculating the gas removal rates. A volumetric speed of

10 liters per second for carbon monoxide has been used in all of the calculations. The speed for hydrogen is used as 40 liters per second.

Tungsten specimens. Because of the rapid contamination of the specimen surface even in the relatively clean ultrahigh vacuum system and because EBID does produce small changes in the surface concentration of adsorbed gases, it is desirable to be able to clean the surface and cover it with the desired gas rapidly and reproducibly. The easiest way to produce a clean surface on tungsten is to heat it to 2200 to 2400°K. Assuming that the tungsten is of reasonable initial purity, the only contaminant not rapidly removed by this treatment is carbon. Carbon can be removed by reaction with 10^{-6} torr pressure of oxygen at 2200°K (reference 71).

Perhaps the easiest way to heat the tungsten surface is to use a specimen in the form of a ribbon that can be heated by passing a large current through it. This also allows one to use thermal desorption to determine the amount and kind of gas present on the surface at the end of an experiment.[72,73] This is also discussed in Appendix B, page 128. The initial tungsten specimens were ribbons 0.3 by 0.0025 by 3 centimeters with [211] poles normal to the surface. For reasons discussed in Chapters IV and V, pages 74 and 89, the final target was 0.5 by 0.025 by 4 centimeters with [100] poles normal to the surface. The targets were decarburized by heating in 10^{-5} torr of oxygen for $1\frac{1}{2}$ hours and 10^{-6} torr of oxygen for about 20 hours at temperatures between 2200 and 2400°K. The 0.025-centimeter-thick ribbon recrystallized to the microstructure as

shown in Figure 21. Although the surface appeared uneven in the optical microscope, no thermal facets or other features except grain boundaries were observed in the electron microscope.

Bombardment cell and mode of operation. The arrangement of the tungsten target and the electron source is shown in Figures 22, 23, and 24. The tungsten target is clamped into the 0.25-inch-diameter copper conductors from the high voltage feedthroughs. It may be heated by passing up to 200 amperes through the ribbon. The target may be raised to voltages up to 10,000 volts positive with respect to ground. Air cooling is provided for the copper rods and the external ends can be maintained near room temperature even when the target is pulsed to 2200°K during a 30 seconds on-30 seconds off continuous cycle for cleaning purposes.

The tungsten target is mounted so that the surface to be bombarded (0.5 centimeter wide and 2 centimeters long) is facing the ion source and is about 3 inches directly in front of the ion cage of the mass spectrometer. This makes it possible to detect and analyze ions as well as neutrals produced by EBID.

The electron source is a 0.0075-centimeter-diameter tungsten wire located 9 millimeters in front of the surface to be bombarded. A tungsten wire mesh shields the electron source from the electrical fields of the mass spectrometer and is about 2 millimeters in front of the electron emitter.

Figure 25 is a schematic diagram of the power supplies for the target heating and bombardment cell. The screen is normally at ground

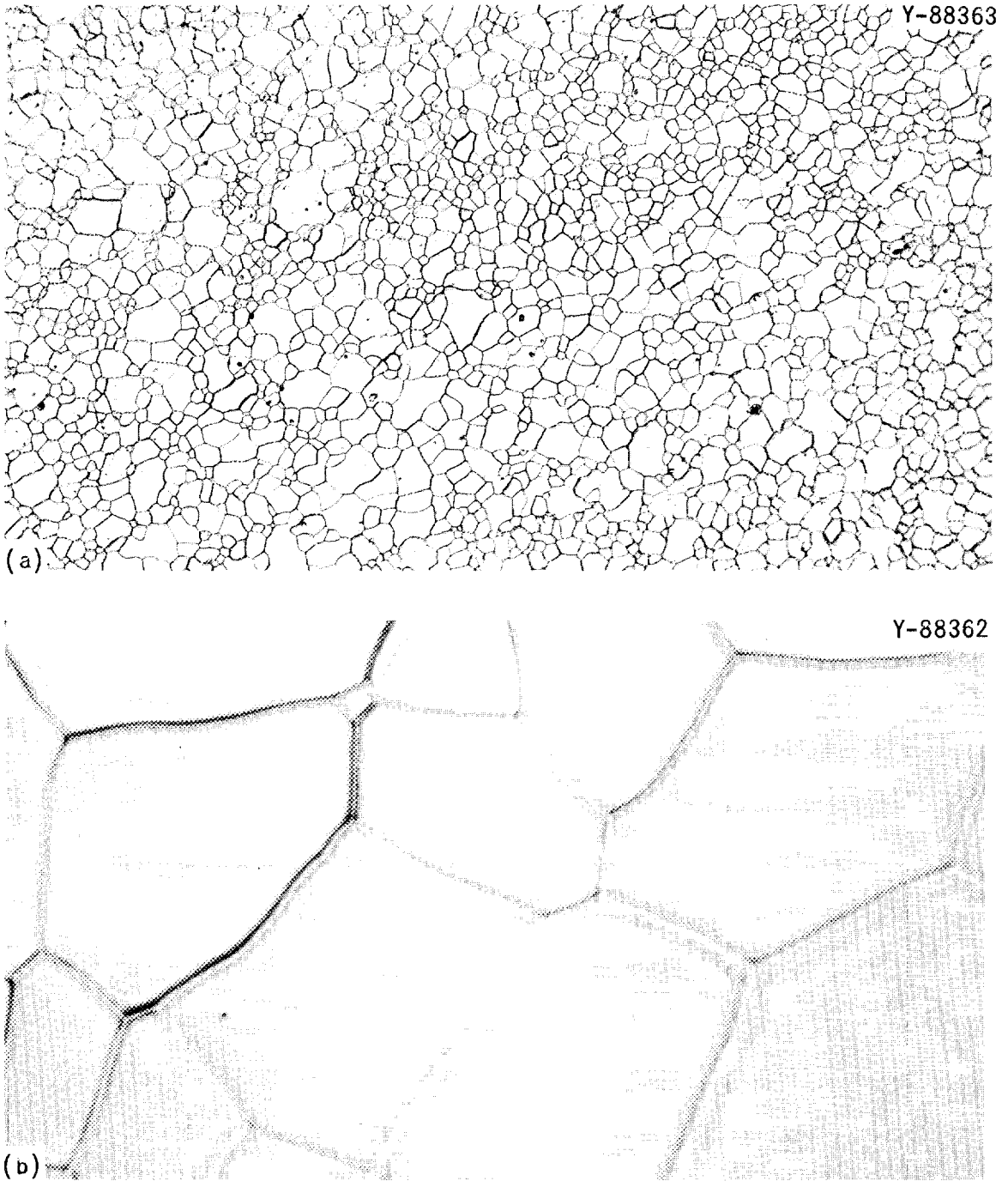

Figure 21. Photomicrograph of the surface of the tungsten target. The specimen was not etched. (a) 75× and (b) 1,000×.

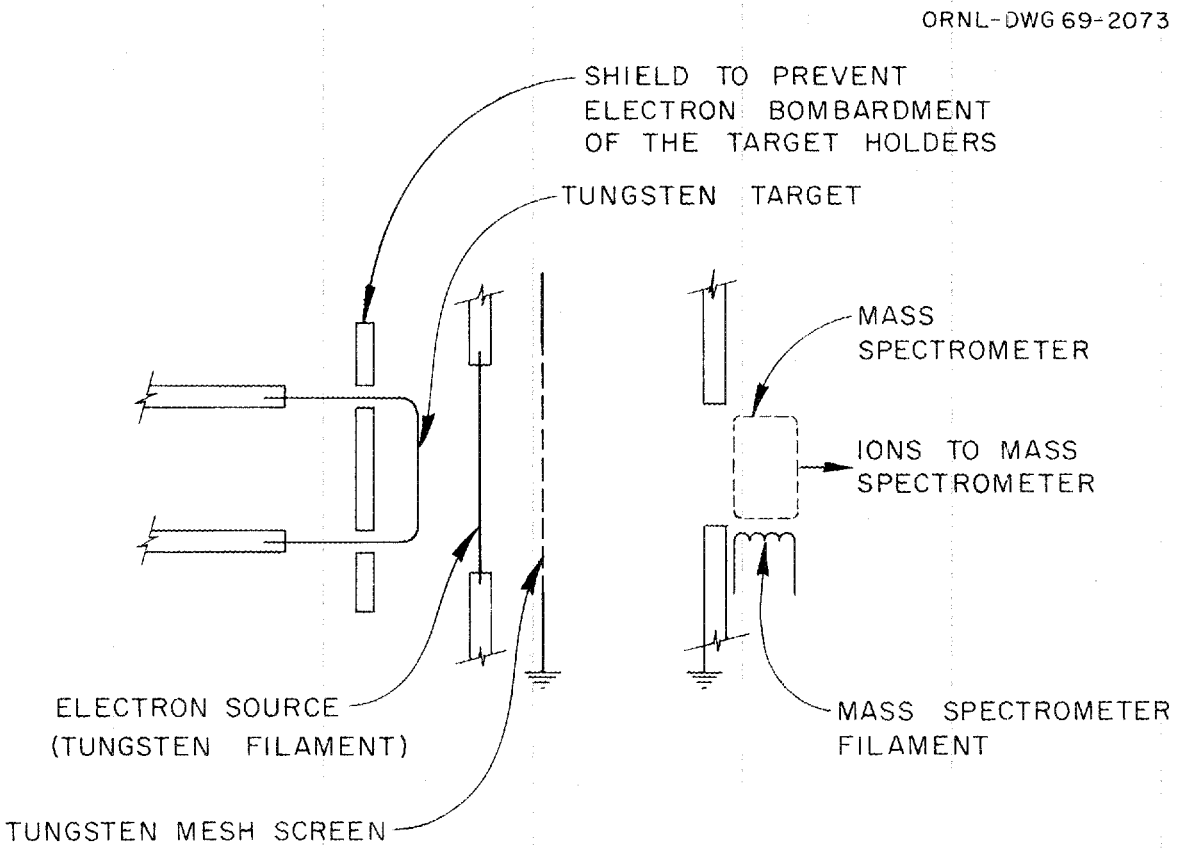

Figure 22. Schematic drawing of the bombardment cell.

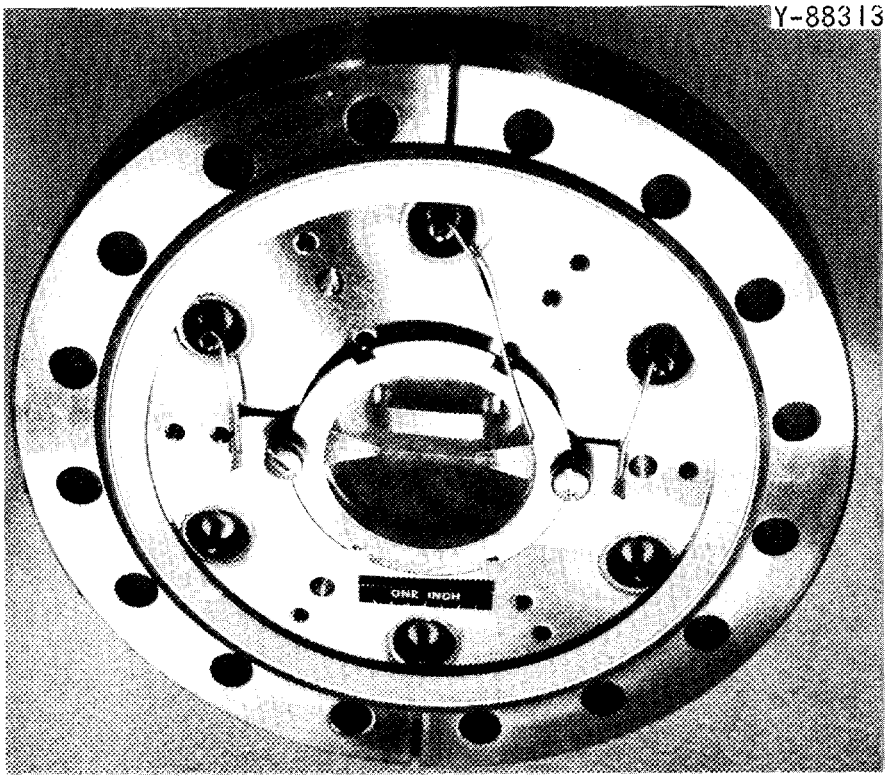

Figure 23. Photograph of the bombardment cell. The target can be seen through the screen and the emitter filament is visible below the target ribbon.

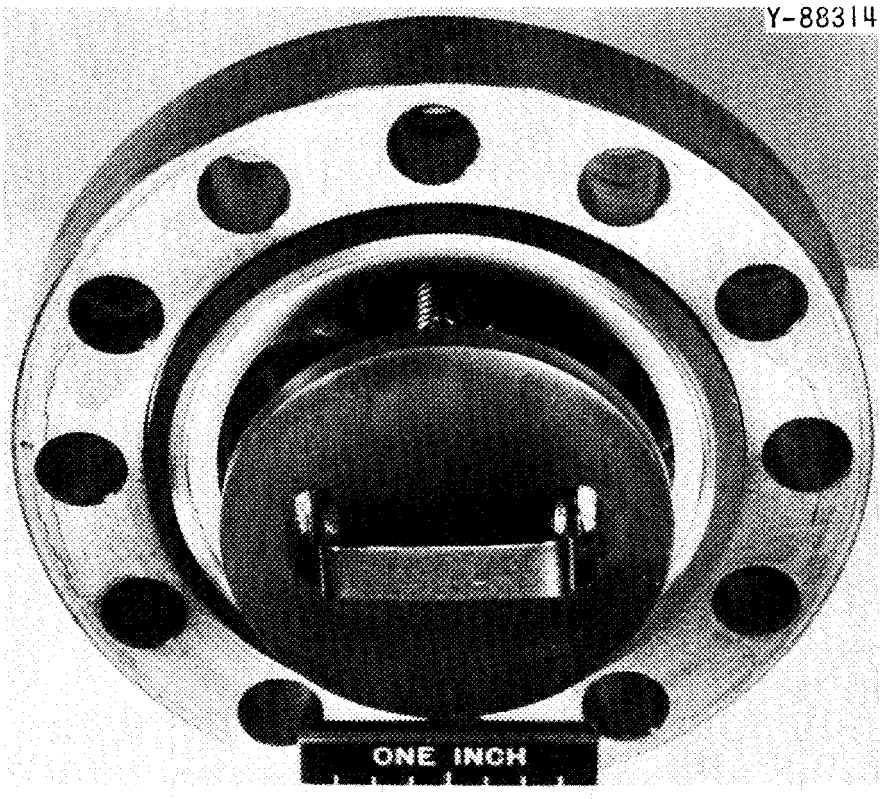

Figure 24. Photograph of the tungsten target in its shielded mounting.

ORNL-DWG 69-2062

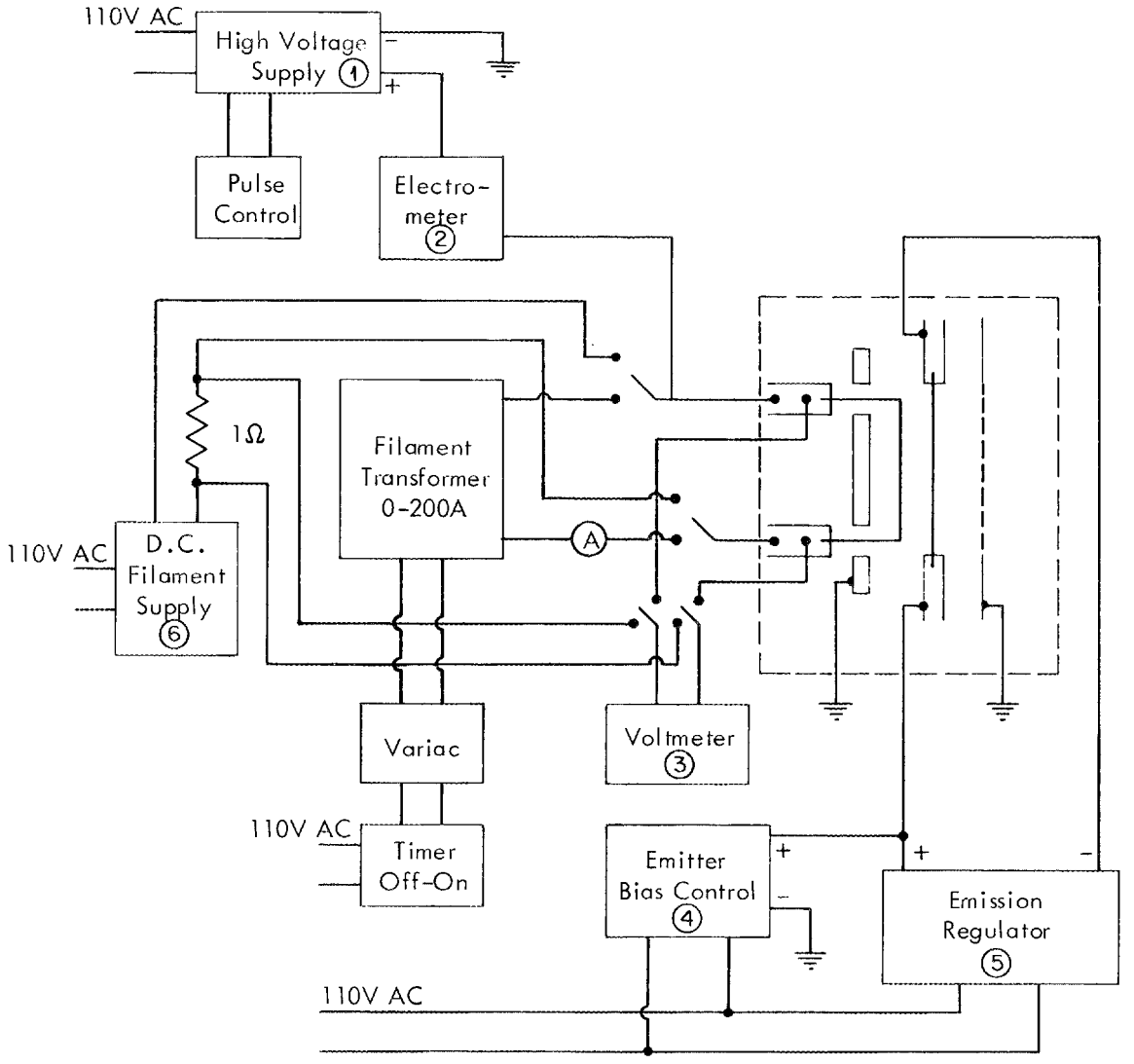

① Fluke Model 410B Regulated 0-10000V DC

② Keithly Model 600A Electrometer

③ Keithly Model 660A Guarded DC Differential Voltmeter

④ Kepco Model ABC 425M Regulated 0-425V DC

⑤ NJE Model TR 18-3 Regulated 0-3A DC

⑥ (1 or 2) Kepco CK 18-3M Regulated 0-3A DC

Figure 25. Schematic diagram of the electrical apparatus associated with target heating and the bombardment cell.

potential, and the negative end of the emitter usually biased about 2 volts positive with respect to ground. Up to 500 volts may be applied to either element. The voltage drop across the emitter including the leads is about 0.6 volt. Thus the center of the emitter is about 0.3 volt positive with respect to the negative terminal. The small positive bias potential prevents electrons with thermal energy from striking gas covered surfaces or getting through the screen and being drawn to the mass spectrometer ion source to produce spurious signals. The target is normally at ground potential, but when it is pulsed to a preselected positive voltage (up to 10,000 volts) electrons are drawn from the emitter to bombard the target. The current is regulated by the temperature of the emitter filament. The normal range is from 5 to 100 microamperes and is decreased as the voltage is increased to limit the heating effect of the bombardment. The filament temperature is not changed during the pulse.

An alternate method of pulsing the electron bombardment is to increase the positive bias of the emitter until the emission falls to zero. This has been done in cases where it was desirable to check for field emission currents to the target or to check the changes in target temperature during bombardment. It was usually more convenient to pulse the accelerating voltage on the target, however.

Target temperature measurement and control. As we shall show in Chapter IV, page 74, small changes in the target temperature can produce

relatively large thermal desorption of some gases. Therefore, it is desirable to be able to measure the temperature change during electron bombardment and to simulate it by other means.

A sensitive indication of the target temperature may be obtained by measuring its electrical resistance. The resistance of the copper leads are less than 1 per cent of that of the filament. If the contact resistance can be assumed negligible, the resistance of the target can be determined from the potential drop between the copper feedthroughs when a known current flows in the circuit. Since the resistivity coefficient changes very little with temperature near room temperature, the resistance measurement will indicate the average temperature of the filament even though the temperature is not uniform over the filament length. These measurements may be somewhat crude and cannot yield accurate absolute temperatures, but they can easily detect changes in the average temperature of the target of 0.2°K and measure changes of 2°K to within 10 per cent by using a measuring current of 3 amperes. This current produces about a 0.2°K rise in the average target temperature. The resistance of the target is about 2.1×10^{-3} ohms at room temperature.

The average temperature increase of the target can be duplicated by ohmic heating; however, the temperature distribution will be different, and the peak temperature will be higher with electron bombardment heating than with ohmic heating.

The problem of comparing the effects of thermal desorption from the two heating methods is discussed in Appendix C, page 134.

Regulated direct current up to 6 amperes is available, and resistance measurements can be made up to this level. If larger currents are required an alternating-current supply is used, and the temperature changes are calculated.

The voltage drop across the feedthroughs is measured with a Keithly Model 660A guarded differential voltmeter, which can be used to read voltage changes as small as 2×10^{-6} volts. The constant current supplies are Kepco CK 18-3M units, which are regulated to better than 0.01 per cent. Each supply will produce 3 amperes, and they can be operated in parallel to give 6 amperes with slightly reduced regulations (that is, 0.02 per cent). A precision 1-ohm resistance in series with the filament allows current measurement to four significant figures.

No provisions have been made for direct temperature measurements during high-temperature heating of the thicker target. The nonuniformity of temperature makes such measurements of limited usefulness. In the temperature range above 2000°K where most of the heat is lost by radiation and the temperatures are reasonably uniform in the center half of the target ribbon, electron emission can be used to estimate the temperature to within about 50°K. No optical temperature readings could be made on the 0.025-centimeter-thick targets, because the target is not visible through the observation port.

On the thinner (0.0025-centimeter-thick) targets, which were mounted somewhat differently, good agreement was obtained between temperatures measured with an optical pyrometer and those calculated from

electron emission at temperatures above 2000°K (provided there was no adsorbed gas on the surface to change its work function). Optical temperature measurements, resistance measurements, and temperatures determined from known gas desorption phenomena allowed a good correlation of the temperature and heating current for this ribbon.

If accurate temperatures are required in future work, tungsten leads could be welded to the back of the target about 1 centimeter from each end of the ribbon to provide accurate resistance measurements. Direct-current heating currents could be used with a superimposed small regulated high-frequency alternating current. The alternating-current voltage across these potential taps would then provide a measurement of the temperature.

Technique

Measurement of neutral gas produced by EBID. The steps in a typical experiment where the yield of carbon monoxide is to be measured as a function of electron energy are described below. It is assumed that the vacuum system is in good operation, has been recently baked at 250°C, and base pressures in the 10^{-10} torr range are indicated.

1. The ion gauges and mass spectrometer are checked for normal operation.
2. The residual gases in the system are monitored with the mass spectrometer. Ion energies of 515 electron volts are usually used, and the spectrum is scanned by varying the magnetic field.

3. The titanium film in the titanium sublimation pump is replenished by operating the sublimator for a few minutes.
4. The residual gases are again monitored as in step two.
5. The mass spectrometer is adjusted to monitor the M/e = 28 peak (which is normally due only to carbon monoxide in these experiments). The instrument is checked until the drift in the magnetic field has stabilized, and no drift of the peak is detectable.
6. The target is cleaned by raising its temperature to 2200 to 2400°K and holding for perhaps 10 seconds, cooling, and flashing again at intervals of 1 or 2 minutes until the pressure rise on flashing is small and does not decrease appreciably from pulse to pulse. This usually requires only three or four pulses.
7. The VacIon pump is valved closed.
8. The target is cooled to room temperature, and carbon monoxide is admitted to a predetermined pressure between 5×10^{-9} and 5×10^{-8} torr to permit adsorption to occur. The pressure is recorded as a function of time and from this data and the volumetric pumping speed the amount of gas adsorbed on the target can be calculated. When adsorption is judged to be complete, that is, the pressure in the working chamber no longer is increasing detectably, the gas supply is turned off, and the pressure falls rapidly to the 10^{-10} scale. Both the total pressure and

the carbon monoxide partial pressure decrease slowly below this pressure. The EBID can begin immediately; however, 5 to 10 minutes are required before the pressure decrease is slow enough for the EBID to begin to produce results that are easy to read and will be reproducible during the next hour or so.

9. Suitable pressure ranges and suppression signals are selected to allow good resolution of the EBID pressure pulses.

10. The EBID is begun by pulsing the target to a high voltage and thereby causing it to be bombarded with electrons having a preselected amount of energy, usually 500 electron volts. A preselected electron current is obtained by adjusting the electron source temperature. The current usually is 10 to 50 microamperes. The pulse is 8 seconds long and is automatically repeated once a minute. From one to three pulses will be used before going to the next voltage, depending upon the magnitude and reproducibility of the pressure pulse. The pressure pulses from both the mass spectrometer and one ionization gauge are recorded on a Sanborn Model 150, dual-channel, high-speed recorder with a Model 150-1800 stabilized direct-current preamplifier. The datum point at 500 electron volts is used as a control and is periodically repeated as a means of assuring that the condition of the target has not changed appreciably during the data acquisition at other electron energies.

11. The EBID is continued using different target voltages and therefore different electron energies until enough data are obtained to produce a complete curve. The electron current may be kept constant or varied to produce the best balance between thermal effects and the height of the pressure pulse.

12. During the EBID run, the target may be pulse heated resistively to produce thermal desorption signals for comparison with the EBID signals. The heating pulse is usually selected to give an increase in the average temperature of the target approximating that produced by the electron bombardment used for the EBID control point and lasts for the same duration as the electron bombardment. Larger heating pulses are also used to compare with the higher power EBID pulses necessary to get data for high-energy electrons.

13. At the conclusion of the EBID run, a complete thermal desorption to 2400°K is made to check on the degree of contamination of the target by other gaseous impurities. This also provides a check on the amount of carbon monoxide adsorbed on the target. The carbon monoxide partial pressure increase integrated over the desorption time and multiplied by the volumetric gas removal rate gives the amount of gas desorbed. This should agree with the amount

adsorbed in step eight unless substantial gas has been removed by the EBID measurements or by some other experimental irregularity.

Measurement of ions produced by EBID. Although the equipment is designed to make measurements of the desorption of gases from the target, it is also possible to make some limited measurements of ions produced on the target surface and desorbed in the direction of the mass spectrometer. The mass spectrometer ion source is turned off, and ions directly from the target are sent through the mass analyzer. The ion accelerating voltage is given by the target voltage since the mass-analyzer slits are at ground potential. The species of ion desorbed can be identified, and changes in the numbers desorbed as functions of temperature and pressure can be determined. It is not possible, however, to determine the numbers desorbed as functions of electron energy because of changes in collection efficiency as the target voltage is changed. It is possible to get an estimate of the ion energy distribution by measuring the peak shape and displacement. The ion energy distributions have been measured much more accurately by Redhead.[33] Some correlations of the ion desorption with the neutral particle desorption have been made but are not reported.

The steps in making measurements of ion desorption are similar to those for measuring neutral gas desorption up through step eight. After the adsorption in step eight when EBID is begun, the mass spectrometer ion source is turned off and its elements brought to ground

potential. The target voltage is then changed to 515 volts so that CO^+ ions released from the target with no initial energy will pass through the mass spectrometer and generate a signal by striking the ion collector of the electron multiplier in the same manner as an ion from the mass spectrometer ion source. Since there is no ion background signal, there is no need for signal suppression or using pulsed EBID. Variations in the ion yield as a function of target temperature or carbon monoxide pressure may be observed continuously and rapidly. Changing the ion species monitored to O^+ involves tuning the magnetic field of the mass spectrometer to pass that ion or changing the target voltage, either of which will result in changes in the ion collection efficiency. Changing the target voltage also changes the energy of the bombarding electrons so that comparisons between ionic species and between ion yields at different electron bombardment energies are not straightforward. A rough estimate of the ion energy distribution can be obtained by varying the target energy in small steps and plotting the amplitude of the output of the mass spectrometer as a function of target voltage.

At the conclusion of an ion measurement, a complete thermal desorption should be made in the same manner as in step twelve describing the measurement of neutral gas produced by EBID, page 71.

CHAPTER IV

EXPERIMENTAL RESULTS

An important result of this investigation is the development of a technique for the measurement of the desorption of neutral particles by EBID that is sensitive enough to permit frequent sampling of surfaces without causing significant changes in the surface. The technique is able to definitely separate and minimize the effects due to thermal desorption from those due to EBID *per se*. A slight modification of this technique would make it compatible with the apparatus required for low energy electron diffraction (LEED) studies and also the measurement of the ions and secondary electrons produced by electron bombardment.

The EBID of Carbon Monoxide as a Function of Electron Energy

Figure 26 shows the neutral desorption of carbon monoxide from tungsten caused by EBID as a function of electron energy. The sample was covered with carbon monoxide at 1×10^{-8} torr. The carbon monoxide partial pressure was reduced to less than 10^{-10} torr, and EBID measurements were made with 30 microamperes of bombardment current. Ohmic heating was used to simulate the thermal desorption effects, and this correction is indicated. Under these conditions thermal desorption is not important until the electron energy exceeds 1,000 electron volts. The sharp increase in the yields at about 5,000 volts is probably due

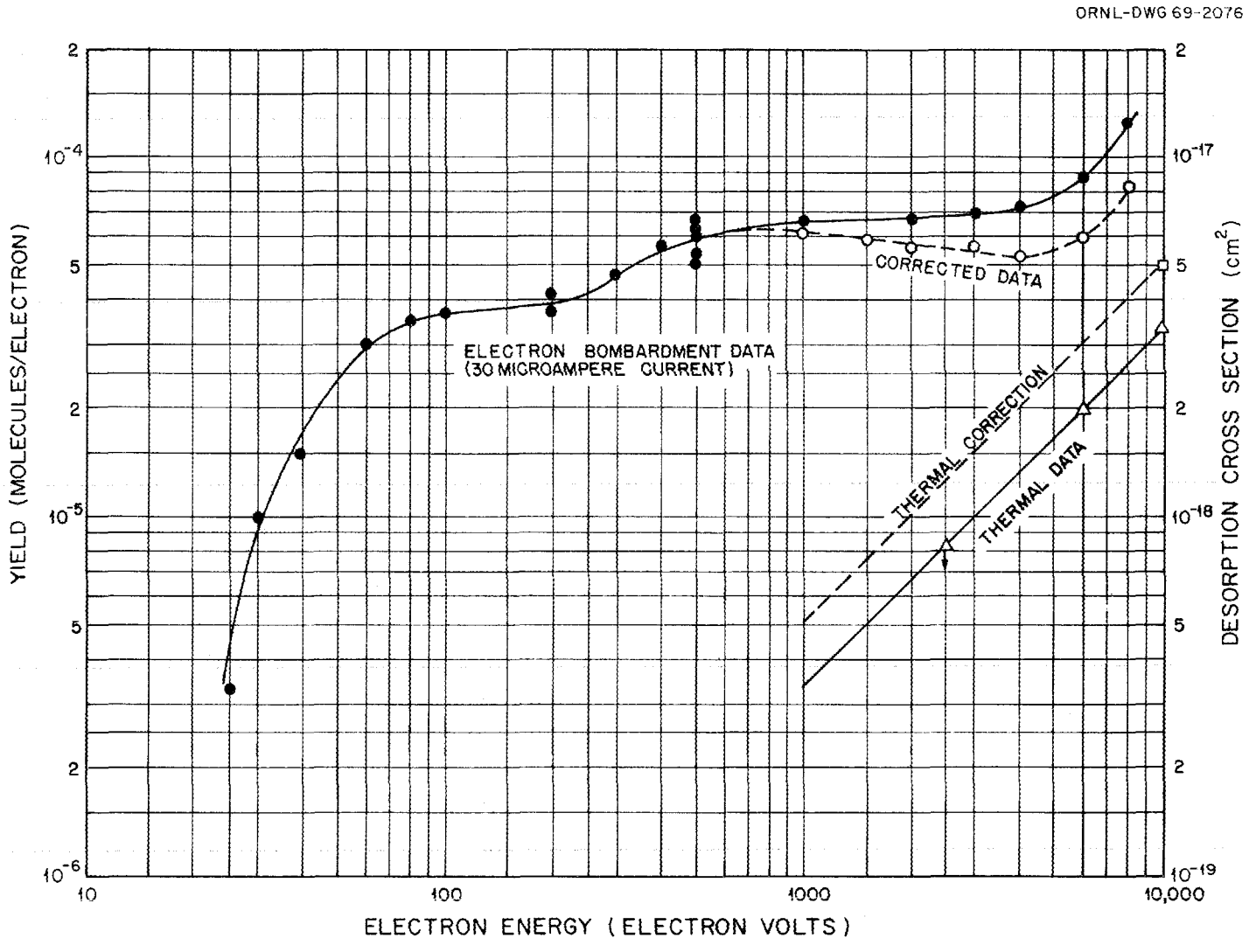

Figure 26. Electron bombardment induced desorption of carbon monoxide from tungsten as a function of electron energy.

to experimental problems with the high voltage insulation, but could be due to an EBID process. The effect was not investigated sufficiently to determine its cause since it occurred at voltages high enough to cause a new set of experimental problems.

The scale on the abscissa of Figure 26 gives both the number of molecules desorbed per electron and the desorption cross section (based on a surface coverage of 10^{13} molecules per square centimeter in the alpha state). Both Menzel and Gomer[34] and Redhead[33] estimated the cross section for the desorption of neutrals to be about 3×10^{-18} square centimeters for 100 electron volt electrons. The excellent agreement with the present results may be fortuitous in view of the large uncertainties in the actual population of the adsorbed alpha-phase layer. The general shape of the curve below 300 electron volts agrees with Redhead's results for ion desorption although Redhead's data fall somewhat faster below 100 electron volts.

The neutral gas desorption is definitely associated with the presence of the low-temperature adsorbed forms of carbon monoxide on the target, since heating the target to an estimated 900° K reduced the EBID signal to below the detection limit. According to Redhead,[33] there are two low-temperature forms of carbon monoxide present at 300° K, one of which desorbs rapidly between 300 and 350° K and another which desorbs rapidly at about 470° K. Heating to an estimated 400° K did reduce the signal slightly but did not eliminate it. Apparently the phase that desorbs at 470° K contributes most of the neutral EBID signal.

Thermal and Pressure Effects on the Desorption Signal

Figure 27 shows the effect of pressure on the amplitude of pressure pulses produced by EBID and by thermal pulses. The thermal and EBID desorptions were produced by pulses of equal power. Appendix C, page 134, shows that the average temperature increases produced by electron bombardment pulses may be as much as 1.5 times larger than by ohmic heating. If we assume the amount of gas desorbed is proportional to the change in the average temperature (which should be true for small temperature changes), thermal effects will be more important than EBID per se at pressures above 2×10^{-7} torr and EBID measurements at pressures below 2×10^{-8} torr would require relatively small corrections. The triangles represent the EBID data corrected for thermal effects. Note that the corrected values are nearly constant and are not pressure sensitive between 10^{-10} and 10^{-8} amperes (5×10^{-10} and 5×10^{-8} torr).

Based on the above results one can explain the discrepancy between the measurements made at 10^{-10} torr on a 0.025-centimeter-thick target and those made earlier at 5×10^{-8} torr on a target ten times thinner and thus ten times more sensitive to thermal effects. The early data shown in Figure 28 are almost a straight line showing the carbon monoxide yield to be proportional to the electron bombardment power (and therefore changes in specimen temperature) over a wide range of power. The yields were many times higher than those observed in the measurements using the heavier target at lower pressures. Thus, virtually the entire desorption from the thinner specimen at higher pressures was due to thermal effects. The thermal contribution to the pressure

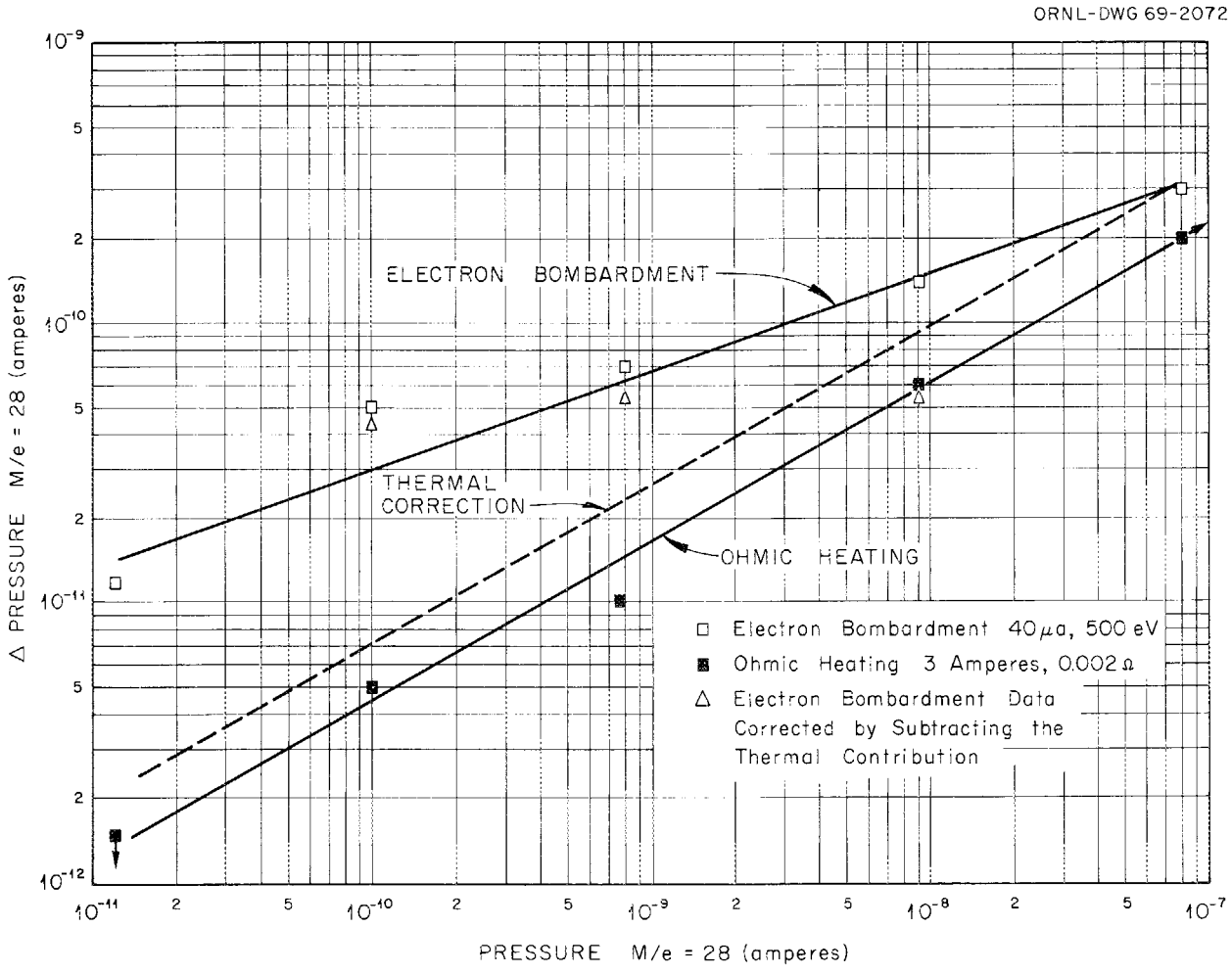

Figure 27. Electron bombardment induced desorption and thermal desorption of carbon monoxide from tungsten at 300°K as a function of the partial pressure of carbon monoxide in the experimental chamber. (The mass spectrometer sensitivity was 0.18 ampere per torr.)

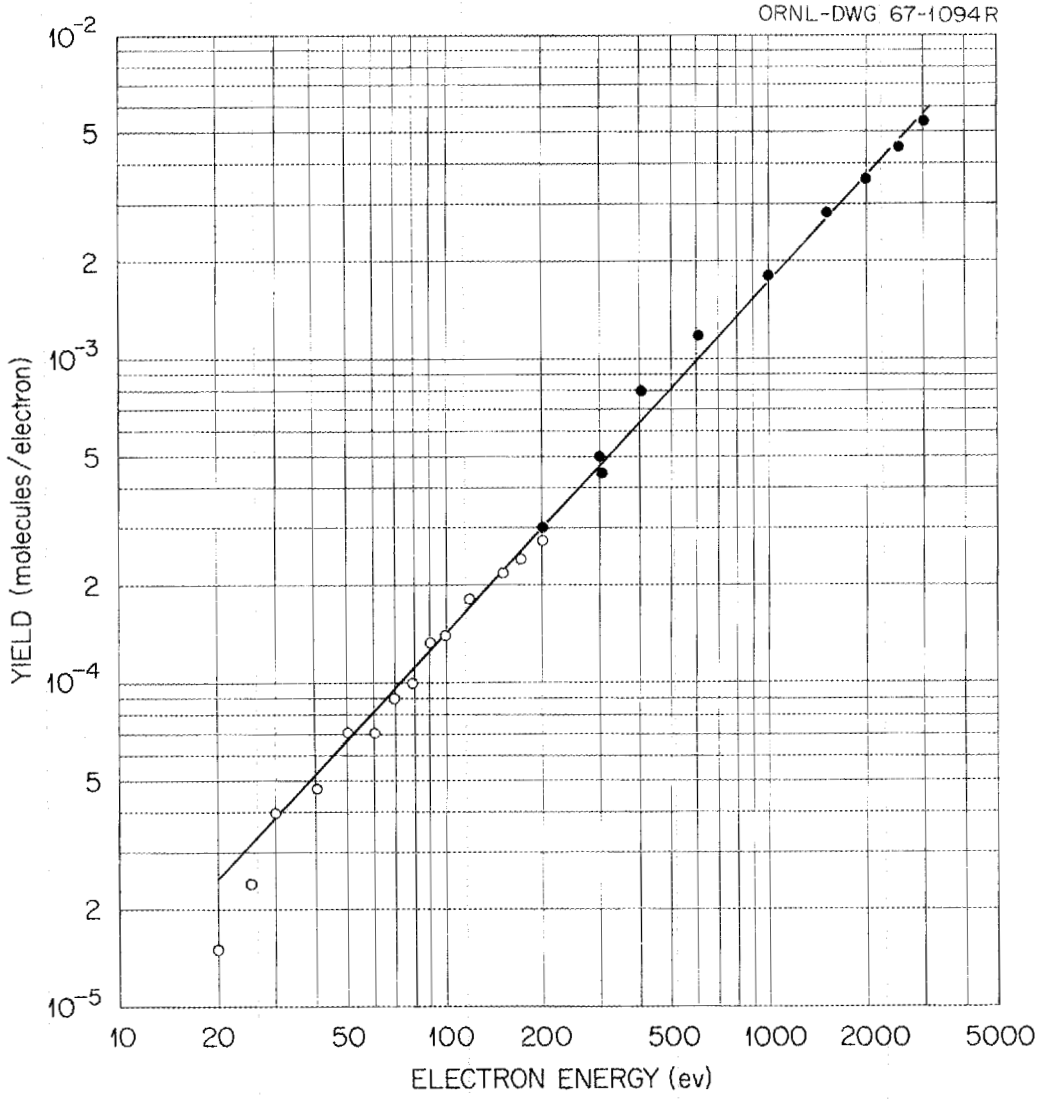

Figure 28. Electron bombardment induced desorption data for carbon monoxide from tungsten taken using the 0.0025-centimeter-thick target and a carbon monoxide pressure of 5×10^{-8} torr. [The desorption is nearly all due to thermal effects. Note that the desorption is proportional to the bombardment power (and therefore the temperature rise of the target during the bombardment pulse) for a very wide range of power. The bombardment current ranged from 5 to 20 microamperes per torr.]

pulses on the heavier target are down by a factor of 300, which is about what one would expect from the pressure effect shown in Figure 27, page 78, and an increase in the heat removal from the specimen by a factor of 10.

Mass Spectrometer Sensitivity

Figure 29 compares the mass spectrometer reading for the carbon-monoxide partial pressure with the ion gauge reading of the total pressure. The pressure was raised from the base pressure of 3.2×10^{-10} torr by leaking in carbon monoxide. The data indicate that the gas present at pressures above 10^{-9} torr was indeed mostly carbon monoxide and provides a pressure calibration for the carbon monoxide peak of the mass spectrometer. The sensitivity of the mass spectrometer for carbon monoxide was 0.18 ampere per torr for the conditions of this experiment, if the ion gauge sensitivity for carbon monoxide is assumed to be unity. The mass spectrometer sensitivity varied, depending upon the particular condition of the electron multiplier, and it was necessary to determine its sensitivity before each series of measurements. Usually this was accomplished after the adsorption of carbon monoxide on the target at a pressure of 10^{-8} torr or higher.

Measurement of the Amount of Carbon Monoxide Adsorbed on the Target

The amount of gas adsorbed on the target can be measured as indicated in Chapter III, "Measurement of Neutral Gas Produced by EBID," page 68, steps eight and thirteen and are discussed in Appendix B, page 128. Measurements made in the present apparatus are consistently

ORNL-DWG 69-2077

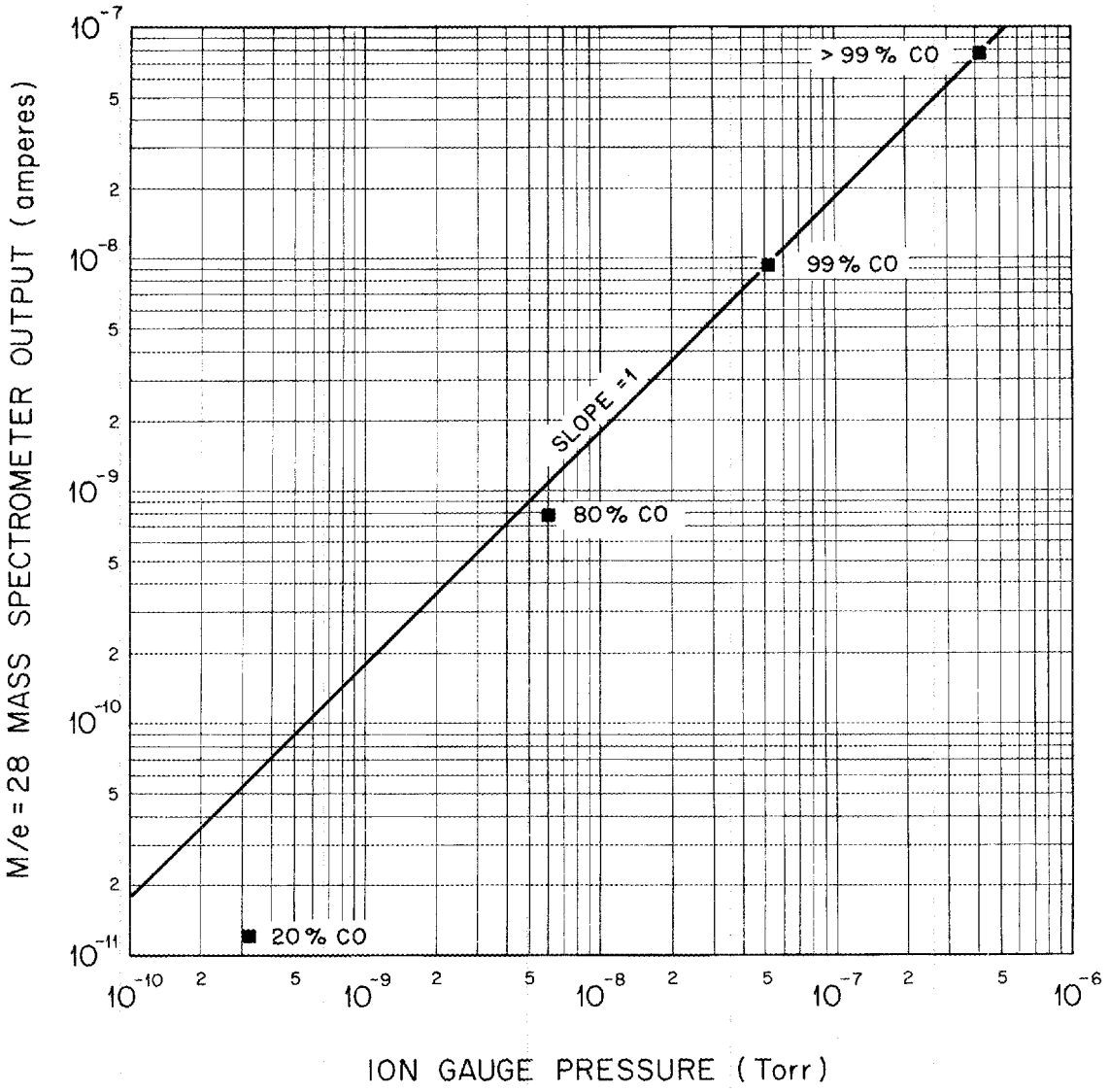

Figure 29. A typical calibration curve for the mass spectrometer output signal as a function of the pressure indicated on the chamber ion gauge. (Carbon monoxide was admitted to the system to raise the pressure.)

lower than the values reported in Table II, page 40, from the literature. Values between 1.5 and 1.8×10^{14} carbon monoxide molecules per square centimeter for full coverage were obtained on adsorption at pressures of about 1×10^{-8} torr and on desorption after exposure at the system base pressure for about 1 hour. The literature values range from these values to 9.5×10^{14} molecules per square centimeter for full coverage. Most values were obtained at pressures considerably higher than the present measurements. The possible reasons for this discrepancy are discussed in Chapter V, page 89. Values were also measured for nitrogen and hydrogen and are compiled along with the values for carbon monoxide and the range of literature values for all three gases in Tables IV and V. The values obtained in this investigation are lower for all three gases, but not by the same ratio. The values for hydrogen and nitrogen are in better agreement with the literature than the carbon monoxide values, as might be expected from the discussion in Chapter V, regarding the possible errors in adsorption measurements for carbon monoxide.

Figure 30 shows qualitatively the way in which the thermal desorption spectra can be used as a means of measuring the kind and amount of gas present on target after an EBID run. The figure shows three sets of desorption spectra. The mass spectrometer partial pressure indication is plotted increasing upward, and the total pressure is plotted increasing downward so that they are easily compared by their symmetry. The first case shows desorption from a specimen with mostly hydrogen on it. The

TABLE IV

FULL COVERAGE VALUES FOR CARBON MONOXIDE ON TUNGSTEN AT 300°K

Maximum Coverage (Molecules/cm^2)	Author	Specimen	Pressure (torr)	Reference
$\times 10^{14}$				
10	Madey *et al.*	Polycrystal Wire	4×10^{-6}	66
10	Nasini *et al.*	Polycrystal Sheet	NA[a]	74
α 0.5 β 9.0	Redhead	Polycrystal Wire	5×10^{-9}	67
7.5	Anderson and Estrup	(100) Crystal	4×10^{-9}	75
α 2 β 5	Ehrlich	Polycrystal Wire	NA	61
6.5	Becker	(411) Plane Ribbon	NA	76
5.3	Eisinger	(311) Plane Ribbon	NA	77
5	Schlier	Polycrystal Wire	NA	78
~4	Degras			79
3.5	Ehrlich	Polycrystal Wire	NA	80
α ~1	Yates *et al.*	Polycrystal Ribbon	NA	43
α 1.1 β 3.6	Rigby	Polycrystal Wire	5×10^{-8}	81
α ~0.1 β ~1.8	Rigby	Polycrystal Wire	b	81
α 0.1 β 1.5	Clausing	Polycrystal Sheet	c	Present Study

[a]Information Not Available

[b]After initial exposure at 5×10^{-8} torr, the surface was exposed to a lower pressure $< 1 \times 10^{-10}$ torr for 15 hours.

[c]Initial exposure at 1×10^{-8} followed by approximately one hour at CO pressures $< 10^{-10}$ torr.

TABLE V

FULL COVERAGE VALUES FOR NITROGEN AND HYDROGEN ON TUNGSTEN AT 300°K

Maximum Coverage (atoms/cm^2)	Author	Specimen	Pressure (torr)	Reference
$\times 10^{14}$				
		Nitrogen		
6 or 7	Eisinger	Sheet (113)	NA[a]	77
very small 4.3	Delchar and Ehrlich	(110) (100)		82
4	Estrup and Anderson	(100) Crystal	NA	83
~3[b]	Redhead	Polycrystal Wire	5×10^{-9}	84
2.5 1.5	Madey and Yates	(100) (110)	NA	85
α 0.06–0.12 β 2.5	Ehrlich	Polycrystal Wire	6×10^{-8}	86
β 1.5	Rigby	Polycrystal Wire	NA	81
β 1	Clausing	Polycrystal Sheet	c	Present Study
		Hydrogen		
23	Estrup and Anderson	(100) Crystal	10^{-9}–10^{-7}	87
12	Rigby	Polycrystal Wire	$> 10^{-8}$	88
10	Redhead	Polycrystal Wire	5×10^{-9}	84
9	Hickmont	Polycrystal Wire	1×10^{-7}	89
8.3	Ricca *et al.*	Polycrystal Sheet	5×10^{-6}	90
7	Eisinger	(113) Crystal	NA	91
7	Eisinger	Polycrystal Sheet	NA	91

TABLE V (Continued)

Maximum Coverage (atoms/cm^2)	Author	Specimen	Pressure (torr)	Reference
6	Rigby	Polycrystal Wire	d	88
6	Clausing	Polycrystal Sheet	e	Present Study

[a]Information Not Available.

[b]These data were obtained at 360°K.

[c]A saturated monolayer was adsorbed at $\sim 2 \times 10^{-8}$ torr and desorbed after approximately ten minutes exposure at a nitrogen pressure of $< 5 \times 10^{-10}$ torr.

[d]A wire with the saturation coverage was pumped at 2×10^{-10} torr for ten minutes and lost 50 per cent of its hydrogen.

[e]Gas was adsorbed at about 2×10^{-8} torr and then the pressure was reduced to $\sim 5 \times 10^{-10}$ torr of hydrogen.

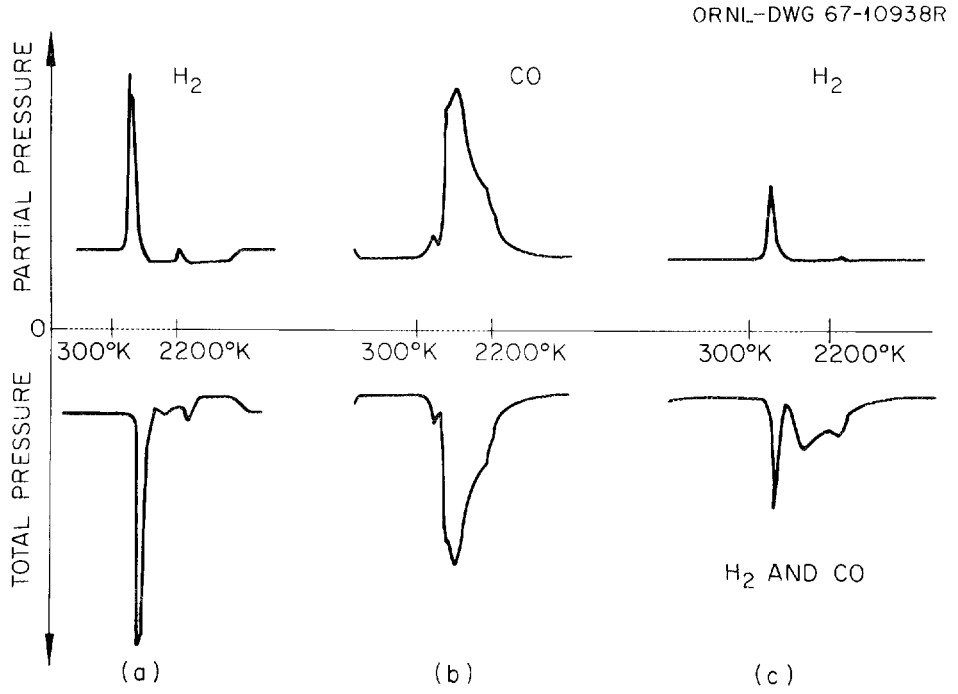

Figure 30. Thermal desorption spectra. [Three examples are given showing desorption from a target covered with (a) mostly hydrogen, (b) mostly carbon monoxide, and (c) a mixture of hydrogen and carbon monoxide.]

hydrogen comes off at 400 to 600° K as the target ribbon is heated. The second case shows mostly carbon monoxide on the target. It begins to come off rapidly at about 1000° K and is largely desorbed before the target reaches 1800° K (desorption of carbon monoxide at about 400 to 500° K is also observed). The final spectra show a case of both carbon monoxide and hydrogen in more nearly equal amounts. The amplitude and duration of the pressure pulses can be related to the amount of gas on the surface. The act of flashing the filament to determine its surface gases, of course, removes the gases from the surface.

Figure 31 shows a pair of adsorption-desorption measurements for carbon monoxide on tungsten. Figure 31(a) shows: (1) the admission of gas starting at the point (0), (2) the relatively constant pressure during the major part of the adsorption, and (3) the increase in pressure and gradual approach to a new constant pressure as the surface is completely covered. The final system pressure is determined according to Equation (2), page 42, by the gas influx from the carbon monoxide leak valve and the volumetric speed of the pumping system. Figure 31(b) shows the desorption. The temperature increase was controlled so that the pressure did not exceed 2×10^{-7} torr and was not linear with time as shown by the approximate temperatures indicated on the chart. The quantity of gas adsorbed by the specimen in Figure 31(a) is shown by the cross-hatched region. The quantity desorbed in Figure 31(b) is similarly shown. The equality of these quantities of gas (areas on the figures) is a necessary but not sufficient condition to ensure that the measurement is accurate.

ORNL-DWG 69-2066

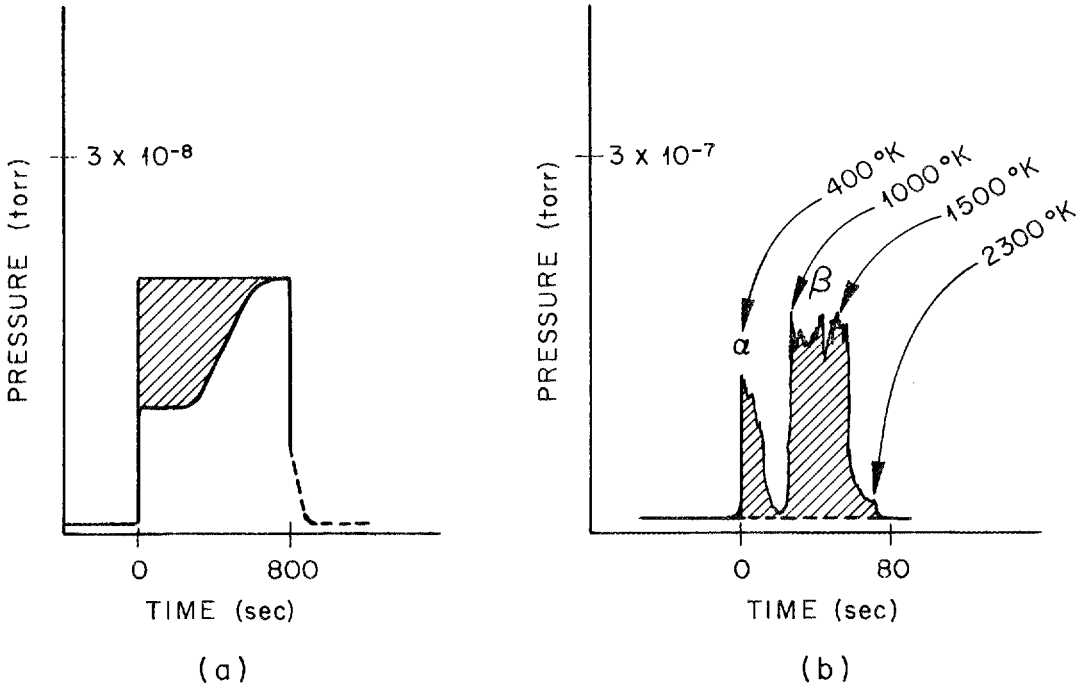

Figure 31. Carbon monoxide pressure as a function of time during (a) adsorption of the gas onto a clean tungsten target and (b) thermal desorption of the gas from the target. [Note the scale change on (b).]

CHAPTER V

DISCUSSION OF THE RESULTS

The Effect of Electron Energy on the Desorption Cross Section

The thermal desorption data of Figure 26, page 75, and the data of Figure 27, page 78, clearly indicate that thermal effects accompanying the electron bombardment are not important below about 5,000 electron volts for the conditions under which the data of Figure 26 were obtained. The shape of the curve for energies up to 100 electron volts suggests that the mechanism for desorption here may be the one proposed by Menzel and Gomer[9] or Redhead[32] and discussed briefly in Chapter II, page 27. Additional explanations are required for the desorptions above 100 electron volts. The mechanisms of Redhead, Menzel, and Gomer require the initial excitation of the adbond in the form of an electronic transition. The interactions are thus basically electron-electron interactions. They should have cross sections that behave qualitatively in the same manner as similar transitions in free molecules. This should certainly be true for adbonds that have localized electrons, as for example those having a predominantly covalent nature. The common gas-phase transitions have cross sections that have thresholds between 10 and 20 electron volts, peak at 100 electron volts, or less, and decrease slowly as the electron energy further increases. Figure 5, page 15, includes a curve for the ionization cross section of atomic oxygen in the gas phase that shows the

typical energy dependence. Redhead's data for ion desorption from oxygen adsorbed on molybdenum (see Figure 5) follows this pattern closely with a threshold at 17.6 electron volts and a maximum at 100 electron volts. His data for carbon monoxide on tungsten have the proper shape below 100 electron volts but continue to increase from 100 electron volts to 300 electron volts. (See Figure 7, page 18.) Lichtman and McQuistan's data for the desorption of protons from stainless steel show the same form at low energies (see Figure 10, page 22) – no data at intermediate energies, but increasing desorption cross sections from about 400 electron volts to above 6,000 electron volts (see Figure 11, page 23). Lichtman and McQuistan also show data for the desorption of Na^+ and Cl^+ with thresholds in the desorption cross sections at 12 and 20 electron volts, respectively, and peaks at 20 and 40 electron volts.[36] These cross sections fall quickly with increasing voltage. From the above evidence it would appear that this desorption mechanism with its predicted characteristics has indeed been experimentally observed, but that only part of the experimental data show decreasing cross sections with increasing energy above 100 electron volts. It should also be noted that the Na^+ desorption should have a very low cross section according to Menzel and Gomer's discussion, but experimental data indicate a rather large cross section.

The present data indicate a threshold for EBID of neutral molecules of carbon monoxide from tungsten in the neighborhood of 20 electron volts. The presence of this threshold for neutral desorption at the same energy as that found for the formation of ions is evidence that the theoretical

treatment is applicable and that the neutrals and ions come from the same initial electronic processes. If better measurements could be made to accurately determine the threshold for neutral desorption, it would be possible to determine if all neutral desorption depended upon an ionized state or if an antibonding state may also be involved. The desorption efficiency rises rapidly to about 100 electron volts, rises only slowly to 200 electron volts, and then more rapidly to 400 or 500 electron volts as though a second desorption process was becoming important. Finally, it rises again at about 5,000 electron volts due to other effects. Figure 32 shows how the data of Figure 26, page 75, could be obtained by adding the effects of several separate desorption phenomena.

Curve I is due to the desorption of neutrals probably by the electron excitation process described and measured by Redhead.[33] This curve is really the sum of desorption from two states according to Redhead, and they are shown by the dotted curves $I_{(1)}$ and $I_{(2)}$. Curve $I_{(2)}$ contributes 90 per cent of the total represented by Curve I and is probably due to desorption from the state called the alpha phase by Redhead,[33] which was described in Chapter II, page 39. This desorption is characterized by its threshold at 18 electron volts and the associated desorption of O^+ ions with an average kinetic energy of 6 electron volts. Curve $I_{(1)}$ is probably due to desorption from the so-called virgin state and has a threshold at about 15 electron volts, and Curve II results from an hypothesized second mechanism as yet undefined. The characteristics of this intermediate process would require a threshold of

ORNL-DWG 69-2075

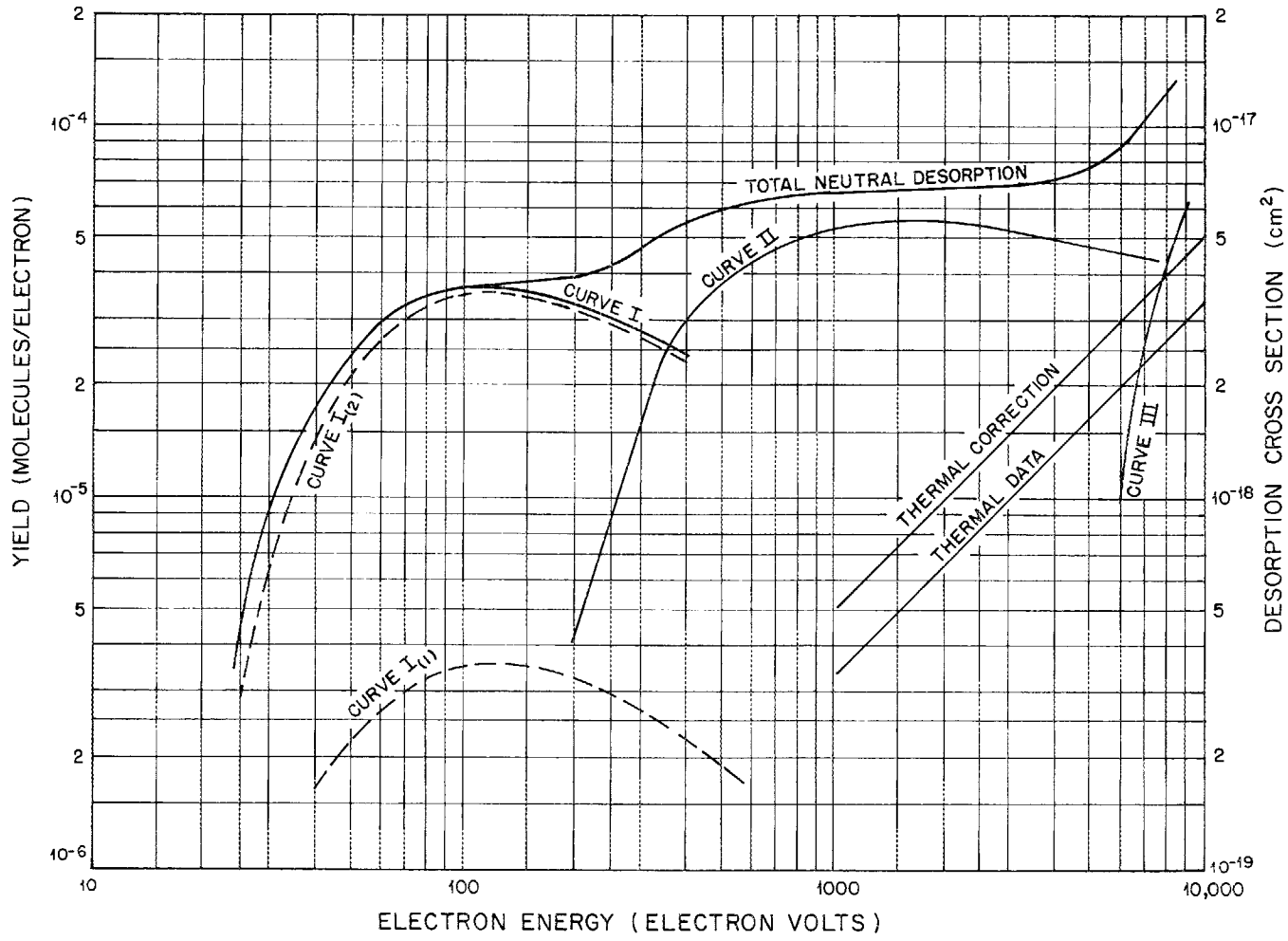

Figure 32. An analysis of the EBID data of Figure 26. (The curve is broken into three regions based on the arguments presented in the text. Each is dominated by a separate desorption process.)

approximately 100 electron volts with a maximum or plateau reached at 500 to 1,000 electron volts.

There are several candidates for this intermediate desorption process, and it is not possible to make a definitive choice at this time. One logical process to consider would be another electron excitation process involving either the activation of higher excited states from the adsorbed states that produce the desorption of Curve I or the electronic excitation of molecules from one or more of the beta states. It is tempting to associate this intermediate process with the desorption of the more strongly held beta state, however, if the beta state is characterized by either the bridge bond or the lying-down mode shown in Table II, page 40, and if an initial electronic excitation process such as Menzel and Gomer's or Redhead's is involved, two bonds would have to be broken by one excitation process to liberate the molecule. This may be possible since the bonding electrons in the bridge bond and perhaps even in the lying-down mode may interact strongly enough with each other and the electrons in the molecule that the whole assembly can be treated as a single entity. There is more than enough energy available to break the beta state bonds from the same excited state that produces the desorption shown in Curve I. According to the paper of Menzel and Gomer,[9] the more tightly bound or the closer the adsorbate is held to the surface the less likely it is to be desorbed. This argument applies to desorption following initial excitation to any energy level. The essence of the argument is that the desorption probability is proportional to the time required for the transition back to the ground state. This time

is in general shorter to more tightly bound states and for closer adsorbate spacings (all of the beta states are more tightly bound and held closer to the surface than the alpha state). The preceding argument would suggest that Curve II is more likely to be due to increased desorption from the alpha phase as the result of the electron impact excitation of an additional ionization or antibonding electronic state than to desorption from the chemisorbed beta state. It is doubtful, however, that the threshold for such an additional electronic excitation would be as high as indicated by Curve II or that its excitation cross section would be large enough to allow it to account for the desorption indicated by Curve II (based on a comparison with ionization and excitation phenomena in the gas phase).[92] This kind of desorption process cannot, however, be ruled out by presently available information.

A second possible explanation concerns the desorption caused by secondary and reflected primary electrons. These electrons leave the surface after the primary impact, but return to the target because of the electric fields near the target. Thus they have two chances to cause desorption. The secondary electron production is energy dependent in a way that matches the requirements of Curve II. The yield of secondaries and reflected primaries is slightly more than unity for electrons of 500 to 1,000 electron volts incident on tungsten.[93,94] Although most of the secondaries have energies below the threshold for causing desorption, a significant fraction (30 to 50 per cent) of the sum of reflected primaries and secondary electrons have energies above 50 electron volts. Since these electrons have two chances to cause desorption

they would nearly double the desorption and could account for all of the increased desorption for primary electrons incident on the surface with more than 200 electron volts of energy. Although there is insufficient data to make an accurate calculation, it is reasonable to assume that the increase in high energy secondaries and the reflected primaries are responsible for the factor of 2 increase in yield observed in the 300 to 1,000 electron volt range.

A third possibility, which should be discussed, is that a momentum transfer process is becoming important in this energy range. This seems unlikely, however, since the maximum energy transferred to the adsorbed molecule is given by

$$E_T = E_o \frac{4 \times \text{Mass of the electron}}{\text{Mass of the CO molecule}} = \frac{E_o}{12,850} , \tag{5}$$

where

E_T = energy transferred to an essentially free molecule,

E_o = the energy of the incident electron.

If E_o is 1,000 electron volts, E_T is one-thirteenth electron volt, which is about three times the average thermal energy of the molecule at 300°K. On the average a molecule receives this amount of energy perhaps 10^{11} times a second due to thermal fluctuations, assuming a frequency factor of 10^{13} in the Arrhenius relation

$$K = \nu \exp(-E/RT) , \tag{6}$$

where

K = the rate of reaction,

ν = the frequency factor,

E = the energy for activation of the reaction.

Even if ν were to be reduced to 10^3 for carbon monoxide adsorbed on tungsten as has been suggested by Pétermann,[95] the carbon monoxide molecule would receive one-thirteenth electron volt of energy about thirty times a second. The cross section (σ_s) for the electron interaction is given approximately by Evans[96] as

$$\sigma_s = 3 \times 10^{-15} \times \frac{Z^2}{E_o^{\ 2}} \text{ cm}^2 , \tag{7}$$

where

Z = atomic number of the atom

$Z^2 = (Z_1^2 + Z_2^2)$ for a diatomic molecule.

This leads to a cross section of about 3×10^{-18} square centimeters for a 1,000 electron volt electron using $Z^2 = 16^2 + 12^2 = 400$. Thus the average carbon monoxide molecule might be given one-thirteenth electron volt of energy every 10,000 seconds due to electron bombardment if the current is 10^{-4} ampere per square centimeter. Any momentum transfer effect should, therefore, be negligible at this electron energy.

Of the explanations offered to explain Curve II, the one involving secondary and reflected electrons appears to be most likely, but a new electronic excitation process followed by desorption cannot be completely ruled out. A measurement of the secondary and reflected primary electron yields and energies should be made to resolve this situation. It would also be helpful if ion desorption measurements of the kind made by Redhead were available to compare with the neutral particle data in this energy range.

It is possible that Curve III represents another new desorption process, but it seems more likely that it is an artifact produced by field emission in the apparatus at the high voltages. High voltage breakdown occurred occasionally at voltages above 8,000 volts.

Electron Bombardment Induced Desorption as a Function of Pressure

Figure 27, page 78, indicates that the total desorption of neutral carbon monoxide molecules is not a very strong function of pressure for 500 electron volt electrons. If the EBID desorption is corrected for thermal effects, the yield is independent of pressure in the range 10^{-10} to 10^{-8} torr. If we assume that Redhead is right in his analysis and that 90 per cent of the carbon monoxide comes from the alpha phase, we can conclude that the concentration of the alpha phase is not very pressure sensitive in the 10^{-7} to 10^{-10} torr range and/or that desorption proceeds very, very slowly from an already formed alpha phase at 300°K. Both these conclusions are consistent with the desorption energy of 25 kilocalories per mole (or 1.1 electron volts per molecule) reported by Redhead.

Thermal Desorption as a Function of Pressure

Figure 27, page 78, shows the thermal desorption of carbon monoxide produced by a small change in the target temperature. The average ΔT caused by the ohmic heating is about 0.7°K at about 300°K. Yet the thermal desorption from the target was detectable down to ambient pressures of 10^{-10} torr. The change in carbon monoxide pressure was, however, less than 2 per cent of the total carbon monoxide pressure at

these pressures. The data have quite a bit of uncertainty; however, it seems that the height of the desorption pulse varies approximately as the square root of the pressure, which implies that the concentration of the adsorbing species also varies in the same manner. No special significance is placed on the square root relationship; there is no reason to predict such a dependence, and the data at low pressures are at the limit of sensitivity of the apparatus and are thus not too accurate. It is significant that the corrected EBID desorption did not change appreciably as the pressure was increased above 10^{-10} torr. This implies that the state responsible for the electron impact desorption is not a function of pressure in this range and therefore that it is not the same state responsible for the thermal signal unless the phase has a relatively large population and a considerable range of desorption energies. It is possible, for example, that there are a few alpha adsorption sites with low activation energies of desorption while the most of the sites have somewhat higher activation energies for desorption. The low energy sites could respond to pressure changes while the higher energy sites remained filled. At this time it is a moot point whether or not to call the low energy sites a separate state. The question could be resolved by knowing if there is a continuous distribution of activation energies of desorption. This could be determined by making a series of measurements such as those in Figure 27, page 78, as the target temperature was slowly increased. In this same manner differential heats of adsorption could also be obtained. Small but measurable quantities of gas were adsorbed during the increase of the carbon monoxide pressure from 6×10^{-9} to 5×10^{-8} torr. One may

not be sure, however, that this was all or even largely adsorbed on the target. Hobson and Earnshaw[97] have observed that carbon monoxide adsorption on vacuum system surfaces may be appreciable when the pressure is changed. This is discussed under the next heading.

Quantity of Gas Adsorbed on the Target at 300°K

Table IV, page 83, shows that the amount of carbon monoxide adsorbed on the target in these experiments was considerably smaller than that measured by other investigators, but that there is also quite a bit of scatter in the literature values. There are several factors that may contribute to both the low values reported here and to the scatter in the literature.

Rigby[81] has shown that the population of both the alpha state and the beta states change with the ambient pressure. A monolayer adsorbed at 5×10^{-8} torr of carbon monoxide has its alpha phase reduced by 90 per cent in just a few minutes and the beta phases reduced by about 20 per cent in 1 hour (and 50 per cent in 15 hours) when the ambient pressure was reduced to his system base pressure of 5×10^{-10} torr (probably $<5 \times 10^{-11}$ torr CO) with his sample at 300°K.

Small differences in the temperature of the sample immediately before the thermal desorption could certainly cause significant differences in the population of the alpha state and perhaps the beta states.

Low energy electron diffraction studies[75,98] have shown that there is a considerable difference between carbon monoxide adsorption on the tungsten (110) surface and the (100) surface. It appears that alpha

and β_1 phases are adsorbed on a macroscopic (110) surface and only β_2 and β_3 states are adsorbed on a macroscopic (100) surface. Redhead[67] and others have also pointed out the obvious importance of the structure of the crystal surfaces to adsorption.

Hobson and Earnshaw[97] have recently pointed out that the use of transient pressure measurements to obtain quantitative adsorption-desorption data may cause substantial errors due to adsorption and desorption from the vacuum system itself. This problem has been recognized by others, but has usually been assumed to be small and no attempts were made to include these effects in their qualitative results. Hobson and Earnshaw have shown that in their system the errors were large for carbon monoxide, considerably smaller but still easily detectable for hydrogen, and negligible for helium, argon, nitrogen, and methane at room temperature. In their apparatus there were, however, large surface areas, small conductances, small pumping speeds (due only to ion gauges), and relatively large pressure changes – that is, two orders of magnitude or more, all of which increase the effect of adsorption on the vacuum system walls.

The importance of this "surface phase" adsorption on system walls is not easy to assess even qualitatively for most of the measurement techniques used to obtain the data in Tables IV and V, pages 83 and 84, because there are two opposing effects. For example, all flash filament techniques involve heating the specimen and measuring the pressure rise

as the sample temperature increases. The act of flashing the filament produces not only thermal desorption from the specimen but also two secondary effects:

1. The system walls are heated slightly by radiant heat.
2. The gas pressure rises, resulting in adsorption onto the system walls.

The first effect would tend to cause the measurement of the desorbed gas to be too large while the second effect would make it too small. It is not possible to determine the magnitude of either of these effects in any simple manner. However, most investigators were aware of these effects and attempted to minimize errors due to them by design and the choice of experimental procedures.

It is tempting to say that the disagreement in the literature is due to real differences in the samples and measurement conditions and that the errors due to the adsorption and desorption of gases from the system walls were not large. This seems likely to be the case, but it cannot be adequately defended since in all cases the tungsten specimen area was 1 per cent or less of the exposed surface area in the working volume; consequently, small changes in the coverage of the system walls would produce large measurement errors.

It is possible to generalize to say that if thermal effects on the gases adsorbed on the vacuum walls are most important the values reported in the literature will be too large, but that if the other effect

dominates — that is, the vacuum system walls act as a source or sink for carbon monoxide as the pressure decreases or increases, the literature values will be too low.

In the present experiment the thermal effects were avoided during the adsorption measurements, because the sample was cleaned by flashing at low pressures, and carbon monoxide was suddenly introduced after the system had returned to ambient temperatures. The amount of adsorption of the system walls due to the pressure change could be measured by causing the sudden pressure change with the tungsten specimen already covered with gas at the lower pressure. The gas adsorbed by the specimen and system under these conditions was less than 5 per cent of the adsorption observed with the specimen flashed clean before the gas admission for the conditions investigated, which approximated those used in the coverage determinations. The desorptions in the reported series of measurements were carried out starting at the system base pressure and raising the specimen temperature at a rate that was adjusted to keep the gas pressure at either 5×10^{-8} or 5×10^{-9} torr. Hence, the pressure rise was limited, but the time the specimen was hot was increased. The amounts adsorbed usually agreed within 20 per cent of the amount desorbed.

An examination of the experimental procedure outlined above indicates that the errors in the adsorption measurement due to this cause would give numbers larger than the true values by as much as 5 per cent and that the errors on desorption could be in either direction.

Other errors affecting the coverage measurements are discussed briefly in the next section. The author estimates that the data for

coverage should be accurate to within much better than a factor of 2 and concludes that the discrepancy with the literature is due either to an actual difference in the specimens and measurement conditions, or to errors in the literature values.

Measurement Errors

The previous section has discussed the errors due to "surface phases" in detail and concluded that they were not large in the present study. These errors should be less important for the EBID neutral particle measurements than for coverage measurements. Two points should be emphasized for this case:

1. There are no significant thermal effects accompanying the EBID measurements at low pressures, and the effects at high pressures are limited to the specimen itself (the specimen holders and other parts of the system experience a completely insignificant temperature change).
2. The pressure changes are short and are quite small ranging from 0.1 to 20 per cent of the ambient pressure [except for a few points taken at low pressures (10^{-10} torr) and high voltages where pressure increases were 100 per cent above ambient].

Other measurement errors are discussed briefly below and, except as noted, apply equally to the measurements of coverage and those of neutral molecule desorption during EBID.

1. The ion gauges were not calibrated. They are usually accurate to ±20 per cent of the true pressure when corrected for the gauge sensitivity for the gas being measured. The three gauges on the system agreed with each other to within ±10 per cent.
2. The pumping speed for gas removal was 10 liters per second through an orifice. The pressure drop across the orifice was usually more than a factor of 10 so that this number should be accurate to within 10 per cent even with no correction for the partial pressure on the downstream side of the orifice.
3. It is possible that the ion gauges in the system have a small pumping speed for carbon monoxide, but this should be considerably less than 1 liter per second (10 per cent of the total gas removal rate) in any case.
4. The sample area could be measured accurately, but it is possible that end effects could decrease the effective area of the sample for the thermal desorption-adsorption measurements by 10 to 20 per cent. This would not produce an error in the EBID measurements.
5. Carbon monoxide molecules desorbed in excited states or with significant kinetic energy or ions desorbed by EBID could interact with gases adsorbed on the vacuum walls and produce erroneous measurements either higher or lower than the true

value depending upon the type of wall interaction. No assessment of the magnitude of this error has been attempted, but it is assumed to be small.

No claim is made for the absolute accuracy of the data, but the results are reproducible within ±25 per cent or better. It seems unreasonable to expect that the summation of all of the errors mentioned above should produce a factor of 2 change from the true value for the EBID results.

CHAPTER VI

CONCLUSIONS AND RECOMMENDATIONS

Conclusions

As the result of this experimental study, the following conclusions may be made:

1. The technique developed measures reproducibly the neutral molecules desorbed by electron impact per se from a metal surface and is sensitive enough to permit frequent sampling of a surface without perturbing the surface gas-metal reactions to any significant extent.
2. The technique is compatible with other methods of studying gas-metal interactions. A combination of techniques including thermal desorption, low energy electron diffraction, secondary electron measurements, and electron-induced ion desorption with the electron-induced neutral desorption seems both feasible and desirable.
3. The desorption of neutral carbon monoxide molecules from tungsten as the result of electron bombardment has been measured at room temperature for electrons with energies between 25 and 8,000 electron volts. Between 3×10^{-6} and 6×10^{-5} molecules were desorbed per incident electron depending upon the electron energy.

4. The results in (3) agree with the predictions made by the indirect measurements of Redhead, Menzel and Gomer, and others and support the theoretical treatments of low energy electron desorption proposed by Redhead and by Menzel and Gomer for electron energies up to 100 electron volts.
5. A new contribution to the desorption process is indicated in the range from 100 to 3,000 electron volts. Several possible mechanisms are discussed, and it is suggested that the results are due to the increased production of reflected primary and energetic secondary electrons.
6. Thermal desorption is not an important desorption influence (for the particular conditions of this experiment).
7. It is possible to separate the desorption caused by thermal effects from the desorption due to direct electron interactions with the adsorbed layer. This is done by simulating the thermal effects by ohmic heating of the sample.
8. The desorption of neutral molecules by impact of 500 electron volt electrons is not very sensitive to the ambient carbon monoxide pressure between 10^{-10} and 10^{-7} torr as long as thermal effects are accounted for separately.
9. Very small increases in the sample temperature cause relatively large desorptions of carbon monoxide when the carbon monoxide pressures are above 10^{-8} torr. This points out a serious problem in the interpretation of flash filament experiments with carbon monoxide at pressures above 10^{-8} torr. Since

it is virtually impossible to eliminate the small changes in the temperature of the vacuum system that accompany the heating and cooling of the filament, it is difficult to separate desorption and adsorption on the filament from accompanying desorptions and adsorptions on the vacuum system walls.

10. Thermal desorption increases approximately as the square root of the pressure over the pressure range from 10^{-10} to 10^{-7} torr, indicating that significant quantities of loosely bound molecules are adsorbed and desorbed as the result of carbon monoxide pressure changes.

Recommendations

1. The mechanism contributing to the intermediate energy process should be investigated further. Toward this end several experiments are suggested. Measurements of the energy distribution and number of secondary and reflected primary electrons should be made as a function of the energy of the incident electron. Calculations could then be made to determine if the intermediate process is due entirely to this effect. A correlation of the neutral desorption data with ion desorption data from the same target during the same experimental run should be made to determine if new electronic excitation processes play any part in the desorption in this energy range. Measurements should be

made with the target temperature selected so as to eliminate the various adsorbed states one at a time until the mechanism is associated with one particular adsorption state. The use of single-crystal surfaces might also be valuable in reducing the number of adsorbed states present.

2. Other gases should be studied using combined ion and neutral desorption techniques. The preliminary results for neutral desorption of hydrogen from tungsten at 300°K reported in Appendix A, page 123, are a good case in point. The data do not display the same form as the carbon monoxide data. This indicates that the dominant desorption mechanisms may be quite different. The momentum transfer process should be observable in this system if it is not overshadowed by another mechanism. Experiments with the specimen near liquid helium temperatures using physisorbed hydrogen might be required.

3. Because electron beams can be directed to small preselected areas or scanned over the surface, it should be possible to measure the diffusion of adsorbates across a surface or the manner in which surface features or structures influence the behavior of adsorbates. Observations of the diffusion of gas from the bulk of the sample to the surface might be made. Perhaps grain boundary diffusion could be studied by the scanning techniques. By measuring the rate at which changes in surface concentrations occur as a function of

temperature the diffusion of some gases such as flourine might be explored in detail – that is, the activation energies could be determined for bulk, grain boundary, and surface diffusion. Depending upon the species to be observed, neutral particles, ions, or Auger electrons might be monitored. If Auger electrons were monitored it would be possible to study not only gaseous species but many other elements as well. In applications using a scanning beam, however, the intensity of the scanning beam required may be so high as to seriously alter the adsorbed state during the observation. This would lead to the necessity to reprocess the sample before the next observation and might in some cases complicate the interpretation of the results by converting one adsorbed state to another.

BIBLIOGRAPHY

BIBLIOGRAPHY

1. G. E. Moore, "The Ionization of Adsorbed Gas by Impact of Slow Electrons," 1959 Sixth National Symposium on Vacuum Technology Transactions (New York: Pergamon, 1960), pp. 16–9.

2. Gert Ehrlich and G. F. Hudda, "Promoted Field Desorption and the Visibility of Adsorbed Atoms in the Ion Microscope," The Philosophical Magazine, 8:1587–91, 1963.

3. B. J. Todd, J. L. Lineweaver, and J. T. Kerr, "Outgassing Caused by Electron Bombardment of Glass," Journal of Applied Physics, 31:51–5, 1960.

4. P. A. Redhead, "The Effects of Adsorbed Oxygen on Measurements with Ionization Gauges," Vacuum, 13:253–8, 1963.

5. P. A. Redhead, "Desorption of CO and O^+ from Polycrystalline Mo Surfaces by Slow Electron Impact," Applied Physics Letters, 4(9):166–7, 1964.

6. David Lichtman, "Adsorption–Desorption of Residual Gases in High Vacuum," The Journal of Vacuum Science and Technology, 2:70, 1965.

7. G. E. Fischer and R. A. Mack, "Vacuum Design Problems of High Current Electron Storage Rings" (paper presented at the Eleventh Annual Symposium of the American Vacuum Society, Chicago, Illinois, September 30–October 2, 1964).

8. L. A. Pétermann, "Gas Desorption Efficiency under Electron Bombardment," Supplemento al Nuovo Cimento, 1:601–11, 1963.

9. Dietrich Menzel and Robert Gomer, "Desorption from Metal Surfaces by Low-Energy Electrons," The Journal of Chemical Physics, 41(11):3311–28, 1964.

10. R. E. Clausing, Exploratory Experiments Concerning the Desorption of Gases by Bombardment with Electrons, ORNL-TM-1166, Oak Ridge National Laboratory Report, November 1965.

11. L. H. Germer, "Low-Energy Electron Diffraction," Physics Today, 17:19–23, 1964.

12. J. T. Mark, Electron "Scrubbing" of High-Vacuum Systems, IEN-2908, Radio Corporation of America Engineering Note, 1965.

13. W. G. Henderson and J. T. Mark, "A Pumping System and Single-Wall Chamber for 10^{-13} Torr" (paper presented at the 12th National Vacuum Symposium of the American Vacuum Society, New York, September 28–October 1, 1965).

14. A. J. Dempster, "A New Method of Positive Ray Analysis," The Physical Review, 11(4):316–25, 1918.

15. F. E. Dart, "Evaporation of Zinc and Zinc Oxide under Electron Bombardment," The Physical Review, 78(6),761–4, 1950.

16. R. H. Plumlee and L. P. Smith, "Mass Spectrometric Study of Solids I. Preliminary Study of Sublimation Characteristics of Oxide Cathode Materials," Journal of Applied Physics, 21:811–9, 1950.

17. G. E. Moore and W. T. Hughes, "Dissociation of Solid Compounds by Electron Bombardment," The Physical Review, 99:1643–4, 1955.

18. G. E. Moore, "Dissociation of Solid SrO by Impact of Slow Electrons," Journal of Applied Physics, 30(7):1086–1100, 1959.

19. P. Wargo and W. G. Shepherd, "Electron-Bombardment-Induced Dissociation of Alkaline Earth Oxides," The Physical Review, 106(4):694–703, 1957.

20. J. R. Young, "Evolution of Gases and Ions from Different Anodes Under Electron Bombardment," Journal of Applied Physics, 31(5): 921–3, 1960.

21. G. E. Moore, "Dissociation of Adsorbed CO by Slow Electrons," Journal of Applied Physics, 32(7):1241–51, 1961.

22. D. A. Degras, L. A. Pétermann, and A. Schram, "Investigation of Gas-Solid Interactions by Electron Bombardment," 1962 Transactions of the Ninth National Vacuum Symposium of the American Vacuum Society (New York: Macmillan, 1962), pp. 497–501.

23. D. A. Degras, "Etude des Phenomenes de Sorption par Bombardements Electroniques," Symposium on Electron and Vacuum Physics, Balatonfoldvár, Hungary, 1962 (Budapest: Akadémiai Kiadó, 1963), pp. 101–11.

24. L. A. Pétermann, "Relative Contributions of Surface and Bulk Gas to the Outgassing Rate of Pure Nickel at Very Low Pressures," Physik und Technik von Sorptions- und Desorptionsvorgängen bei neideren Drücken Vortrag des 2. Europäischen Symposium "Vakuum," Frankfurt am Main, 1963 (Taunus, Germany: R. A. Lang Verlag, 1963), pp. 157–68.

25. P. Marmet and J. D. Morrison, "Second Reactions in the Ion Chamber of a Mass Spectrometer," The Journal of Chemical Physics, 36:1238, 1962.

26. W. D. Davis, "Sputter-Ion Pumping and Partial Pressure Measurements Below 10^{-11} Torr," 1962 Transactions of the Ninth National Vacuum Symposium of the American Vacuum Society (New York: Macmillan, 1962), pp. 363–70.

27. J. L. Robins, "Mass Peaks from Adsorbed Gases in a Single-Focusing Mass Spectrometer," Canadian Journal of Physics, 41:1385–7, 1963.

28. P. A. Redhead, "Variations in the 'X-Ray Limit' of Hot-cathode Gauges," Vacuum, 12:267, 1962.

29. T. E. Hartman, "Anomalous Residual Currents in the Ultrahigh Vacuum Use of Bayard-Alpert Ionization Gauges," The Review of Scientific Instruments, 34(11):1190–5, 1963.

30. W. C. Schuemann, J. L. deSegovia, and D. Alpert, "Effects of Electron-Surface Interaction in Ionization Gauges," 1963 Transactions of the Tenth National Vacuum Symposium of the American Vacuum Society (New York: Macmillan, 1963), pp. 223–7.

31. S. Garbe, "Desorption Process in Ionization Gauges During Bombardment of Oil Covered Surfaces with Slow Electrons," Vakuum-Technik, 12:201–5, 1963.

32. P. A. Redhead, "Interaction of Slow Electrons with Chemisorbed Oxygen," Canadian Journal of Physics, 42:886–905, 1964.

33. P. A. Redhead, "Electron-Impact Desorption of Carbon Monoxide from Tungsten," Supplemento al Nuovo Cimento, 5(2):586–97, 1967.

34. Dietrich Menzel and Robert Gomer, "Desorption from Surfaces by Slow-Electron Impact," The Journal of Chemical Physics, 40:1164–5, 1964.

35. David Lichtman, "Mass Spectrometer System for Beam Surface Interaction Studies" (paper presented at the Eleventh Annual Conference on Mass Spectrometry and Allied Topics, San Francisco, California, May 19–24, 1963).

36. David Lichtman and R. B. McQuistan, "Slow Electron Interaction with Adsorbed Gases," Progress in Nuclear Energy Series IX. Analytical Chemistry (Vol. 4, New York: Pergamon, 1965), pp. 95–135.

37. David Lichtman, "Electron Induced Surface Ionization Mass Spectrometry" (paper presented at the 12th Annual Conference on Mass Spectrometry and Allied Topics, Montreal, Canada, June 7–12, 1964).

38. David Lichtman and T. R. Kirst, "Electron Probe Study of Fluorine-Contaminated Titanium," The Journal of Vacuum Science and Technology, 3:224, 1966.

39. David Lichtman and T. R. Kirst, "Electron Probe Surface Mass Spectrometry Study of Oxygen on Molybdenum," Physics Letters, 20(1):7–9, 1966.

40. David Lichtman, T. R. Kirst, and R. B. McQuistan, "Some Observations on the Reactions of H_2 and CO on 100 Nickel," Physics Letters, 20(2):129–30, 1966.

41. David Lichtman, R. B. McQuistan, and T. R. Kirst, "Electron Probe Surface Mass Spectrometry Study of CO on Molybdenum," Surface Science, 5:120–36, 1966.

42. Dietrich Menzel and Robert Gomer, "Electron-Impact Desorption of Carbon Monoxide from Tungsten," The Journal of Chemical Physics, 41(11):3329–51, 1964.

43. J. T. Yates, Jr., T. E. Madey, and J. K. Payn, "Desorption by Electron Impact: Carbon Monoxide, Nitric Oxide and Oxygen on Tungsten," Supplemento al Nuovo Cimento, 5(2):558–81, 1967.

44. J. W. Coburn, "The Dissociative Electronic Desorption of Carbon Monoxide from Tungsten," Surface Science, 11:61–81, 1968.

45. D. A. Degras and J. Lecante, "Desorption et dissociation de l'oxyde de carbone adsorbe sur le molybdene par des electrons lents," Proceedings of the Seventh International Conference on Phenomena in Ionized Gases, Belgrade, 1965 (Vol. 1, Belgrade: Gradevinska Knjiga, 1965), pp. 124–29.

46. D. A. Degras, Thesis, Université de Paris, 1966.

47. D. R. Sandstrom, J. H. Leck, and E. E. Donaldson, "Electron-Bombardment Desorption of Carbon Monoxide Adsorbed on Tungsten," Journal of Applied Physics, 38(7):2851-2, 1967.

48. J. H. Singleton, "Errors in Pressure Measurement and Impurity Generation in Hydrogen using Bayard-Alpert Ionization Gauges," The Journal of Vacuum Science and Technology, 4(3):103-10, 1966.

49. D. A. Degras and J. Lecante, "Interactions between Low-Energy Electrons and Adsorbed Carbon Monoxide," Supplemento al Nuovo Cimento, 5(2):598-605, 1967.

50. D. Theodorou and J. Love, "Technique for Monitoring the Desorption Efficiency of Gases from a Surface under Electron Bombardment," Supplemento al Nuovo Cimento, 5(1):179-91, 1967.

51. E. Sugata, H. Kim, and S. Ishii, Electron-Microscopy (Tokyo), 1:245, 1966.

52. A. Klopfer, "Interactions of Electrons with Adsorbed Water," Supplemento al Nuovo Cimento, 5(2), 606-11, 1967.

53. Yu. V. Zubenko, S. A. Shakirova, I. L. Sokol'skaya, and Yu. I. Belyakov, "Use of the Omegatron in the Analysis of Gases Produced by Electron Bombardment of Coatings of Vacuum Devices," Radio Engineering and Electronics (USSR) (English Translation of Radiotekhnika i Elektronika), 9(2):285-7, 1964.

54. R. E. Clausing, "Release of Gases from Surfaces by Energetic Electrons" (paper presented at the Eleventh National Vacuum Symposium, Chicago, Illinois, September 30-October 2, 1964).

55. M. Bernardini and L. Malter, "Vacuum Problems of Electron and Positron Storage Rings," The Journal of Vacuum Science and Technology, 2:31, 1965.

56. V. L. Auslender and G. B. Minchenkov, "Outgassing of Metal Surfaces by Electron Bombardment," Soviet Physics-Technical Physics (English Translation of Zhurnal Tekhnicheskoi Fiziki), 11(11): 1535-8, 1967.

57. P. H. Dawson, "Outgassing of Glass by 100 to 1000 volt Electron Bombardment," Supplemento al Nuovo Cimento, 5(2):612-9, 1967.

58. E. W. Hoyt and E. L. Garwin, "Thermal and Electron Bombardment Desorption of Gases from Engineering Surfaces" (paper presented at the International Conference on Vacuum Metallurgy, New York, June 13-16, 1967).

59. G. M. McCracken, R. S. Barton, and W. Dillon, "Electron-Induced Desorption of Gas from Stainless-Steel Surfaces," Supplemento al Nuovo Cimento, 5(1):146–52, 1967.

60. H. S. W. Massey and E. H. S. Burhop, Electronic and Ionic Impact Phenomena (London: Oxford University Press, 1956), pp. 229–49.

61. Gert Ehrlich, "Low-Temperature Chemisorption. II. Flash Desorption of Carbon Monoxide," The Journal of Chemical Physics, 34(1): 39–46, 1961.

62. L. W. Swanson and Robert Gomer, "Field Desorption of Carbon Monoxide from Tungsten," The Journal of Chemical Physics, 39(11):2813–36, 1963.

63. Robert Gomer, "Surface Diffusion of CO on W," The Journal of Chemical Physics, 28:168, 1958.

64. R. P. Eischens, S. A. Francis, and W. A. Pliskin, "The Effect of Surface Coverage on the Spectra of Chemisorbed CO," The Journal of Chemical Physics, 60:194–201, 1956.

65. R. P. Eischens and W. A. Pliskin, "The Infrared Spectra of Adsorbed Molecules," Advances in Catalysis and Related Subjects (Vol. X, New York: Academic Press, 1958), pp. 2–56.

66. T. E. Madey, J. T. Yates, Jr., and R. C. Stern, "Isotopic Mixing in CO Chemisorbed on Tungsten. A Kinetic Study," The Journal of Chemical Physics, 42(4), 1372–8, 1965.

67. P. A. Redhead, "Chemisorption of Polycrystalline Tungsten," Transactions of the Faraday Society, 57:641–56, 1961.

68. A. A. Bell and Robert Gomer, "Adsorption of Carbon Monoxide on Tungsten, Abundances, Dipole Moments, and Sticking Coefficients," The Journal of Chemical Physics, 44(3):1065–80, 1966.

69. D. O. Hayward and B. M. W. Trapnell, Chemisorption (2nd ed., London: Butterworths, 1964).

70. S. Dushman, Scientific Foundations of Vacuum Technique (New York: Wiley, 1949), p. 17.

71. J. A. Becker, E. J. Becker, and R. G. Brandes, "Reactions of Oxygen with Pure Tungsten and Tungsten Containing Carbon," Journal of Applied Physics, 32:411–23, 1961.

85. T. E. Madey and J. T. Yates, Jr., "Work Function Studies: Chemisorption of Diatomic Molecules on Single-Crystal Tungsten," Supplemento al Nuovo Cimento, 5(2):483–505, 1967.

86. Gert Ehrlich, "Low-Temperature Chemisorption. I. Flash Desorption of Nitrogen," The Journal of Chemical Physics, 34(1):29–38, 1961.

87. P. J. Estrup and J. Anderson, "Chemisorption of Hydrogen on Tungsten (100)," The Journal of Chemical Physics, 45(6): 2254–60, 1966.

88. L. J. Rigby, "The Adsorption and Replacement of Hydrogen on Polycrystalline Tungsten," Canadian Journal of Physics, 43: 1020–35, 1965.

89. T. W. Hickmott, "Interaction of Hydrogen with Tungsten," The Journal of Chemical Physics, 32(3):810–23, 1960.

90. F. Ricca, R. Medana, and G. Saini, "Adsorption and Desorption of Hydrogen on Polycrystalline Tungsten," Transactions of the Faraday Society, 61:1492–1506, 1965.

91. Joseph Eisinger, "Properties of Hydrogen Chemisorbed on Tungsten," The Journal of Chemical Physics, 29(5):1154–60, 1958.

92. H.S.W. Massey and E.H.S. Burhop, Electron and Ionic Impact Phenomena (2nd ed., London: Oxford University Press, 1956), pp. 217–81.

93. H.S.W. Massey and E.H.S. Burhop, Electron and Ionic Impact Phenomena (2nd ed., London: Oxford University Press, 1956), pp. 282–329.

94. G.W. Simmons, Georgia Institute of Technology, Atlanta, Georgia (unpublished data on secondary and reflected electrons from tungsten and titanium surfaces, July 1968).

95. L. A. Pétermann, "Bond Strength and Mean Time of Adsorption for Active Gases on Metals," Supplemento al Nuovo Cimento, 5(2): 364, 1967.

96. R. D. Evans, The Atomic Nucleus (New York: McGraw-Hill, 1955), p. 592.

97. J. P. Hobson and J. W. Earnshaw, "Pressure Equations for the Residual Gases in an Ultrahigh Vacuum System," The Journal of Vacuum Science and Technology, 4(5):257–73, 1967.

98. J. W. May and L. H. Germer, "Adsorption of Carbon Monoxide on a Tungsten (110) Surface," The Journal of Chemical Physics, 44(8):2895–2902, 1966.

99. L. R. Apker, "Surface Phenomena Useful in Vacuum Technique," Industrial and Engineering Chemistry, 40(5):846–7, 1948.

100. J. A. Becker, "Adsorption on Metal Surfaces and Its Bearing on Catalysis," Advances in Catalysis and Related Subjects (Vol. II, New York: Academic Press, 1955), pp. 136–211.

APPENDICES

APPENDIX A

EBID OF HYDROGEN FROM TUNGSTEN AT 300°K

Figure 33 shows data for the EBID of hydrogen from tungsten at 300°K as a function of electron energy. The target was covered at 2.3×10^{-8} torr with 6×10^{14} hydrogen atoms per square centimeter and still had more than 5×10^{14} hydrogen atoms per square centimeter on the surface at the end of the run. The data are normalized to a bombardment current of 100 microamperes. The actual conditions for the measurements are given on Figure 33. Although there was considerable scatter in both the EBID and thermal desorption data, it is apparent that any reasonable correction for thermal desorption will still leave an important desorption due to electron interactions with the adsorbate. The figure shows a curve through the data, a curve with a correction based on $1\frac{1}{2}$ times the observed thermal desorption (as discussed in Appendix C, page 134) and an overcorrected curve. The overcorrected curve was drawn to show what would happen qualitatively if the thermal desorption was much larger than estimated. Note that neither the corrected curve nor the overcorrected curve is like that observed for carbon monoxide. Data from Menzel and Gomer[9] can be used to estimate that their neutral desorption was about 1×10^{-5} molecules per electron for 100 electron volt electrons, which is in good agreement with the present data.

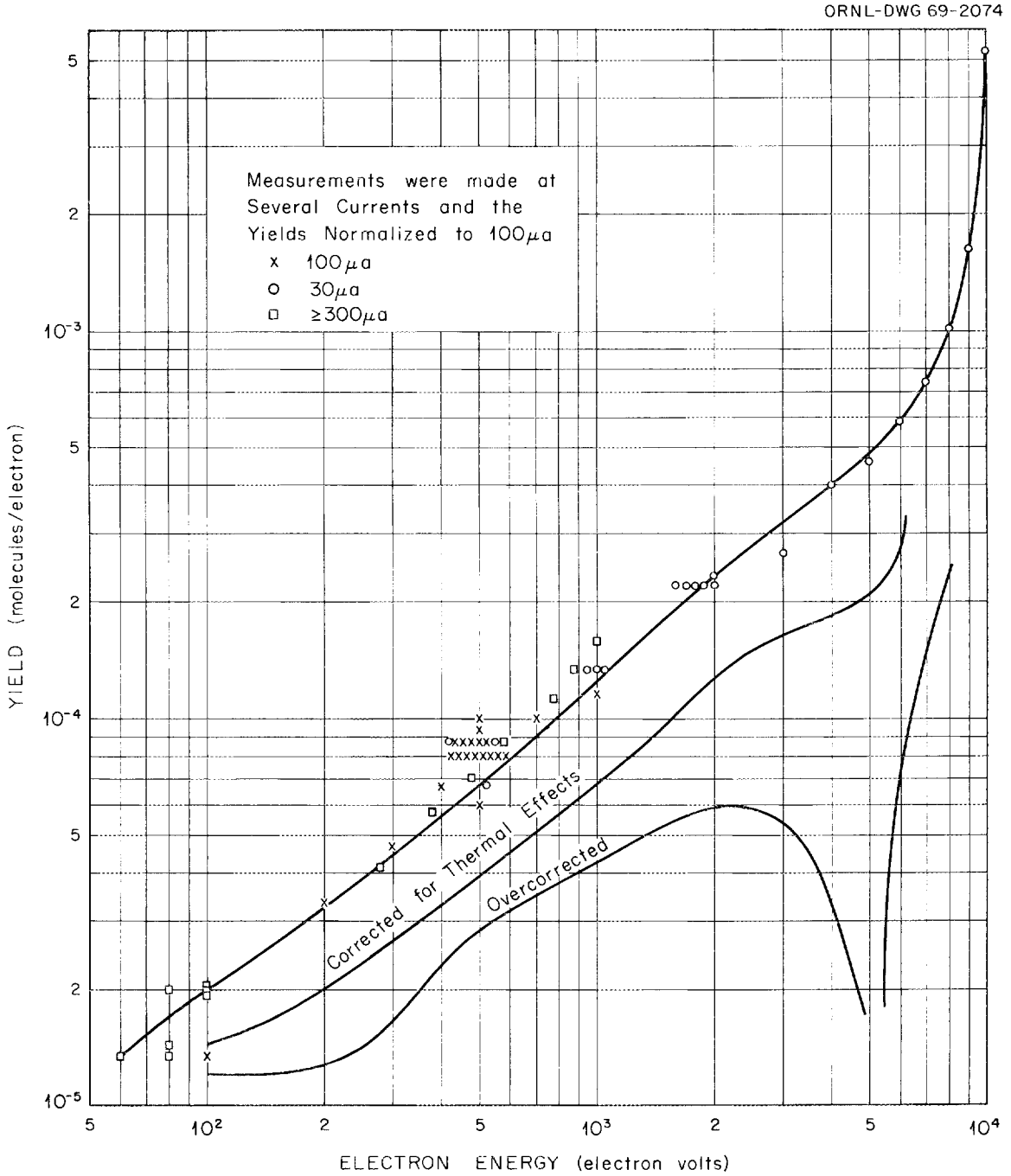

Figure 33. Electron bombardment induced desorption of hydrogen from tungsten at 300°K as a function of electron energy.

Figure 34 shows the EBID and thermal desorption of hydrogen from tungsten initially at 300°K as a function of hydrogen pressure. The procedure used was similar to that used for carbon monoxide and reported in Chapter III, page 68. The bombardment and thermal desorption parameters are given on Figure 34. The data points are numbered to indicate the sequence in which they were obtained. The thermal points show the desorption to be approximately proportional to the square root of the hydrogen pressure. It was found from the thermal desorption spectra at the end of the run that the specimen was contaminated with 1.5×10^{14} carbon monoxide molecules per square centimeter during the experiment. There is reason to believe that nearly all of the contamination occurred at the highest hydrogen pressure and that the carbon monoxide displaced some of the hydrogen.

The EBID data exhibit less pressure dependence if only the uncontaminated points 2, 3, and 4 are considered. If a correction for thermal effects is made, the desorption due to direct electronic interaction with the adsorbate is virtually independent of pressure as it was in the case of carbon monoxide (see Figure 27, page 78). The contamination of the specimen with carbon monoxide causes the EBID of hydrogen to increase whereas the thermal yields decreased. If the thermal desorption yields are subtracted from the EBID yields for the contaminated specimen the electronic interactions again seem to be nearly independent of pressure, but they are roughly three times higher than for the uncontaminated hydrogen. This seems to indicate that the

ORNL-DWG 69-2064

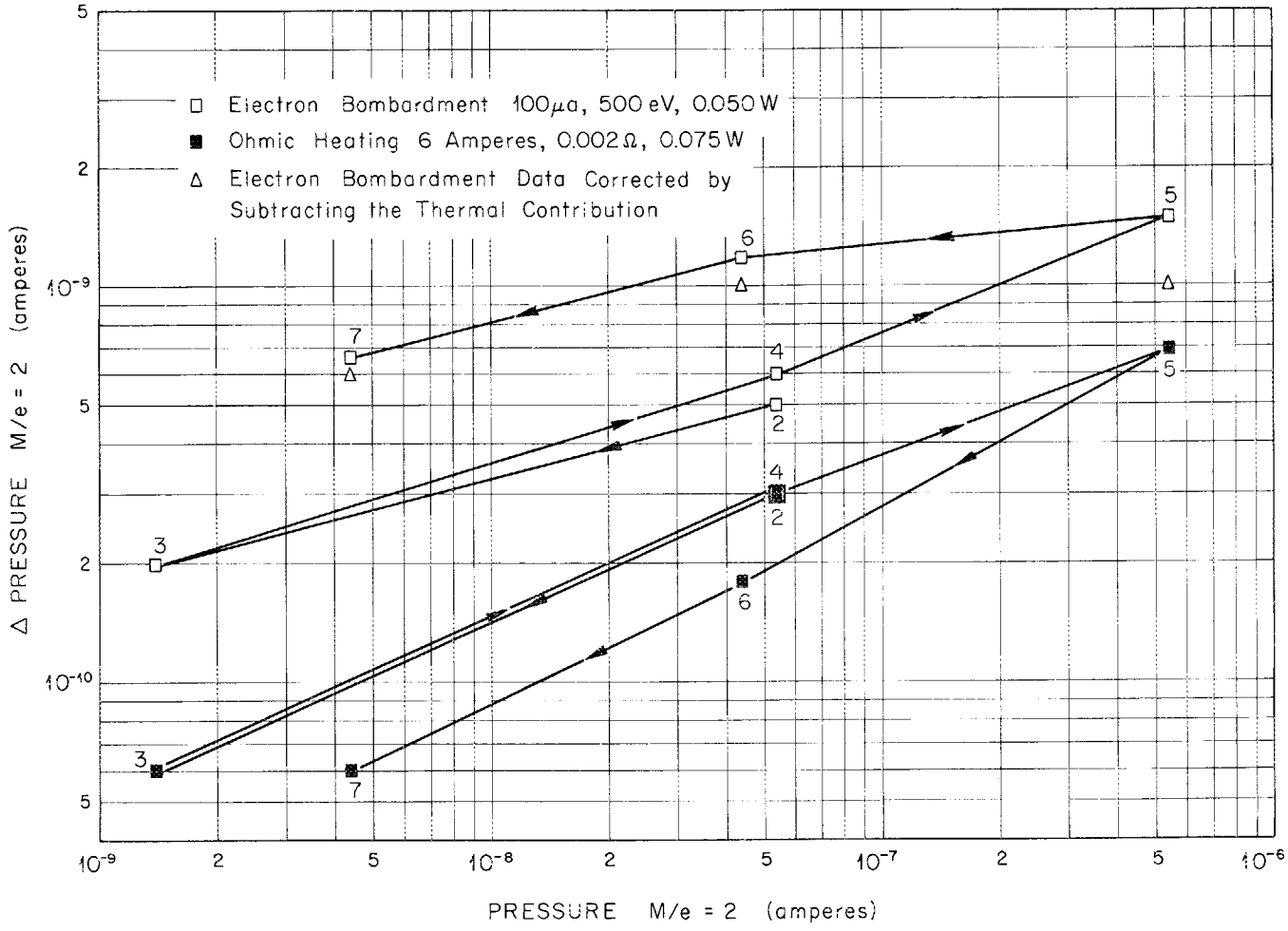

Figure 34. Electron bombardment induced desorption and thermal desorption of hydrogen from tungsten at 300°K as a function of the partial pressure of hydrogen in the experimental chamber. (The mass spectrometer sensitivity was 0.5 ampere per torr.)

remaining hydrogen (approximately 3×10^{14} atoms per square centimeter) is now in a state which is much more vulnerable to desorption by electron impact.

Electron bombardment induced desorption of hydrogen ions (H^+) has been observed from this target. It was noted that the H^+ signal decayed as the hydrogen was desorbed by raising the target to 500 or 600°K, but no other significant data were obtained. Figures 8, 9, 10, and 11, pages 19, 20, 22, and 23, show some data from the literature for EBID of H^+ from molybdenum and type 303 stainless steel.

APPENDIX B

THERMAL DESORPTION

When a gas is adsorbed on a surface, its rate of evaporation is given by an Arrhenius equation

$$-\frac{dn}{dt} = n^x \nu_x \exp\left(\frac{E}{RT}\right), \tag{B-1}$$

where

n = the surface concentration per square centimeter,

t = time in seconds,

x = order of the desorption reaction (1 or 2),

ν_x = frequency factor usually approximated as 10^{13} per second,

E = activation energy for desorption, heat of adsorption, plus the activation energy of adsorption,

R = gas constant = 8.7×10^{-5} electron volt per atom per °K,

T = absolute temperature, °K.

If ν is approximately 10^{13}, it is easy to verify that gases with E less than 5 electron volts (approximately 120 kilocalories per mole) will be desorbed at 2400°K with half-lives of much less than a second. This means that all of the common gases are quickly desorbed from a tungsten surface at that temperature. We can also see that as the temperature of the tungsten is raised slowly, gases with a small activation energy of desorption will come off first and that gases with particular activation

energy for desorption will come off rapidly in a fairly narrow temperature range. These facts can be used in the study of the interactions of gases with surfaces to great advantage.

By simply heating a ribbon of tungsten to 2400°K in a closed system and monitoring the pressure, we can determine the quantity of gas that was on the surface. By observing the temperature at which the desorption occurred, we can estimate the activation energy for desorption. This provides a very powerful experimental technique. Ehrlich[72] and Redhead[73] have analyzed the thermal desorption process in detail, and many investigators have used it to study gas-metal interactions. Several important variations of these techniques will be outlined below.

Apker[99] and others[100] used thermal desorption to measure the quantity of gas adsorbed on surfaces as a means of determining the adsorption rates and equilibrium concentration of gases on surfaces under known conditions. They simply allowed adsorption to occur for a given time in a specified environment and then flashed the gas off to measure the quantity adsorbed by the pressure rise in the system.

Ehrlich monitored the pressure as a function of the ribbon temperature during heating and calculated E values. A typical curve for the desorption of carbon monoxide from tungsten is shown in Figure 35(a). This curve may be differentiated to obtain the desorption rates as a function of temperature.

Redhead used an experimental system that had a large known pumping speed from the desorption chamber. He obtained the desorption rate directly since the pressure in the chamber under these conditions is

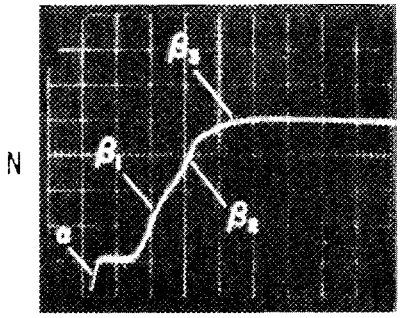

(a)

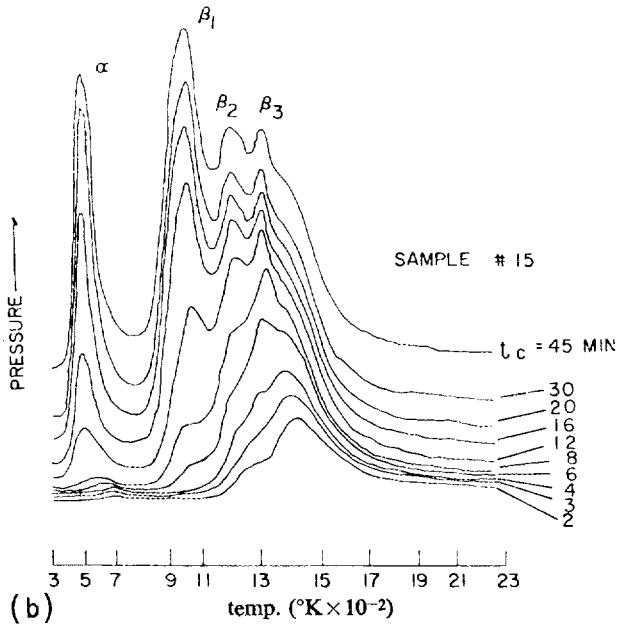

(b)

Figure 35. Typical thermal desorption data for carbon monoxide from tungsten. (a) Using Ehrlich's technique. [Adsorption at 336°K. Time scale of desorption: N is proportional to the total number of desorbed molecules; t is the time (1 division equals 0.1 second). Surface concentrations: β_1 equals 206×10^{12} molecules per square centimeter, β_1 equals 202×10^{12}, and β_2 equals 62×10^{12}. Reprinted from G. Ehrlich, "Kinetic and Experimental Basis of Flash Desorption," Journal of Applied Physics, 32(1):4, 1961.] (b) Using Redhead's technique. [Desorption spectra for various adsorption times, t_c, at a temperature of 300°K, heating rate equals 35°K per second. The zero levels of the curves have been shifted to prevent overlap. Reprinted from P. A. Redhead, "Chemisorption on Polycrystalline Tungsten," Transactions of the Faraday Society, 57:646, 1961.]

proportional to the rate of gas desorption rather than to the total amount desorbed as it is in Ehrlich's experiment. Figure 35(b) shows some of Redhead's data. The temperature at which the desorption rates peak are easy to observe, but the total amount of gas desorbed must be obtained by integrating the rate of desorption as a function of time. Redhead has worked out several relationships for his system that avoid tedious calculations and directly relate the peak pressure to the activation energy for desorption provided certain prescribed heating rates are followed.

If the temperature, the desorption rate, the frequency factor, and the concentration are known, one can determine E by a simple calculation using Equation (B-1). If $\ell n\ n^x \frac{dn}{dt}$ is plotted against $\frac{1}{RT}$ the correct value of x will give a straight line from which one can determine E without knowing the frequency factor. He may then go back and find it, assuming that it is not a function of temperature in the range of the plot.

With the idea that we need to know $\frac{dn}{dt}$, T, and n to determine E and subsequently ν, still another technique is suggested — that is, increasing the temperature in steps rather than continuously. Bell and Gomer[68] did this, and some of their data for carbon monoxide on tungsten is shown in Figure 36. Their system was pumped continuously so that the plot shows $\frac{dn}{dt}$ as a function of temperature, and the sum of the lengths of all of the columns at temperatures below the one being considered is proportional to the amount of gas desorbed up to that temperature. The sum of the lengths of all of the columns indicates the total quantity of

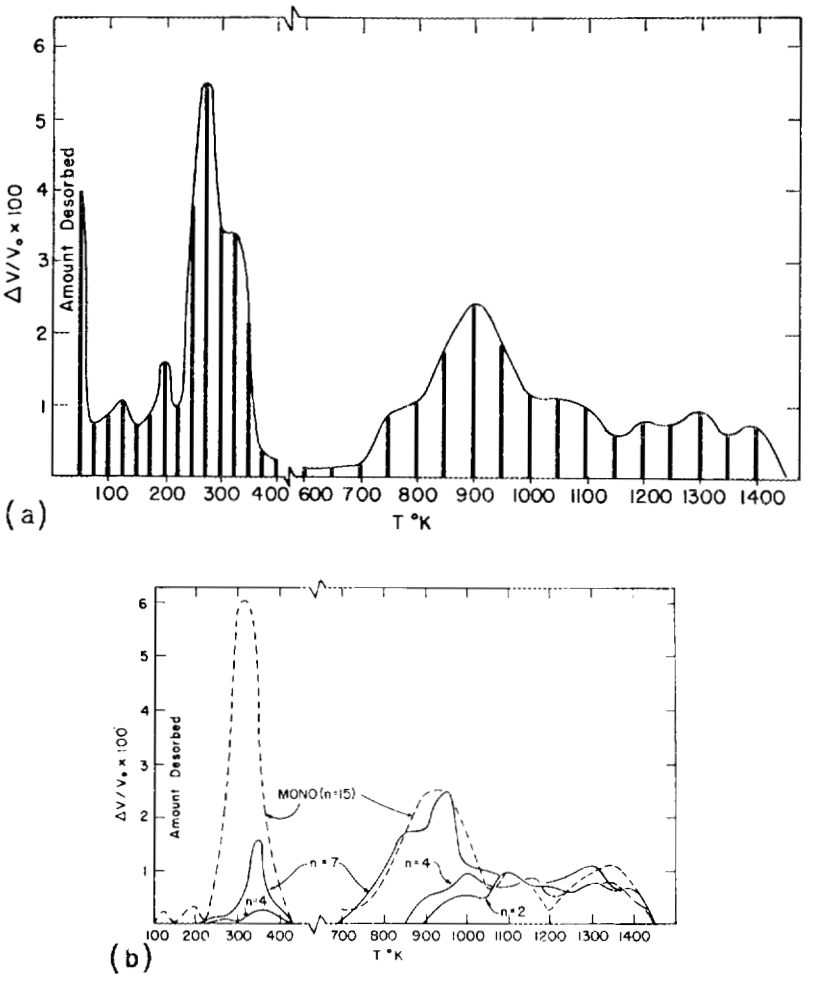

Figure 36. Thermal desorption of carbon monoxide from tungsten using the technique of Bell and Gomer. (a) Alpha (and beta) step-desorption spectrum, obtained by heating a full 20°K layer to 600°K for 60 seconds, and then redosing with an excess of carbon monoxide. (The desorption below 100°K corresponds to physisorbate. Heating time per step was 10 seconds.) (b) Step-desorption spectra of full and partial 20°K layers [n refers to the number of doses deposited at 20°K on the ribbon before a desorption sequence (n equals 15 constitutes a full layer). Note the absence of β_1 (700 to 900°K desorption) for $n < 4$. Only the spectrum envelopes are shown, for ease of presentation. Reprinted from A. A. Bell and R. Gomer, "Adsorption of Carbon Monoxide on Tungsten Abundances, Dipole Moments, and Sticking Coefficients," The Journal of Chemical Physics, 44(3):1075–76, 1966.]

gas adsorbed on the specimen at the beginning of the series of desorption steps. Note on Figure 36(b) that the desorption spectra can be very complex; not only are there many adsorption states, but it would appear that the activation energy for desorption changes with the amount adsorbed in at least some of the states. If the various adsorbed states overlap in their desorption temperatures and if E is not constant, the analysis becomes much more difficult.

In summary, thermal desorption techniques make it possible to determine the amount of gas on the surface, the activation energy for desorption, and the frequency factor. Using this information we can study reaction rates at metal surfaces and the populations of various states as functions of other variables such as the pressure and the structure of the surface.

APPENDIX C

TEMPERATURE DISTRIBUTION IN THE TARGET DURING EBID AND OHMIC HEATING

In order to obtain a measure of the thermal contribution to the EBID pulses so that purely electronic interactions could be examined, it was found useful to simulate the heating effect of electron bombardment by ohmic heating. Since the temperature distribution is not the same in the two cases, an exact simulation is not possible. It was decided that if the change in target temperature was small it would be acceptable to assume that the amount of desorption is proportional to the average temperature of the ribbon and that it would therefore be suitable to reproduce the average temperature change by ohmic heating. This assumption is given experimental support by data such as that shown in Figure 28, page 78, where the major part of the desorption is due to thermal effects, and the desorption is proportional to the energy of the bombarding electrons and hence, the power input and finally the average ΔT of the target during the pulse. In the case of Figure 28, page 78, the average ΔT was much greater than in any of the other data reported in this dissertation.

Although the temperature changes could be measured to 0.2°K, the increase in average temperature was less than 1°K for most of the carbon monoxide work so an analytical approach was needed to decide how much ohmic heating was required to simulate the electron bombardment heating.

Since the temperature changes are small and the heat deposition from electron bombardment is probably fairly uniform over the portion (the center half) of the surface bombarded, a one-dimensional heat-transfer model was used, and several cases were examined. For all cases it was assumed that the only heat loss from the ribbon was from its ends by conduction to a heat sink at constant temperature. Only one end of the ribbon is studied since it is symmetrical.

The basic heat transfer relationship we will use is given by

$$\frac{dT}{dx} = \frac{q}{KA},$$

where

$\frac{dT}{dx}$ = the temperature gradient,

T = temperature,

x = distance from the heat sink,

q = the heat flux,

K = the thermal conductivity of the sample,

A = the cross-sectional area of the sample.

For the sake of simplicity we will choose to compare the various cases on the basis of equal power dissipation in the target, which means that the q at the heat sink is the same in all cases. For convenience we will choose our units such that the right-hand side of the equation is unity at the heat sink, and KA is unity so that q is unity at $x = 0$. The distance x is chosen zero at the heat sink and unity at the center of the ribbon.

Case I Uniform Heat Generation in the Ribbon – Ohmic Heating

The heat flux, $q(x)$, is unity at $x = 0$ and decreases linearly to zero at $x = 1$. Therefore $q(x) = 1 - x$ and $dT/dx = 1 - x$. Solving

$$T = T_0 + x - \tfrac{1}{2}x^2.$$

Then

$$\begin{aligned} T_{av} &= T_0 + \int_0^1 T dx \\ &= T_0 + \tfrac{1}{2}x^2 - \tfrac{1}{6}x^3 \Big|_0^1 \\ &= T_0 + \tfrac{1}{3} . \end{aligned}$$

The average temperature change $(\Delta T)_{av} = 0.333$ and the maximum temperature change $(\Delta T)_{max} = 0.500$.

Case II Source Only at Center of Strip – An Extreme Case for Electron Bombardment Heating

The heat flux is unity along the whole specimen. Therefore $q(x) = 1$ and $dT/dx = 1$. Solving

$$T = T_0 + x .$$

Then

$$\begin{aligned} T_{av} &= T_0 + \int_0^1 x \\ &= T_0 + \tfrac{1}{2}x^2 \\ &= T_0 + 0.500 . \end{aligned}$$

Thus the average temperature change $(\Delta T)_{av} = 0.500$ and the maximum temperature change $(\Delta T)_{max} = 1.00$.

Case III Center Half of Ribbon Uniformly Heated — An Idealization of the Electron Bombardment Situation

The heat flux, $q(x)$, is given by $q(x) = 1$ for $0 < x < \frac{1}{2}$; and $q(x) = 1 - 2x$ for $\frac{1}{2} < x < 1$. By calculations similar to those of Cases I and II we find the average temperature change $(\Delta T)_{av} = 0.415$ and the maximum temperature change $(\Delta T)_{max} = 0.750$.

Case IV Center Third of Ribbon Heated Uniformly — An Approximation to the Expected Electron Bombardment Situation

The heat flux, $q(x)$, is given by $q = 1$ for $0 < x < \frac{2}{3}$ and $q = 1 - 3x$ for $\frac{2}{3} < x < 1$. By calculations similar to those above we find the average temperature change $(\Delta T)_{av} = 0.480$ and the maximum temperature change $(\Delta T)_{max} = 0.833$.

Figure 37 shows the calculated temperature distributions for the cases above. Curve V shows the temperature distribution for ohmic heating which would be produced by increasing the heating power by a factor of 1.5 to obtain the same average temperature as given by Curve II. This gives the same $(\Delta T)_{max}$ as Curve III, the idealized electron bombardment heating case, and gives a slightly lower $(\Delta T)_{max}$ but slightly higher $(\Delta T)_{av}$ than the slightly more realistic approximation given by Curve IV.

Following this analysis, it was decided to make the power used in the ohmic heating either $1\frac{1}{2}$ times the power in the electron bombardment pulses or to multiply the ohmic desorption values by $1\frac{1}{2}$ if pulses of the same power were used.

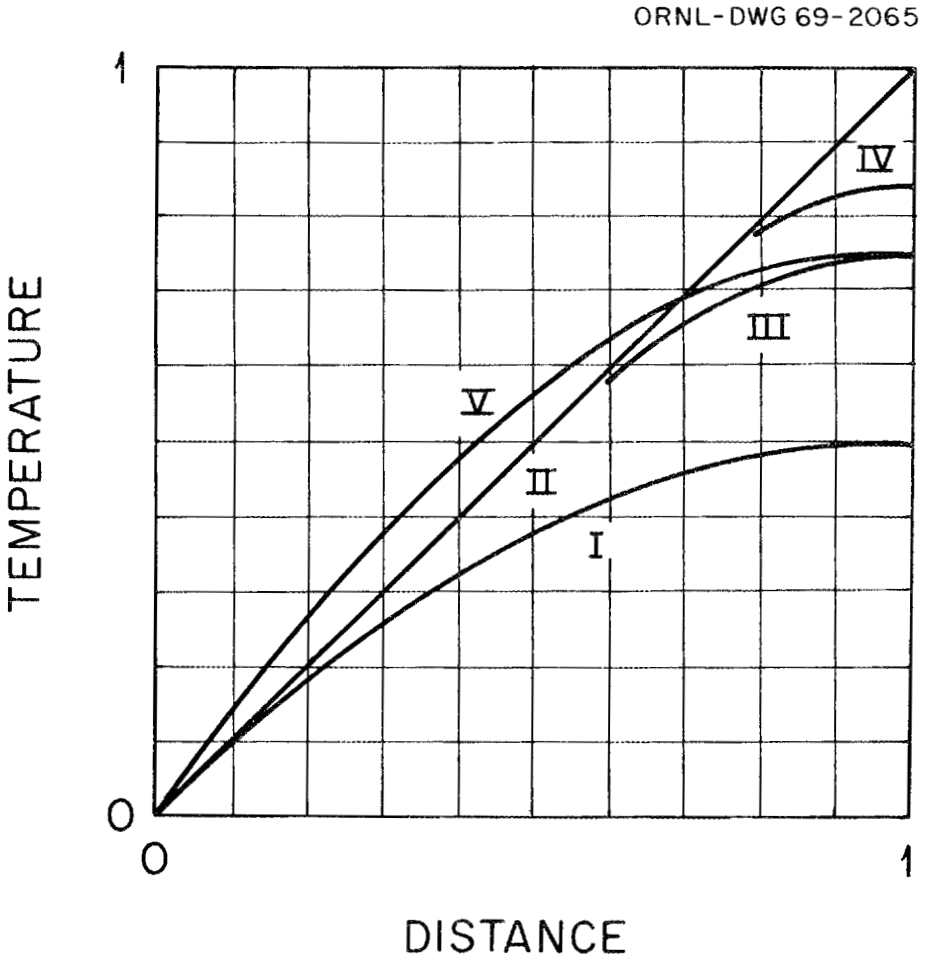

Figure 37. Temperature distributions in a one dimensional model of the tungsten target (I), ohmic heating (II), electron bombardment only at the midpoint of the target (III), electron bombardment of the center half of the target (IV), electron bombardment of the center third of the target (V), and ohmic heating with 150 per cent of the power input of Curves I, II, III, and IV.

INTERNAL DISTRIBUTION

1–2. Central Research Library
3–4. ORNL – Y-12 Technical Library
Document Reference Section
5–15. Laboratory Records
16. Laboratory Records, R.C.
17. ORNL Patent Office
18. I. Alexeff
19. G. M. Adamson, Jr.
20. C. F. Barnett
21. B. S. Borie
22. G. E. Boyd
23. J. V. Cathcart
24–53. R. E. Clausing
54. J. E. Cunningham
55. R. A. Dandl
56. J. H. DeVan
57. J. L. Dunlap
58. D. S. Easton
59. A. C. England
60. J. H Frye, Jr.
61. W. F. Gauster
62. G. E. Guest
63. G. R. Haste
64–66. M. R. Hill
67. H. Inouye
68. W. D. Jones
69. G. G. Kelley
70. N. H. Lazar
71. C. J. McHargue
72. J. H. McNally
73. O. B. Morgan, Jr.
74. R. V. Neidigh
75. P. Patriarca
76. R. E. Pawel
77. H. Postma
78. D. M. Richardson
79. E. D. Shipley
80. W. L. Stirling
81. R. F. Stratton
82. R. A. Strehlow
83. D. A. Sundberg
84. R. L. Wagner
85. E. R. Wells
86. O. C. Yonts

EXTERNAL DISTRIBUTION

87. D. F. Cope, RDT, SSR, AEC, Oak Ridge National Laboratory
88. D. K. Stevens, AEC, Washington
89. Laboratory and University Division, AEC, Oak Ridge Operations
90–104. Division of Technical Information Extension